Transporter and Metabolic-based Drug-Drug Interactions:

The Blood-Brain Barrier and The Liver

Li Liu

A dissertation submitted in partial fulfillment of the

requirements for the degree of

Doctor of Philosophy

University of Washington

2012

Reading Committee:

Jashvant D. Unadkat, Professor, Chair

Kenneth E. Thummel, Professor

Yvonne Lin, Assistant Professor

Qingcheng Mao, Associate Professor

Program Authorized to Offer Degree:

Pharmaceutics

University of Washington

Abstract

Transporter and Metabolic-based Drug-Drug Interactions:

The Blood-Brain Barrier and The Liver

Li Liu

Chair of the Supervisory Committee:

Professor Jashvant D. Unadkat

Department of Pharmaceutics

The HIV Protease inhibitor (PI)-based DDIs are complex, unpredictable and often paradoxical. Investigations dedicated to evaluating PIs' potential as inducers of the CYPs and drug transporter, and PIs' as substrates of hepatic uptake transporters haven been scarce, especially those using human hepatocytes, an advanced *in vitro* systems that provides the most comprehensive and *in vivo*-like hepatocyte cellular characteristics. These investigations are much needed to better understand and predict the *in vivo* DDIs with PIs as precipitant and/or object drugs. Therefore, we used human hepatocytes and performed 1) comprehensive quantification of the net induction potential of the eight PIs for nine major hepatic CYPs

(CYP3A, 2B6, 1A, 2C8, 2C9, 2C19, 2D6, 2E1, 2A6) at the activity level, as well as their induction of the mRNA transcripts of the same CYPs, and the hepatic drug transporters (P-gp, OATPs, MRPs), and 2) transport studies to examine whether the hepatic uptake of PIs is transporter mediated. We showed that the majority of PIs (particularly amprenavir) produced significant induction in CYP3A4 mRNA expression. They were also net and modest inducers of CYP2B6 (mRNA and activity), and OATP1B1 and P-gp (mRNA). Based on these findings, we were able to establish qualitative agreement between our *in vitro* results and those observed *in vivo*. Furthermore, from these studies, we also learned that the hepatic uptake of ritonavir, lopinavir, and nelfinavir was dominated by passive diffusion. However, amprenavir was transported into human hepatocytes, but not by OATP-mediated transport.

P-gp is functionally important at the human blood-brain barrier (BBB). However, we question whether BBB P-gp can be maximally inhibited or induced by a drug at its clinically-approved concentration, and whether such P-gp mediated DDIs are clinically significant, and be translated to improve the treatment of CNS diseases. To address these questions, we recruited healthy human volunteers to conduct positron emission tomography (PET) imaging to quantify the magnitude of change in BBB P-gp activity in comparison to baseline by quinidine (model P-gp inhibitor), and after chronic treatment of rifampin (model P-gp inducer) using ^{11}C-verapamil as our P-gp PET substrate. In addition, we evaluated whether the level of P-gp inhibition can be predicted using preclinical data. Our findings show quinidine can significantly inhibit P-gp at the human BBB, and therefore has the potential produce clinically significant DDIs with P-gp substrate drugs with narrow therapeutic index and/or significantly effluxed from brain by P-gp. The quinidine-verapamil P-gp-based DDI at the human BBB was also successfully predicted by the macaque model, but not by the rat model. Conversely, we found that chronic rifampin

treatment did not induce P-gp at the human BBB, and highlighted the need for future investigation to determine whether nuclear receptors (e.g., PXR, CAR, VDR, GR) known to regulate P-gp in other tissues are present at the human BBB.

In summary, we addressed and explained many unanswered questions and key issues that we believe have contributed to the complexity of DDIs associated with HIV protease inhibitors and those mediated by P-gp at the human BBB. However, many new and interesting questions are raised from these studies, and remained to be addressed.

TABLE OF CONTENTS

LIST OF FIGURES

LIST OF TABLES

ACKNOWLEDGEMENTS

My most sincere and deepest gratitude to my doctoral advisor and life mentor Professor Jashvant D. Unadkat. Everything that I have accomplished during my PhD career is not possible without his encouragement, support, and guidance. Professor Unadkat played a central role in my scientific growth and future professional pursuits. He is the most influential person in my adult life, and was like a father to me in fostering my personal growth. I am forever indebted to him, and will always carry his advice and insights with me in life.

To my thesis doctoral and reading committee advisors and members, Professors Thummel, Ho, Mao, Lin, and Anderson, I wish to express my appreciation for their unwavering motivation and support through the years. Special thanks to Professor Thummel, for believing in me and providing me with opportunities when I needed them the most. His commitment to my education and success is critical in my accomplishments

I also wish to express my sincere appreciation to my clinical study team members, with special thanks to Drs. Collier, Mankoff, Link, Domino, and Richards, and study coordinator Eric Helgeson. I have learned so much from their dedication and professionalism. I will always carry the relationships I have built with them wherever I go.

DEDICATION

To my parents, Sheldon Liu and Najia Geng, there is not enough “thank you”s in the world for me to say to you for your love, confidence, motivation and encouragements. I owe this doctoral degree to you, and thank you for making everything possible for me to succeed in my pursuits and to make my dream come true. I love you, mom and dad!

To my brother, Eugene Liu: you came into my life ~17 years later, but the role you have played in my life in the past 10 years has been essential to my success. Through the years of my doctoral pursuit, we have battled through and conquered some much hardship that life has thrown at us. You have so much love, happiness and laughter to give, your confidence and pride in me have given me the strength and determination to pull through all of my difficult times. I will always love you, and be forever thankful that you are in my life.

To my academic siblings and labmates, thank you for all the scientific discussions and wonderful conversations that made grad school life so fun and enjoyable. It was a pleasure getting to know each of you, and I look forward to our growth together in the future.

Chapter 1: Introduction

Drug-drug interactions (DDIs) have long been recognized to limit drug efficacy and produce adverse effects and toxicity. However, DDIs can be adapted to improve drug therapy. My thesis research is divided into two major themes, and centers on both the prevention and utility of DDIs to improve treatment of HIV/AIDS and CNS diseases. The following sections present a broad background on these two themes. Detailed background for each aim is provided in the respective chapter describing the aim.

1.A HIV Protease Inhibitors DDIs

Protease inhibitors (PIs)-based HIV regimens continue to serve as the backbone of Highly Active Antiretroviral Therapy (HAART) [Thompson et al., 2012]. With proper adherence, HAART can suppress viral replication for decades, and dramatically increase the life expectancy of the HIV-infected patients. However, the efficacy of HAART is dependent on drug adherence and tolerability, and can be significantly impaired by DDIs amongst antiretroviral agents and with other coadministered medications [Arts et al., 2012]. PIs are known to produce complex, unpredictable and unexpected DDIs due to their complex pharmacokinetic properties involving extensive drug metabolism and transport [Kirby et al., 2011a, 2011b]. In humans, after oral administration of a single dose of radiolabeled PIs, these drugs are found to be cleared from the body via extensive hepatic elimination (>80%), of which 88% is accounted for by CYP3A metabolism, and ~12% by biliary excretion [Denissen et al., 1997; Kumar et al., 2004; Sadler et al., 2001]. Therefore, understanding PIs' interactions with the various hepatic CYPs

and transporters is critical in obtaining a better mechanistic understanding of how they elicit their precipitant effects. Many PI-based DDIs have been attributed to decreased CYP activity (e.g., CYP3A inhibition and/or inactivation), while others have also been linked to PIs' ability to induce the expression and therefore, activity of metabolic enzymes and transporters [Dickinson et al., 2010; Kirby et al., 2011a, 2011b]. However, detailed quantitative characterization of PIs' induction potential of the major hepatic CYPs and drug transporters has been limited to ritonavir and nelfinavir on selective CYP enzymes and transporters [Dixit et al., 2008]. In addition, it is increasingly recognized that drug transporters (ATP-binding cassette, ABC and solute carrier family, SLC, transporters) could have an important role in PI disposition and could potentially contribute to DDIs of clinical significance [Kis et al., 2010]. While PIs have been identified as substrates, inhibitors, and/inducers of multiple efflux transporters (e.g., P-gp, MRP2, and BCRP), whether PIs are transported into the human hepatocytes remain an open question [van der Sandt et al., 2001; Huisman et al., 2002; Hsiao et al., 2008; Ye et al., 2010; Gupta et al., 2004; Dixit et al., 2008]. Therefore, the goals of our investigations were: **Chapter 2**) to quantify the net induction potential of PIs for hepatic CYPs and transporters in the presence of other concurrent DDI mechanisms (e.g., inhibition of CYPs and drug transporters) in human hepatocytes, and **Chapter 3**) evaluate whether the hepatic uptake of the PIs is transporter-mediated by using a physiologically relevant *in vitro* system such as human hepatocytes. Conducting these studies is essential in obtaining an integrative understanding of the PI-based DDIs (both metabolic and transporter mediated mechanisms) to improve their accurate prediction, and to evaluate the clinical implication of hepatic uptake transporters in PIs disposition and in PI-based DDIs.

1.A1 Hypothesis

PIs exhibit multifaceted interactions with both metabolic and transporter-mediated processes. Delineating their interactions with and induction potential for the hepatic CYPs and transporters will help achieve an integrative understanding and provide a more accurate *in vitro-in vivo* prediction of PI-based DDIs.

1.A2 Specific Aims

Aim A1 Chapter 2: Quantification of Human Hepatocyte Cytochrome P450 Enzymes and Transporters Induced by HIV Protease Inhibitors Using Newly Validated LC-MS/MS Cocktail Assays and RT-PCR

Sub Aim A1.1: To validate two cocktail assays that can simultaneously quantify the activity of nine CYPs using probe substrates via LC-MS/MS, to maximize the efficient use of precious or low-yield samples (e.g., microsomes isolated from human hepatocytes)

Sub Aim A1.2: To apply the two cocktail assays to quantify the net induction potential of eight PIs (amprenavir, ritonavir, nelfinavir, saquinavir, atazanavir, lopinavir, tipranavir, and indinavir) for the major hepatic CYPs (CYP3As, 2B6, 2C8, 2C9, 2C19, 1As, 2A6, 2E1, and 2D6) in microsomes isolated from PI-treated human hepatocytes.

Sub Aim A1.3: To quantify the induction of the same hepatic CYPs and transporters (OATP1B1, 1B3, 1A2, P-gp, MRP2 and MRP4) at the mRNA level by these PIs in human hepatocytes.

Aim A2 Chapter 3: Interaction between HIV Protease Inhibitors (PIs) and Hepatic Transporters in Sandwich-Cultured Human Hepatocytes: Implication for PI-based DDIs

Sub Aim A2.1: To determine whether the hepatic uptake of the PIs is transporter-mediated in sandwich-cultured human hepatocytes (SCHH).

Sub Aim A2.2: To evaluate whether the sinusoidal influx transport (if any) of the PIs is contributed by hepatic OATPs using SCHH and selective OATP stably transfected MDCKII cells.

1.A3 HIV-1 Life Cycle and Drug Targets

The advancement in the understanding of the HIV-1 replication cycle has presented many opportunities for therapeutic intervention, and hence accelerated the development of six classes of antiretroviral drugs inhibiting various steps of the virus life cycle [Art et al., 2012]. Figure 1.A1 illustrates the HIV-1 replication scheme with the most advanced antiretroviral drug targets, the time window of the replication cycle during which each class of antiretroviral acts upon, and the list of both FDA approved antiretrovirals or those in development [Art et al., 2012]. Our focus is on the HIV-1 protease inhibitors (PIs) that block proteolysis of the viral gag and gag-pol

polyprotein precursors, a step essential for the production and maturation of infectious viral particles [Dickinson et al., 2009].

1.A4 HIV Protease Inhibitors: Therapeutic Use

Ten PIs are currently approved for use in humans, amprenavir (APV, Agenerase), fosamprenavir (FPV, Lexiva; prodrug of APV), atazanavir (ATZ, Reyataz), darunavir (DRV, Prezista), indinavir (IDV, Crixivan), lopinavir (LPV, Kaletra), nelfinavir (NFV, Viracept), ritonavir (RTV, Norvir), saquinavir (SQV, Fortovase/Invirase), and tipranavir (TPV, Aptivus) [Art et al., 2012]. As part of the initial antiretroviral therapy (ART), PIs are typically used in combination with two nucleos(t)ide reverse transcriptase inhibitors (NRTIs) [Thompson et al., 2012]. According to the 2012 recommendations for antiretroviral treatment of adult HIV infection published by the International Antiviral Society, PIs remain a vital role in HAART along with two other classes of antiretroviral agents (NRTIs and nonnucleoside reverse transcriptase inhibitors) [Thompson et al., 2012]. Though PIs are extremely potent in decreasing viral-load, their poor bioavailability as stand-alone therapy requires coadministration with "booster agent" (e.g., low-dose RTV, or cobicistat) to inhibit CYP3A4 (a major metabolic enzyme of the PIs) to provide the pharmacoenhancement necessary to reach desirable systemic concentration and pharmacological efficacy [Hill et al., 2009]. Currently, RTV-boosted ATV or DRV are the most clinically recommended frontline PIs, followed by alternatives such as RTV-boosted LPV, FPV or SQV [Thompson et al., 2012].

In general, PIs are associated with several characteristic adverse events, including metabolic disorders (hyperlipidemia, lipodystropy, and insulin resistance) and gastrointestinal

disorders (nausea, vomiting, and diarrhea) [Art et al., 2012]. Reports of cardiac conduction abnormalities (QT interval prolongation), and hyperbilirubinemia leading to clinical jaundice have also been published for selective PIs [Art et al., 2012].

1.A5 HIV Protease Inhibitors: Pharmacokinetics

As a general class, PIs are large molecular weight (500 – 720 daltons), lipophilic compounds with relatively high LogP (1.8 – 6.8) and high permeability (Table 1.A). They are structurally similar (Figure 1.A2), and divided into peptidomimetics (RTV, SQV, IDV, ATV and LPV) and non-peptidomimetics (FPV, APV, NFV, TPV, and DRV). Consistent with their physicochemical properties, most PIs are highly plasma protein bound (≥ 98%), favoring α1-acid glycoprotein over albumin. All PIs are extensively metabolized by CYP3A4 and efficiently effluxed by P-gp, with relatively short plasma elimination half-lives. For selective PIs (e.g., RTV, NFV), CYP2C9, 2C19 and 2D6 also play minor roles. After a single dose of oral administration of radiolabeled PIs, these drugs are found to be cleared from the body via extensive hepatic elimination (>80%), of which 88% is accounted by CYP3A metabolism, and ~12% by biliary excretion [Denissen et al., 1997; Kumar et al., 2004; Sadler et al., 2001]. However, given that many of the PIs are able to inactivate CYP3A almost completely, upon chronic administration boosted with RTV (how PIs are normally administered), the contribution from CYP3A metabolism in PIs elimination could be minimal, and that from biliary elimination is likely to be higher. In addition, multiple dosing studies (e.g., RTV, NFV, or TPV) have also demonstrated time-dependent decrease in their plasma concentrations, suggesting autoinduction of their respective clearance pathways [Chen et al., 2007].

1.A6 DDIs with the PIs:

1.A6.1 PIs as Precipitants of DDIs:

As precipitant drugs, PIs are capable of generating DDIs through a complex balance of inhibition, inactivation and/or induction of the CYPs and transporters. PIs' potent CYP3A inhibition and inactivation capacities (e.g., RTV, APV, LPV, ATV) have been well-characterized. These studies permitted both the mechanistic understanding and the building of preliminary prediction models for PI-based DDIs [Kirby et al., 2011a, 2011b]. However, this mode of action alone cannot account for many other DDIs, particularly those involving induction mechanisms. The latter is being increasingly recognized since almost all current PI-based HIV therapy is RTV-boosted and administered chronically, where the major route of PIs clearance (CYP3A metabolism) is inactivated. Under such circumstances, the systemic exposure and intracellular concentration of the coadministered PIs are elevated to further magnify their precipitant effects (e.g., induction, inhibition/inactivation of CYPs and transporters). PIs' inhibition towards various CYPs [Unadkat and Wang, 2000] and transporters (P-gp, MRP2, BCRP, and OATPs) [Hsiao et al., 2008; Ye et al., 2010; Annaert et al., 2010; Gupta et al., 2004] have been well-studied. Therefore our focus was to investigate and quantify the net induction potential of PIs for the hepatic CYPs and transporters.

Selective PIs have been identified as ligands of the nuclear receptor, pregnane X receptor (PXR) [Dussault et al., 2001]. In addition, *in vitro* results from caco2-cells showed that PIs are not ligands of constitutive androstane receptor (CAR) [Gupta et al., 2008]. However, PIs' capability to induce PXR and CAR co-regulated CYPs were observed in various *in vivo* DDI studies, such as the 60% decrease in bupropion AUC (CYP2B6 probe), and 40% decrease in S-

and R-warfarin AUC (CYP2C9 probe) was observed after chronic dosing of LPV/RTV [Hogeland et al., 2007; Lim et al., 2004]. Induction of hepatic glucuronidation pathways (PXR regulated) was also proposed when 40%-50% decrease was observed in the AUC of lamotrigine, a compound primarily cleared by phase II enzymes (UGT1A4, 2B7), after multiple ATV/RTV or LPV/RTV administration [Burger et al., 2008; van der Lee et al., 2006]. In addition to metabolic induction, induction of transporters co-regulated by PXR and CAR was also observed. P-gp induction by chronic RTV-boosted TPV or APV therapy was believed to contribute to the decreased AUCs of loperamide (60%), and paroxetine (55%) [Mukwaya et al., 2005; van der Lee et al., 2007]. Moreover, OATP and MRP2 induction were proposed to explain the 50% pravastatin AUC decrease after chronic administration of ATV/RTV, SQV/RTV, or NFV [Ray et al., 2009]. Last, but not least, activation of Aryl hydrocarbon receptor (AhR) by PIs was also suggested when the AUCs of CYP1A2 (AhR-regulated) probes drugs (theophylline, caffeine) were decreased by 40%-75% after chronic administration of RTV [Unadkat and Wang, 2000].

Despite these clinical observations, detailed identification and quantification of the net induction potential of PIs (with the exception of NFV and RTV) for both hepatic CYPs and transporters are limited [Dixit et al., 2008]. Thus to fulfill this gap in knowledge and to improve our ability to accurately predict PI-based DDIs, studies proposed in **Specific Aim 1** and detailed in **Chapter 2** were conducted to delineate the net induction potential of eight PIs on various hepatic CYPs (activity and mRNA expression) and transporters (mRNA expression) using human hepatocytes.

1.A6.2 PIs as Objects of DDIs:

Since the clearance of PIs is primarily dominated by CYP3A, with minor involvement of other metabolic enzymes, the majority of the DDIs involving PIs as object drugs are attributed to CYP3A-mediated mechanism. Therefore, understandably, the exposure of the PIs is generally not significantly affected when other non-CYP3A enzymes are modulated. However, PIs are known substrates of multiple hepatic transporters. Since most PI-regimens are RTV-boosted and chronically administered, biliary excretion of the PIs is likely to become the predominate route of PI elimination to compensate for the loss of CYP3A metabolism. Thus, the contribution hepatic transporters (sinusoidal and canalicular) in PI disposition becomes more pronounced, and the likelihood of transporter-based DDIs involving PIs as object drugs could also increase.

Most PIs have been well characterized to be substrates of the canalicular efflux transporters (P-gp, MRP2), with the exception of BCRP, which has been shown to not transport PIs [van der Sandt et al., 2001; Huisman et al., 2002; Gupta et al., 2004]. However, whether PIs are transported by the hepatic uptake transporters remain inconclusive, due to the limited and conflicting results on their interactions with the OATPs as substrates [Hartkoorn et al., 2010; Su et al., 2004; Parker et al., 2008; Kis et al., 2010]. More importantly, evaluation of PIs uptake in human hepatocytes remains uninvestigated. If the sinusoidal influx transporters (including, but not limited to OATPs) are involved in PI hepatic uptake, then DDIs involving modulation (inhibition or induction) of such transporters could have clinically significant implication on PIs disposition and efficacy. Therefore, studies proposed in **Specific Aim 2** and detailed in **Chapter 3** were performed to evaluate the hepatic uptake of PIs in the most physiologically relevant *in vitro* system.

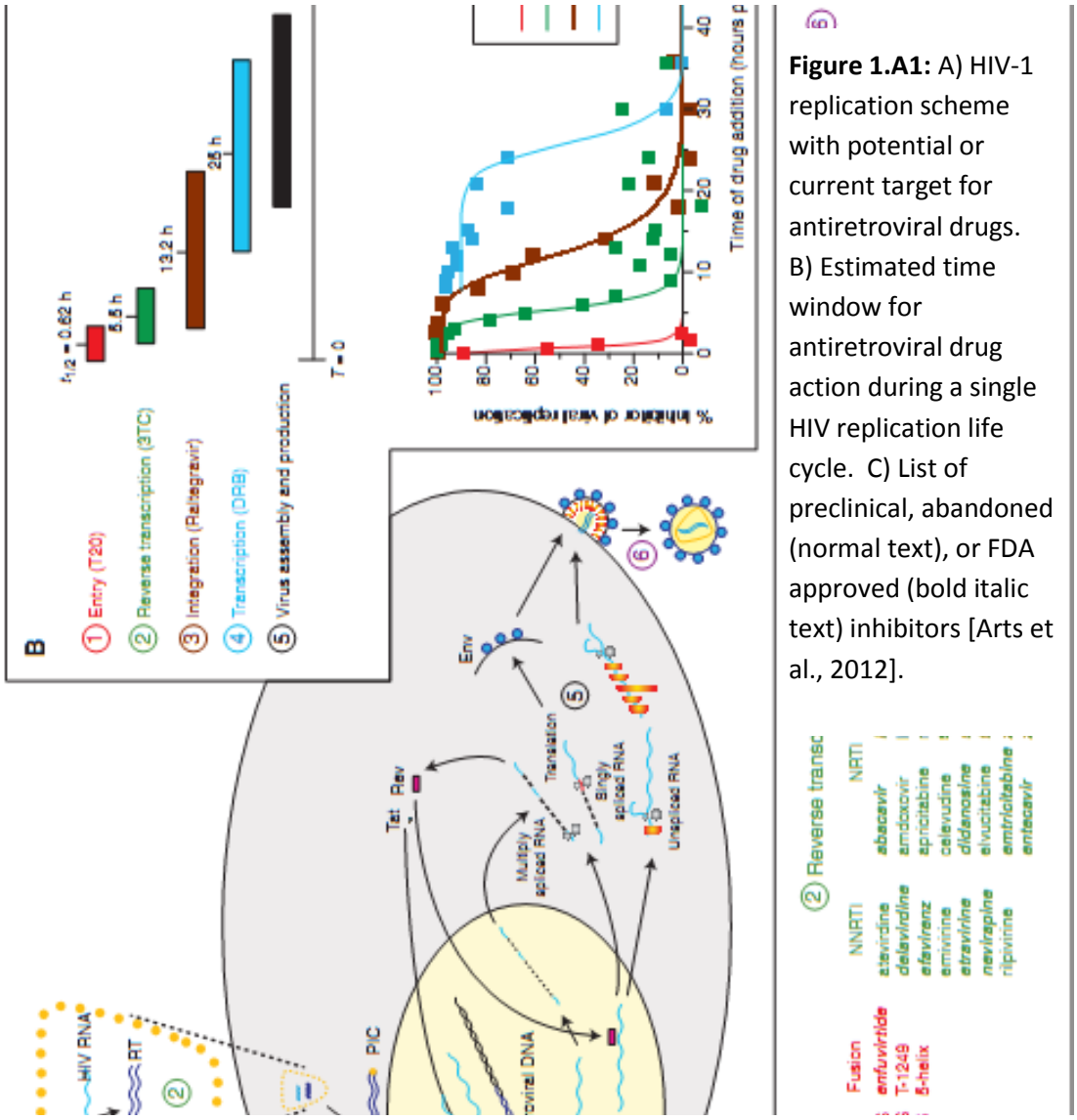

Figure 1.A1: A) HIV-1 replication scheme with potential or current target for antiretroviral drugs. B) Estimated time window for antiretroviral drug action during a single HIV replication life cycle. C) List of preclinical, abandoned (normal text), or FDA approved (bold italic text) inhibitors [Arts et al., 2012].

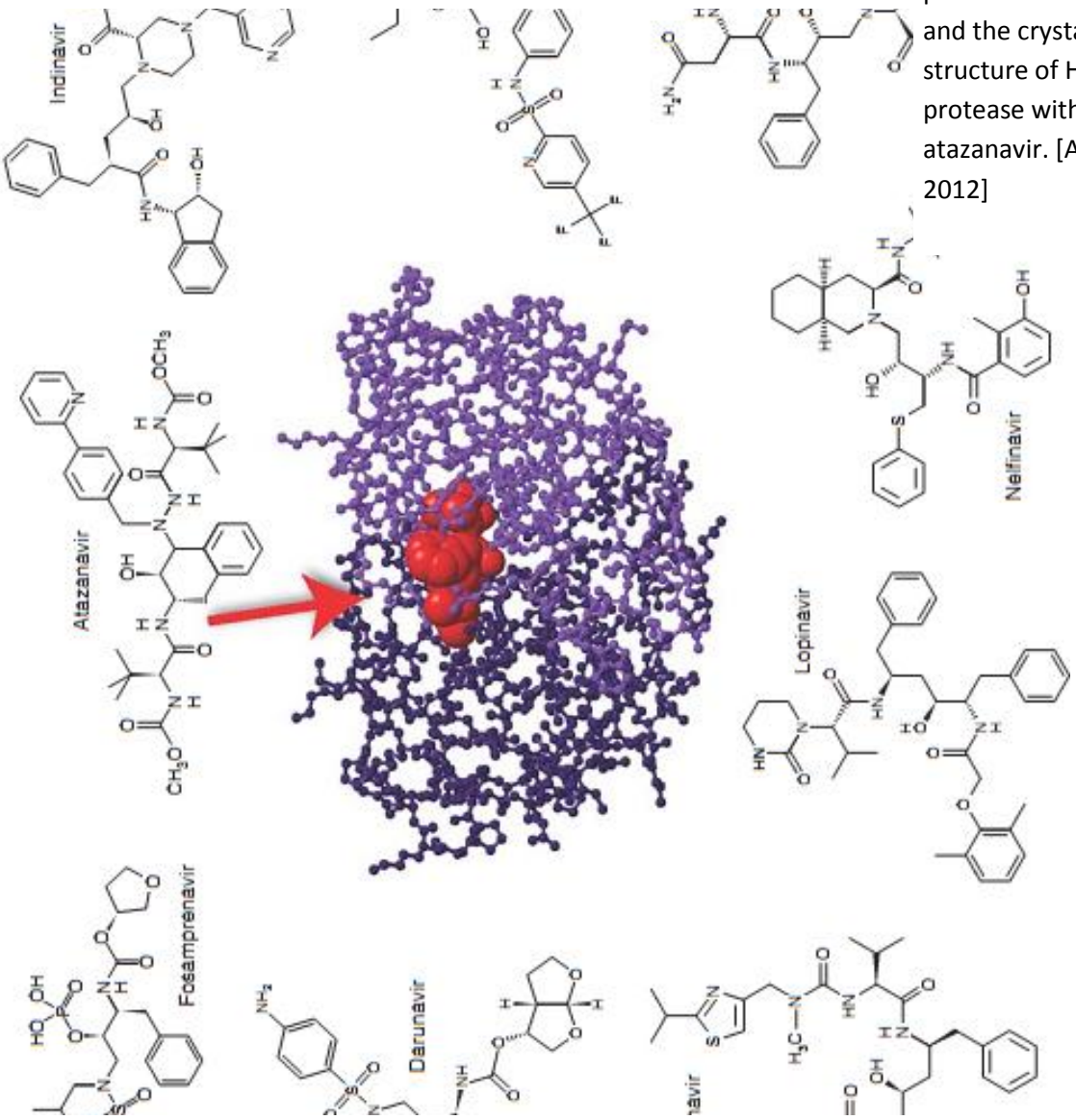

Figure 1.A2: Chemical structures of HIV protease inhibitors, and the crystal structure of HIV-1 protease with atazanavir. [Arts et al., 2012]

	Ritonavir	Lopinavir	Tipranavir	Darunavir
Molecular Weight	720.9	628.8	602.6	547.6
Solubility (mg/mL)	0.001	0.002	0.0002	0.07
Log P	3.9	3.9	6.9	1.8
Half-life (hours)	14.2	14.0	7.8	14.2
Protein Binding	99%	99%	>99.9%	~95%
Volume of Distribution (L)	84-150	98	20	161
Clearance (L/hr)	4	5	5	15 (+RTV)
Protease Inhibitors				
Excretion (urine)	11% urine	10% urine	4.4% urine	14% urine
Excretion (feces)	86% feces	83% feces	82% feces	80% feces
HIV-2	4% urine	2% urine	3% urine	8% urine
HIV-1	34% feces	20% feces	80% feces	41% feces

1.B PET Imaging: P-gp Mediated DDIs at the Human Blood-Brain Barrier

Penetration of hydrophilic or lipophilic compounds (MW > 500 daltons) into the central nervous systems (CNS) is strictly regulated by the presence of the blood-brain barrier (BBB). The active drug efflux transporters of the ATP-binding cassette (ABC) gene family expressed at the BBB are increasingly recognized as key determinants of drug distribution to and elimination from the CNS [Abbott et al., 2010]. Permeability-glycoprotein (P-gp) with its high expression

and wide substrate selectivity (e.g., endogenous compounds and > 30% of the approved drugs) is considered the most important efflux drug transporter at the BBB [Sun et al., 2003].

The functional importance of P-gp at the BBB was first confirmed in both P-gp chemical inhibition and knockout studies performed in rodents, where P-gp activity ablation resulted in drastic increase in the CNS distribution of P-gp substrates (7-36 fold increase for protease inhibitors: nelfinavir, indinavir, saquinavir; 6-28 fold for anticancer drugs: taxanes, paclitaxel, and docetaxel; 8.5-10 fold for digoxin and verapamil) [Kim et al., 1998; Kemper et al., 2003; Kemper et al., 2004a; Kemper et al., 2004b]. Direct evidence of P-gp's importance at the **human BBB** was demonstrated through Positron Emission Tomography (PET) imaging, where the brain uptake of P-gp specific radiolabeled substrate, ^{11}C-verapamil, was modestly increased by 88% in the presence of P-gp inhibitors, cyclosporine-A (CsA) [Sasongko et al., 2005].

Therefore, DDIs mediated by P-gp at the human BBB are possible due to inhibition or induction of P-gp, and potentially have several clinically significant consequences. Chemical inhibition of P-gp can be utilized to circumvent the BBB P-gp to increase the CNS delivery of chemotherapeutics, anti-HIV protease inhibitors, and antiepileptic drugs, to improve the efficacy of their treatment for CNS disorders that is compromised due to P-gp active efflux at the BBB. [Loscher et al., 2005a] In contrast, induction of P-gp activity at the human BBB could be utilized to increase the BBB protection for the CNS against neurotoxins or non-CNS targeted P-gp substrate drugs. The linkage between reduced BBB P-gp expression and Alzheimer's disease (AD) and the implication of beta-amyloid (pathological peptide of AD) being effluxed out by P-gp, suggest that P-gp induction could be a novel therapeutic strategy to treat AD by increasing the clearance and decreasing the brain accumulation of beta-amyloid [Cirrito et al., 2005; Ohtsuki et al., 2010]. In addition to the efficacious DDIs that BBB P-gp modulation could

generate, inadvertent DDIs due to BBB P-gp inhibition or induction is also possible. Thus, there is a tremendous clinical and scientific need to better understand and investigate BBB P-gp inhibition and induction in humans.

Quantitative evaluation of P-gp activity and its modulation at the human BBB is not possible until the recent application of a non-invasive and sensitive PET imaging technique. P-gp inhibition at the human BBB has been studied via PET-imaging, and cyclosporine A (CsA) at supertherapeutic concentration showed significant, but modest P-gp inhibition [Sasongko et al., 2005]. This begs the question, whether potent P-gp inhibition at the human BBB can be achieved by using a FDA-approved drug at a clinically relevant concentration? Amongst the clinically approved drugs that can potently inhibit P-gp at clinically relevant concentrations, quinidine is the most promising in its potential to produce a significantly greater inhibition of P-gp at the human BBB than that previously obtained with CsA [Hsiao et al., 2008]. This is essential for translating the concept of P-gp inhibition into clinical usage to improve the treatment of CNS diseases (e.g., brain tumors, HIV dementia) [Linnet et al., 2008]. In addition, we have previously shown that pre-clinical animal models (e.g., rat) can successfully predict the CsA-verapamil DDI at the human BBB [Hsiao et al., 2006]. However, P-gp is known to contain multiple ligand binding sites, and species and inhibitor-dependent characteristics [Martin et al., 2000; Zolnerciks et al., 2011], thus confirmation studies with additional P-gp inhibitors (e.g., quinidine) are needed. Lastly, amongst the PET-imaging studies conducted so far to evaluate P-gp activity at the human BBB, controversy still remains regarding the preferred index (e.g., distribution clearance, efflux rate constant, or extraction ratio of radiolabeled P-gp PET tracer) that should be used to characterize BBB P-gp activity and modulation [Bauer et al., 2012; Kreisl et al., 2010; Bart et al., 2003; Lubberink et al., 2007]. Therefore, our goals (**chapter 4)** were to

quantify the P-gp inhibition at the human BBB by quinidine in healthy human volunteers using PET-imaging and ^{11}C-verapamil; to evaluate the prediction of quinidine-verapamil BBB P-gp mediated DDI from experimental models (e.g., rat and macaque), and finally, to propose an optimal index for evaluating P-gp activity and its modulation at the human BBB. Conversely, P-gp induction at the human BBB has never been evaluated, thus we conducted an additional healthy human volunteer PET-imaging study (**chapter 5)** to evaluate whether P-gp at the human BBB can be induced by a FDA-approved drug, rifampin, a potent and positive control inducer of P-gp.

1.B1 Hypothesis

P-gp is functionally significant at the human BBB. Modulation of its activity via inhibition or induction will lead to significant changes in the brain penetration of its model substrate, ^{11}C-verapamil, a P-gp selective PET tracer and experimental surrogate for other CNS drugs and neurotoxins transported by P-gp.

1.B2 Specific Aims

Aim B1 Chapter 4: Quinidine inhibition of P-glycoprotein at the Human Blood-Brain Barrier as Measured by Positron Emission Tomography Imaging

Sub Aim B1.1: To quantify the magnitude of P-gp inhibition at the human BBB by a model P-gp inhibitor, quinidine, in healthy human volunteers, using PET imaging analysis and P-gp radiolabeled substrate, ^{11}C-verapamil.

Sub Aim B1.2: To predict quinidine-^{11}C-verapamil P-gp mediated DDI at the human BBB using a combination of preclinical experimental models (rat and macaque) and *in vitro* MDR1 over-expressing cells.

Sub Aim B1.3: To confirm that the best index for quantifying P-gp activity and modulation at the human BBB is the cerebral blood flow (CBF)-normalized distribution clearance (ER) of ^{11}C-verapamil.

Aim B2 Chapter 5: Can P-glycoprotein at the Human Blood-Brain Barrier be Induced by Rifampin? A PET Imaging Study

Sub Aim B2.1: To quantify the magnitude of P-gp induction at the human BBB by a model P-gp inducer, rifampin, in healthy human volunteers, using PET imaging analysis and P-gp radiolabeled substrate, ^{11}C-verapamil.

1.B3 Human Blood-Brain Barrier

In the brain and spinal cord of mammals, all well-developed CNS have a BBB that regulates and protects the microenvironment of the brain. The BBB is formed by a monolayer of brain capillary endothelial cells with tight junctions in between, no fenestrae and little pinocytotic vesicular activities [Pardridge et al., 1999]. These endothelial cells are surrounded

and the BBB is further strengthened by an extracellular matrix (basal membrane), pericytes, and astrocyte foot processes (Figure 1.B1) [Loscher et al., 2005b]. The physiological properties of the BBB provide an extremely efficient physical barrier for the brain [Pardridge et al., 1999]. However, the BBB has an additional dynamic layer with the expression of numerous membrane transporters involved in the influx or efflux of various essential substrates (e.g., amino acids, glucose, electrolytes, nucleosides; Figure 1.B2A), and xenobiotics (Figure 1.B2B) [Lee et al., 2001]. In addition to this transporter barrier, the BBB also exhibits a metabolic barrier by expressing enzymes that metabolize molecules in transit through the endothelial cells [Abott et al., 2010]. The synergy between the physical, transporter and metabolic barriers at the BBB has led many to propose the delivery of drugs to the CNS as one of the final frontiers of pharmacotherapy [Miller et al., 2010].

1.B4 P-gp

P-gp (multidrug resistance protein, MDR1) was the first ABC transporter that was detected in the endothelial cells of the human BBB [Cordon-Cardo et al., 1989; Thiebaut et al., 1989]. P-gp is expressed on the luminal side of the brain capillary endothelium [Beaulieu et al., 1997]. This 170 kDa membrane-bound efflux pump is known to exhibit a broad polyspecificity for hundreds of compounds (mostly hydrophobic) ranging from 330 to 4000 daltons [Aller et al., 2009]. Due to its high expression and wide substrate selectivity, P-gp is considered the most important efflux drug transporter at the BBB. Recent X-ray crystallography confirmed that P-gp exhibits multiple and overlapping binding sites, supporting the cooperative binding or allosterism that has been previously proposed [Martin et al., 1999; Aller et al., 2009]. Despite P-gp's ability

to transport numerous endogenous substrates (e.g., beta-amyloid, steroids, lipids and peptides), the endogenous function of P-gp is not fully understood [Kim et al., 2002]. The hydrophobic "vacuum cleaner" (extracts substrates from the lipid bilayer and pumps them out of the cell) and flippase (scans and binds to substrates prior to their extrusion by "flipping" the phospholipids from the inner to outer leaflets of the lipid bilayer) models have both been propose to described P-gp mediated drug efflux [Losher et al., 2005a]. Both mechanisms are not mutually exclusive and a combination of both can occur.

1.B4.1 P-gp Substrates Drugs and Modulators

P-gp's polyspecificity extends to numerous drugs (Table 1.B1). A list of known P-gp modulators (inhibitors and inducers) is provided in Table 1.B1. Detailed pharmacokinetics parameters of verapamil, quinidine and rifampin are provided in Table 1.B2, as these three drugs were used in our human PET-imaging studies.

1.B5 Regulation of P-gp

Xenobiotics, stress and disease can act through various and specific signaling pathways to alter the expression P-gp [Miller et al., 2010]. We have the most complete understanding on the transcriptional regulation of P-gp. Xenobiotics (drugs and environmental toxins) can bind directly to ligand-activated transcription factors (pregnane X receptor, PXR; constitutive androstane receptor, CAR; glucocorticoid receptor, GR; vitamin D receptor, VDR; farnesoid X receptor, FXR) to increase P-gp expression [Reschly et al., 2006; Aiba et al., 2005; Martin et al., 2008]. However, most of the evidence for P-gp induction were done primarily in cell lines (e.g.,

caco-2, hepG2), and studies on p-gp induction at the BBB remain limited and were primarily conducted in preclinical rodent models. In fact, it is unclear and controversial whether these nuclear receptors are even expressed in the human BBB endothelial cells [Dauchy et al., 2008]. In addition, the transcription factor Nf-κB has been implicated to mediate the effects of three signaling pathways: 1) proinflammatory signaling (e.g., TNF-α, ET-1), 2) HIV-Tat protein signaling (RhoA, Rac, and myosin light chain kinase), and 3) seizure-induced signaling (COX-2) [Miller et al., 2010]. It is important to note that these signaling pathways are not P-gp selective, and can also affect protein expression of other ABC transporters and enzymes at the BBB [Miller et al., 2010].

1.B6 P-gp and CNS Diseases

Due to P-gp's polyspecificity toward a wide range of therapeutic agents, P-gp is commonly recognized at an obstacle in the treatment of many CNS disorders. Altered P-gp expression has also been linked to various CNS diseases. For example, P-gp expression is reduced in Alzheimer's disease (AD), Creutzfeldt-Jakob disease, Parkinson's disease, HIV infection, and normal aging [Loscher et al., 2005a]. For AD, recent findings suggest that P-gp at the human BBB may be involved in the reduced beta-amyloid efflux and clearance from the brain, thereby increasing the brain accumulation of this pathological peptide that is the hallmark of AD [Cirrito et al., 2005; Ohtsuki et al., 2010]. Conversely, increased P-gp expression is associated with other CNS disorders (e.g., epileptic seizures, depression) [Eyal et al., 2009]. Increasing evidence connects P-gp overexpression with pharmacoresistance in antiepileptic drugs, which have also been identified as P-gp inducers [Linnet et al., 2008]. Better

understanding of the linkage between P-gp expression and CNS diseases could better provide additional insights in developing novel and innovative therapy for such CNS disorders via modulation of P-gp at the human BBB.

1.B7 P-gp Mediated CNS DDIs

DDIs mediated by P-gp at the BBB are possible due to inhibition or induction of P-gp. Table 1.B1 lists known P-gp inhibitors and inducers. The majority of the studies evaluating P-gp mediated DDIs are conducted using mice devoid of functional P-gp. These studies have helped demonstrate that P-gp at the BBB can exert profound effect on CNS delivery of numerous therapeutic agents (e.g., cardiovascular drugs, opioids, HIV protease inhibitors, chemotherapeutics) [Loscher et al., 2005a]. While P-gp is undoubtedly functionally important, clinical observation suggesting a role for P-gp in relation to DDI at the BBB is sparse, and further studies are need to draw a definite conclusion regarding P-gp's clinical significance at the human BBB [Linnet et al., 2008]. However, current observations do suggest the potential risk of neurotoxicity when potent inhibitors are co-administered. A good representative example is the study by Sadesque et al. (2000), which showed that after co-administering quinidine with the antidiarrheal agent loperamide, serious respiratory depression associated with loperamide was observed in the healthy volunteers. It is believed that P-gp at the human BBB was potently inhibited by quinidine, therefore allowing the CNS penetration of loperamide, a peripheral opioid and P-gp substrate that is normally effluxed out by P-gp and does not across the BBB. However this DDI is controversial as it could not be reproduced by other groups [Vandenbossche et al., 2010]. This is further complicated by the finding from a separate study that showed

coadministering a similar dose of quinidine did not enhance the CNS effects of morphine [Sharke et al, 2003]. Other less well-documented P-gp mediated CNS DDIs have also been reported, such as the interaction between colchicine and verapamil, where this combination resulted in enhanced neurotoxicity of colchicine in the form of tetraparesis [Troger et al., 2005].

1.B7.1 Prediction of P-gp Mediated CNS DDIs

In drug development, rodents are frequently used as experimental models in preclinical studies to screen and evaluate candidate drug distribution into the CNS, particularly those that have been identified as P-gp substrates. Extrapolation from rodents to humans regarding the brain penetration of P-gp substrate candidate drugs is based on the assumption that P-gp activity as well as other characteristics of the human BBB are well-represented by those of the rodent BBB. These same assumptions have also been applied to the prediction of P-gp mediated DDIs at the human BBB. Using rodent models, we were able to successfully predict CsA's inhibition on the BBB P-gp mediated transport of ^{11}C-verapamil observed in our human PET study [Hsiao et al., 2006; Sasongko et al., 2005]. However, this needs to be confirmed with another substrate-inhibitor pair. This is especially important given that species-dependent differences have been reported between the P-gp expression at human and rodent BBB [Shawahna et al., 2011; Ito et al., 2011]. In addition, rodent cerebral blood flow (CBF) is reportedly twice that in humans [Yuen et al., 2008].

1.B8 PET Imaging of P-gp Activity at the Human BBB

Numerous experimental and diagnostic tools have been developed and applied to study P-gp mediated efflux transport in the brain, however, PET-imaging is the only available non-invasive and quantitative tool that enables the evaluation of P-gp function and modulation at the BBB in real-time in humans [Elsinga et al., 2004]. Several radiopharmaceuticals (e.g., ^{11}C-verapamil, ^{11}C-colchicine, ^{11}C-daunorubicin, ^{11}C-N-desmethyloperamide, ^{11}C-tariquidar) have been evaluated for the quantification of P-gp mediated transport by PET [Elsinga et al., 2004]. Amongst the PET tracers used for evaluating P-gp activity at the human BBB, ^{11}C-verapamil exhibits the most optimal overall characteristics in its specificity towards P-gp and sufficient brain uptake to evaluate P-gp inhibition or induction at the human BBB.

1.B8.1 P-gp PET Tracer: ^{11}C-verapamil

The applicability of ^{11}C-verapamil as a P-gp PET tracer has been extensively studied in several experimental setups, [Elsinga et al., 1996; Hendrikse et al., 1998] and its human use was first validated by Sasongko et al. (2005). Verapamil is an excellent P-gp substrate (well established, approved for human IV administration and relatively safe) [Unadkat et al., 2008]. However, as a PET-tracer, it suffers from a drawback in that it undergoes extensive hepatic metabolism, mediated by CYP3A4 and CYP2C enzymes [Tracy et al., 1999]. Therefore, when conducting PET studies, it is extremely important to limit the extent of ^{11}C-verapamil metabolism by conducting PET-imaging studies in short durations, and also quantify the ^{11}C-radioactivity content in the plasma to account for radioactivity contributed by verapamil metabolites using validated methods that allow real-time metabolite separation and analysis [Unadkat et al., 2008]. The metabolic scheme of ^{11}C-verapamil is illustrated in Figure 1.B3. The ^{11}C-N-dealkylated and ^{11}C-O-demethylated metabolites (not detectable in human

circulations) of verapamil formed by CYP2Cs enzymes have been shown to be P-gp substrates [Tracy et al., 1999; Pauli-Magnus et al., 2000]. Based on rodent data, the ^{11}C-polar metabolites formed by CYP3A4 are composed of mostly ^{11}C-formaldehyde and other small polar molecules, which are believed to diffuse freely across the BBB [Luurtsema et al., 2005]. The ^{11}C-metabolites in the brain are likely derived systemically, since CYP3As and CYP2Cs have been reported to be undetectable in the human brain microvessel endothelial cells, and the overall CYP content in the human brain is low, ~1-5% of that in the liver [Shawahna et al., 2011].

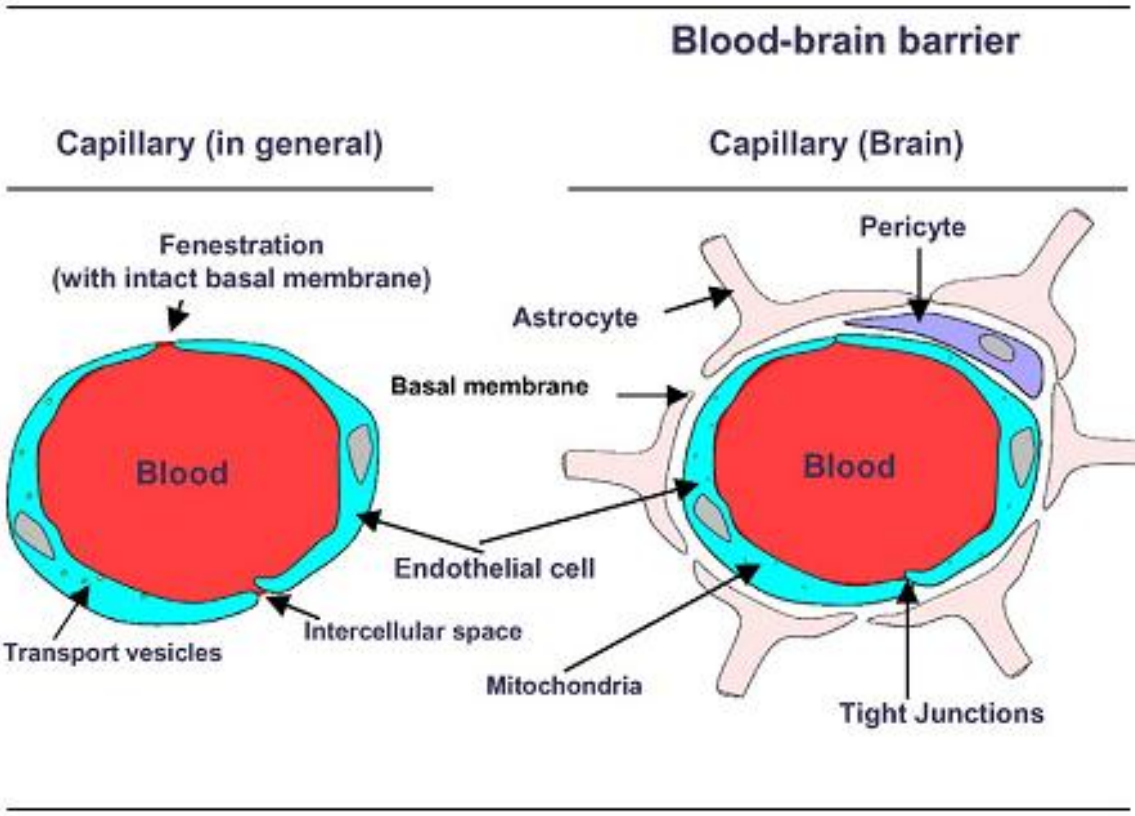

Figure 1.B1: Illustration of a brain capillary compared with a periphery capillary [Loscher et al., 2005a].

A)

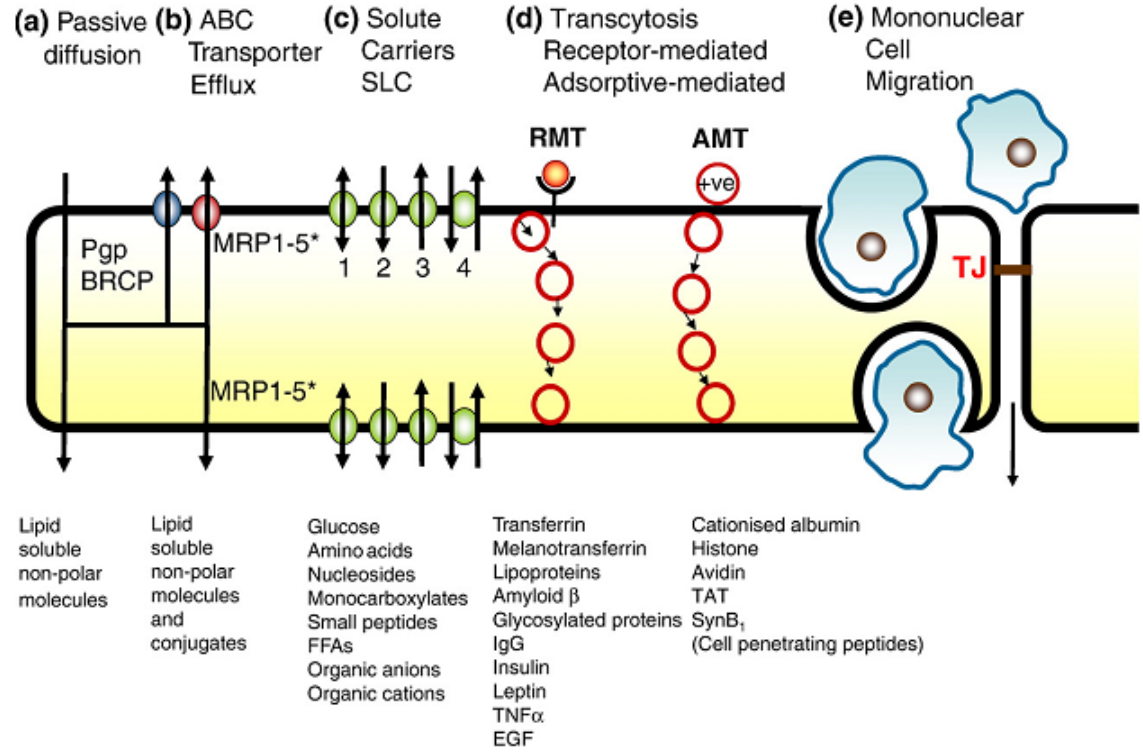

B)

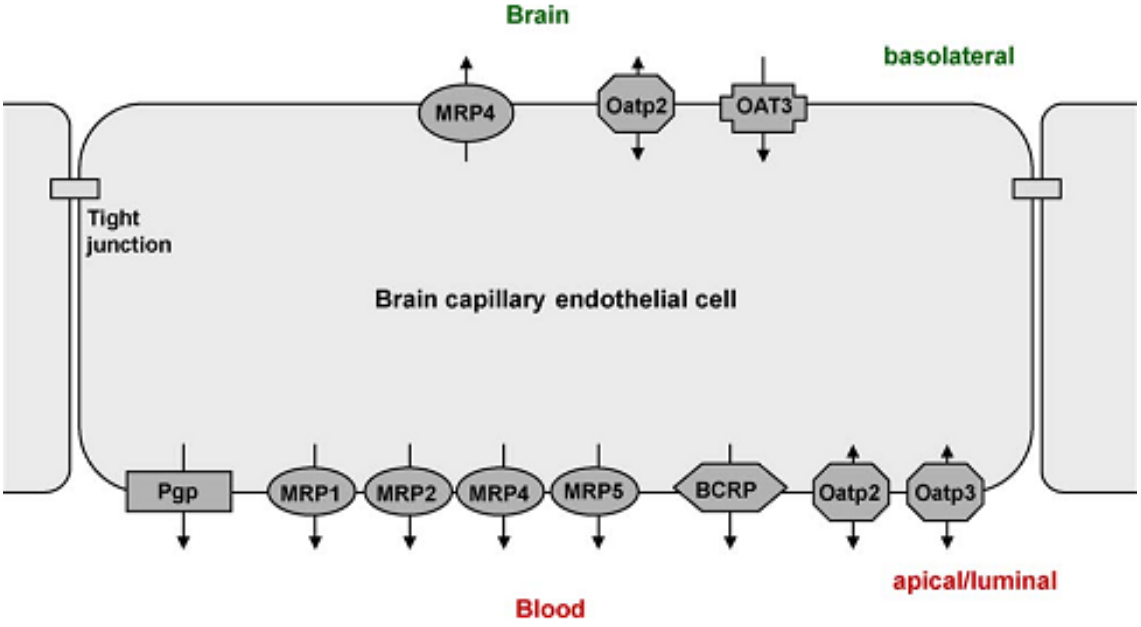

Figure 1.B2: A) Routes of transport across, and B) Drug transporters on the brain capillary endothelial cells that form the BBB [Abbott et al., 2010; Loscher et al., 2005a].

Table 1.B1: P-gp Substrate Drugs, Inhibitors and Inducers [Elsinga et al., 2004; Kim et al., 2002]

Substrates	Inhibitors	Inducers
Analgesics: Asimadoline, Morphine	**Quinidine**	**Rifampin**
Anticonvulsants: Carbamazepine, Felbamate, Lamotrigine, Phenobarbital, Phenytoin	Atorvastatin	Dexamethasone
Antidepressants: Amitriptyline, Nortriptilyne	Bromocriptine	St John's wort
Antiemetics: Domperidone, Ondansetron, Ramosetron	Carvedilol	Clotrimazole
Antibacterial agents	Cyclosprine-A	Morphine
Antifungal agents: Itraconazole	Erythromycin	Phenothiazine
Antihistamines: Cetrizine	GF120918, Elacridar	Retinoic acid
Beta-blockers: Bunitrolol, Carazolol, Carvedilol	Itraconazole	Amprenavir
Ca^{2+} channel blockers: Verapamil, Loperamide	Ketoconazole	Indinavir
Cardiac glycosides: Digoxin	LY335979, Zosuquidar	Saquinavir
Cytotoxic agents: Paclitaxel, Vinblastine	Meperidine	Ritonavir
HIV protease inhibitors	Methadone	Indinavir
Immunosuppressive drugs: Cyclosporin-A	Nelfinavir	
Neurokinin antagonists	Ritonavir	
Pesticides: Ivermectin	Saquinavir	
Sigma ligands: Pentazocine	Pentazocine	
Steroids	Progesterone	
	Tamoxifen	
	PSC-833, Valspodar	
	Verapamil	

Tyrosine kinase inhibitors

Table 1.B2: Pharmacokinetic parameters for drugs used in human PET studies [Goodman & Gilman, 10th ed.]

Drug Name	MW	Oral Bioavailability	Plasma Protein Binding	Clearance (mL/min/kg)	Volume of Distribution (L/kg)	Half-life (hr)
Verapamil	**454.6**	**23%**	**90%**	**15**	**5**	**4**
Quinidine	**324.4**	**71-80%**	**87%**	**4.7**	**2.7**	**6**
Rifampin	**822.9**	**90%**	**60-90%**	**3.5**	**1**	**3.5**

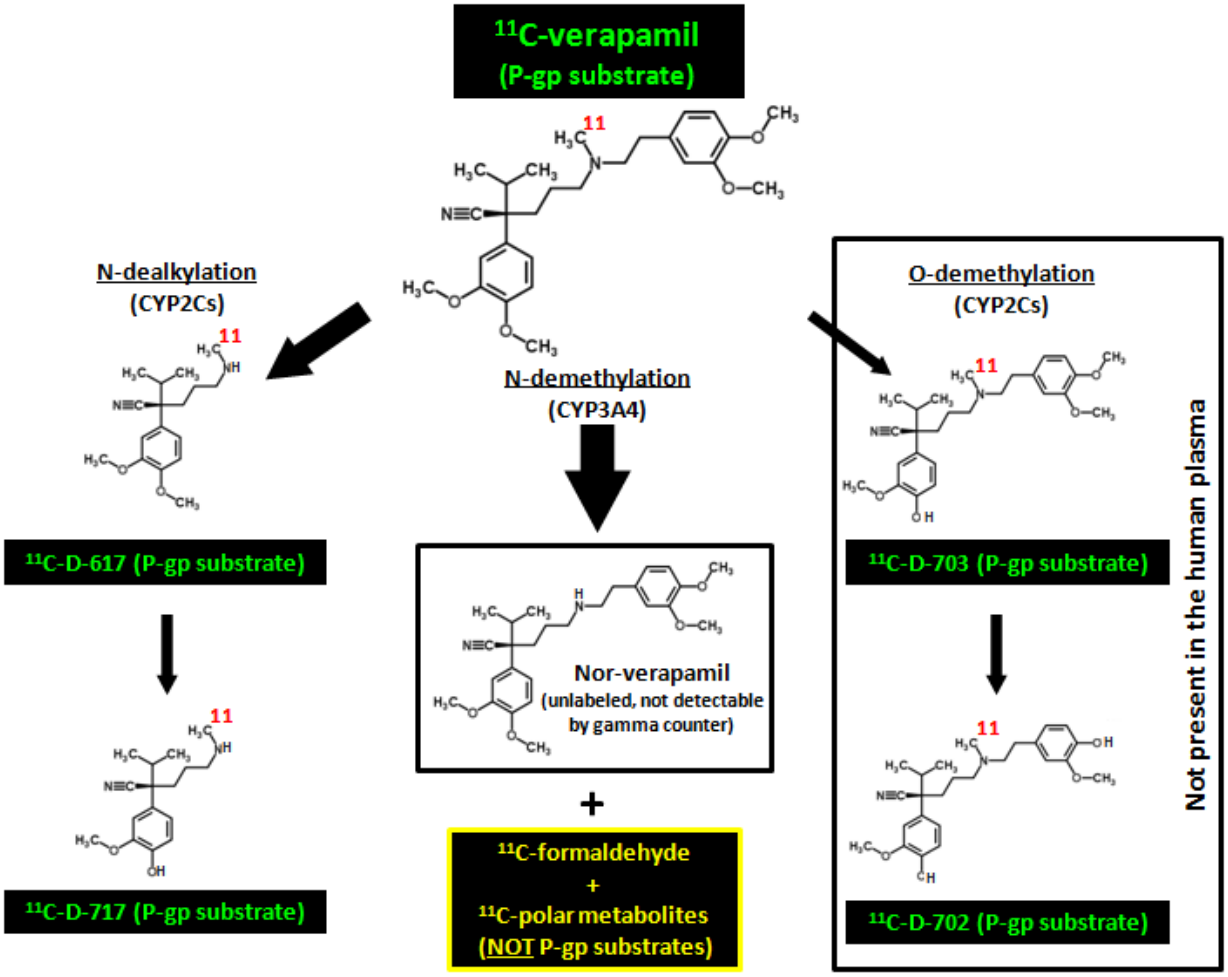

Figure 1.B3: Metabolic pathway of verapamil. In humans, only verapamil, D-617 and the polar metabolites (identity unknown) were detectable [modified from Unadkat et al., 2008].

1.C Introduction Summary

As described previously, DDIs with the HIV protease inhibitors are complex and in much need of further investigation. Our proposed studies in **Chapters 2 and 3** to better characterize the PIs' net induction potential for and interaction with the hepatic enzymes and transporters using a most *in-vivo* like *in vitro* model (human hepatocytes), will provide an improved mechanistic understanding that are essential in explaining and predicting the PI-based DDIs. In addition, the novel experimental techniques (e.g., CYP activity cocktail assays) that we have established and validated will also be of great value for future applications using human hepatocytes or liver microsomes.

In addition, as elaborated in section 1.B, P-gp is functionally important at the human BBB, and its DDIs could have both beneficial and adverse clinical CNS consequences. Quantifying P-gp modulation (inhibition and induction) at the human BBB using PET-imaging enables us to evaluate open questions that have long been asked, but unanswered. Our proposed studies in **chapter 4 and 5** to evaluate whether 1) more potent P-gp inhibition at the human BBB can be achieved by quinidine at its clinically relevant concentrations; 2) this level of P-gp inhibition can be accurately predicted using preclinical data; and 3) P-gp at the human BBB can be induced by a FDA-approved and potent P-gp inducer, rifampin, are pivotal in determining the clinical significance of P-gp in mediating CNS DDIs, and in evaluating the potential of modulating BBB P-gp activity as innovative therapeutic strategies for the treatment of CNS diseases that have unmet medical needs.

Chapter 2: Quantification of Human Hepatocyte Cytochrome P450 Enzymes and Transporters Induced by HIV Protease Inhibitors Using Newly Validated LC-MS/MS Cocktail Assays and RT-PCR

The data presented in this chapter has been previously published by the journal - Biopharmaceutics and Drug Disposition 33:207-217, 2012.

2.1 Abstract

HIV protease inhibitors (PIs) produce profound and unpredictable drug-drug interactions (DDIs) that cannot be fully explained by their inhibition/inactivation of CYP3A enzymes. Delineating and quantifying the CYPs and transporters inducible by PIs are crucial in developing an integrative mechanistic understanding and prediction of PI-based DDIs. To do so, we modified and validated two LC-MS/MS cocktail assays to simultaneously quantify the CYP activity of CYP3A, 2B6, 2C8, 2C9, 2C19, 1A, 2E1, 2A6 and 2D6 enzymes. We applied these new assays to evaluate the induction potential of eight PIs in microsomes isolated from PI-treated human hepatocytes. The mRNA expression of these CYPs and transporters (OATP1B1, OATP1B3, OATP1A2, MDR1, MRP2, and MRP4) was also evaluated using relative RT-PCR. The majority of PIs were net inducers of CYP3As and 2B6 at both the mRNA and activity level (> 2-fold), while ritonavir, saquinavir, nelfinavir, or lopinavir did not induce CYP3A activity (< 2-fold) presumably due to CYP3A inactivation. OATP1B1 and MDR1 were the only two hepatic transporters induced (> 2-fold) by the PIs. Amprenavir was the most potent net inducer.

In conclusion, our validated cocktail assays can be implemented to comprehensively quantify CYP activities in human liver microsomes and hepatocyte studies. Our results also provide the much needed data on the net induction potential of the PIs for hepatic CYPs and transporters. A qualitative agreement was observed between our results and published PI-based DDIs, suggesting that human hepatocytes are a useful platform for more extensive and quantitative *in vitro-in vivo* prediction of PI-based DDIs.

2.2 Introduction

As one of the six major classes of human immunodeficiency virus (HIV) medications, protease inhibitors (PIs) continue to serve as a crucial component in Highly Active Antiretroviral Therapy (HAART). However, their propensity to produce clinically deleterious drug-drug interactions (DDIs), resulting in either significantly increased or decreased plasma concentration of the coadministered drugs, greatly complicates their usage in HIV/AIDS poly-therapy. Adding an additional level of complexity is that many of the PI-based DDIs are unpredictable and paradoxical that cannot be entirely explained by many PIs' potent capacity to inhibit or inactivate (mechanism-based inactivator, MBI) CYP3A enzymes [Unadkat and Wang 2000]. For example, ritonavir (RTV) and amprenavir (APV) have both been shown to be equipotent inactivators of CYP3A enzymes [Earnest et al., 2005], yet their effect on saquinavir's (SQV, primarily metabolized by CYP3As) area under the plasma concentration-time profile (AUC) are dramatically different, resulting in >2000% increase or ~19% decrease after chronic administrations of RTV or APV, respectively [Buss et al., 2001; Boffito et al., 2004]. Thus, other contributing mechanisms have been proposed, such as the PIs' ability to inhibit and/or

induce various CYPs other than CYP3A and transporters (e.g., P-gp, MRP2, BCRP, and OATPs) [Kirby et al., 2011a]. Since PIs are capable of eliciting multifaceted precipitant effects through a complex balance of inhibition, inactivation and/or induction of the CYPs and transporters, it is important to evaluate and characterize the relative importance of PIs' induction potential in the presence of other concurrent DDI mechanisms (e.g., CYP and transporter inhibition) using a physiologically relevant *in vitro* system such as human hepatocytes.

We have extensively characterized the net induction potential of RTV and nelfinavir (NFV) in human hepatocytes. Both PIs produced net induction of CYP2B6, 2C8, and 2C9 mRNA transcripts and activity, but reduced CYP3A activity via inactivation [Dixit et al., 2007a]. But, the ability of other PIs to induce CYPs and transporters is not known. This gap in knowledge continues to limit our ability to fully understand and accurately predict many of the PI-based DDIs. Therefore, the goals of this investigation were: 1) to validate two cocktail assays that can simultaneously quantify the activity of nine CYP enzymes using CYP probe substrates via LC-MS/MS; 2) to apply these assays to quantify in the net induction potential of eight PIs for the major hepatic CYP enzymes (CYP3As, 2B6, 2C8, 2C9, 2C19, 1As, 2A6, 2E1, and 2D6) in microsomes isolated from PI-treated human hepatocytes; and 3) to quantify the mRNA induction of these CYP enzymes and transporters (OATP1B1, OATP1B3, OATP1A2, MDR1, MRP2, and MRP4) by these PIs in human hepatocytes.

2.3 Materials and Methods

2.3.1 Cocktail Assay Development and Validation

2.3.1.1 Chemicals

All PIs used in this study were obtained from the National Institutes of Health AIDS Research and Reference Reagent Program, with the exception of darunavir, which was not available. Acetaminophen, tolbutamide, dextromethorphan, testosterone, phenacetin, bupropion, omeprazole, 7-hydroxycoumarin, and nicotinamine adenine diphosphate (NADPH) were purchased from Sigma-Aldrich (St Louis, MO). Hydroxy-bupropion, dextrorphan, 4-hydroxytolbutamide and desethylamodiaquine were purchased from GenTest (Woburn, MA). Hydroxyomeprazole was a gift from AstraZeneca (Molndal, Sweden). 6-β-hydroxytestosterone was purchased from Steraloids Inc (Newport, RI). Coumarin, 7-hydroxycoumarin and chlorzoxazone were purchased from Sigma-Aldrich (St Louis, MO). 6-hydroxychlorzoxazone was a generous gift from Dr. Kenneth Thummel (Department of Pharmaceutics, University of Washington). D5-diazepam was purchased from Cerilliant (Round Rock, TX). HPLC grade solvents (methanol, acetonitrile and water) were purchased from Fisher Scientific. All other chemicals were purchased from Sigma Chemical Company (St Louis, MO) or Fisher Scientific (Pittsburg, PA) and were of the highest purity available.

2.3.1.2 Validation Assays (human live microsomal incubations)

Microsomes were isolated from livers in the University of Washington (UW) School of Pharmacy Human Liver Bank. These tissues were procured and stored as described previously [Paine et al., 1997]. Activity of CYP3As, 2B6, 2C8, 2C9, 2C19, 1As, 2E1, 2A6, and 2D6 enzymes in isolated human liver microsomes (HLM, n=3 livers) was evaluated using specific CYP substrates divided into two cocktails and based on those recommended by the Food and Drug Administration (FDA) [FDA DDI guidance]. Solutions of CYP substrates were made in

water (bupropion, amodiaquine, dextromethorphan, coumarin), methanol (testosterone, tolbutamide, omeprazole, chlorzoxazone) or ethanol (phenacetin). Standard stock mixture of cocktail 1 or cocktail 2 substrates were prepared, and diluted in microsomal incubations to final concentrations listed in Table 2.1, and with the final concentration of all organic solvents at 1%. Microsomal incubation protocol and conditions followed closely to those established in Dixit et al, 2007a and 2007b [Dixit et al., 2007b; 2007a]. Briefly, HLM (0.1 mg/mL) were pre-incubated for 5 min in a 37°C shaking water bath with either a single CYP substrate or a cocktail of substrates in a total volume of 100 µL containing 5 mM MgCl2, 0.1 M phosphate buffer (pH 7.4). Reactions were initiated with 1 mM NADPH and incubated for an additional 30 min, and then stopped by adding 100 µL of ice-cold acetonitrile containing internal standard, D5-diazepam. The incubate was then centrifuged for 10 min at 13000 g, and the supernatant was extracted, vacuum dried, and reconstituted in 100 µL of 10% acetonitrile and 0.1% formic acid in water (initial HPLC elution gradient condition). Until analysis, samples were stored at 4°C, and 20 µL were injected onto LC-MS/MS. All microsomal incubations were performed in duplicates.

2.3.1.3 Calibrations and Quality Controls

Two separate (e.g., independent weighing) standard metabolite mixtures of probes for cocktail 1 (6-OH-testosterone, 4-OH-tolbutamide, acetaminophen, dextrorphan, and 7-OH-coumarin), or cocktail 2 (OH-bupropion, n-desmethylamodiaquine, 5-OH-omeprazole, and 6-OH-chlorzoxazone) were prepared, and used to prepare ten calibrators and four quality controls (QCs). Both the calibrators and QCs contained the same components as for incubations, 0.1 mg/mL HLM, 5 mM $MgCl_2$, and 0.1 M phosphate buffer (pH 7.4). The calibrators or QCs were

incubated along with the microsomal incubations at 37°C for 30 min without NADPH, followed by addition of 100 µL of ice-cold acetonitrile containing NADPH and D5-diazepam, and were subsequently processed and reconstituted in 100 µL of 10% acetonitrile and 0.1% formic acid water. The calibrator or QC concentrations ranged as the following, 7-OH-coumarin, n-desmethylamodiaquine, dextrorphan: 0.025-8 µM or 0.05-6.4 µM; acetaminophen, 6-OH-chlorzoxazone, 5-OH-omeprazole: 0.125-80 µM or 0.625-80 µM; 6-OH-testosterone, OH-bupropion: 0.625-160 µM or 1.25-160 µM; 4-OH-tolbutamide: 1.25-320 µM or 2.5-320 µM, respectively.

2.3.1.4 Analytical Instrumentation

CYP probe metabolites were analyzed using LC-MS/MS. All instruments and conditions are specified in Table 2.1. For all assays, HPLC separation was achieved using Agilent XDB C18 2.1x150 mm, 5 µm column, and compounds were eluted with 0.25 mL/min of 0.1% formic acid in water (solvent A) and 0.1% formic acid in acetonitrile (solvent B) using the following gradient. For the first 1.5 min, 90% solvent A, then a linear decrease to 70% solvent A until 4 min. The gradient was maintained at 70% A until 6 min followed by linear decrease to 25% solvent A until 9 min. The gradient was held at 25% solvent A until 13 min to wash out substrates and then cycled back to initial conditions. The column was re-equilibrated for 4 min before injecting the following sample.

2.3.2 Human Hepatocyte Induction Study

2.3.2.1 Induction Study Design and Sample Preparation

Primary cultures of human hepatocytes from five different donors (Table 2.2) were provided by the Liver Tissue Procurement and Distribution System (Pittsburgh, PA) in collagen-coated 6-well plates (1 x 10^6 cells/well), 24 well plates, and T-25 cm^2 flasks formats. Hepatocytes were maintained in Williams's E medium (BioWhittaker; Walkersville, MD), as described previously [Desai et al., 2002]. Stock drug solutions were prepared in DMSO and β-cyclodextrin (0.05%). 72 h induction studies were performed, with media containing test compounds and 0.2% DMSO changed every 24 h. All the PIs and rifampin (RIF; positive control) were incubated with the hepatocytes at 10 µM, with the exception of NFV and tipranavir (TPV), where the concentrations were reduced to 1 µM due to cell toxicity observed at 10 µM. At the end of 72 h, the cells were incubated in drug-free medium for 3 h to wash out residual PIs and RIF. Viability of the cells was determined using 3-[4, 5-dimethylthiazol-2-y] 2, 5-diphenyl-tetrazolium bromide (MTT) assay, as per the manufacturer's instructions. Microsomes were prepared from treated hepatocytes, as described previously [Dixit et al., 2007b]. Total cellular RNA was isolated using TRIzol reagent according to the manufacturer's protocol (Invitrogen, Carlsbad, CA).

2.3.2.2 CYP Activity Determination (Isolated Human Hepatocyte Microsomal Incubations)

Activity of CYP3A, 2B6, 2C8, 2C9, 2C19, 1A, 2E1, 2A6, and 2D6 enzymes was determined in isolated hepatocyte microsomes (0.1 mg/mL) following the procedures described above for the cocktail validation assays using HLM.

2.3.2.3 Relative mRNA Expression Quantification

Changes in the mRNA levels of CYP enzymes (CYP3A4, 3A5, 2B6, 2C8, 2C9, 2C19, 1A1, 1A2, 2A6, 2E1, and 2D6) and transporters (OATP1B1, OATP1B3, OATP1A2, MDR1, MRP2, and MRP4) in human hepatocytes produced by the PIs and RIF were quantified by real-time quantitative PCR (qPCR) as previously described [Dixit et al., 2007a].

2.3.3 Statistical and Data Analysis

CYP (mRNA and activity) and transporter (mRNA) induction levels in the treated groups were expressed relative to those observed in the vehicle control. Due to significant inter-individual variability known to be associated with human hepatocytes [11], we defined, as per usual practice, our primary index for significant induction as greater than 2 fold-change in mRNA and activity level relative to that of the vehicle control [Dixit et al., 2007a; Fahmi et al., 2010]. In addition, we also performed a paired two-tailed Student's T-test as a secondary index to evaluate if drug treatments significantly altered CYP and transporter transcript expression and CYP activity. Lastly, as per the FDA DDI draft guidelines, CYP3A induction by the PIs was expressed relative to that obtained by the positive control treatment of 10 μM RIF.

2.4 Results

2.4.1 Cocktail Assay Validation

We previously showed that amodiaquine (CYP2C8 substrate) inhibits dextromethorphan (CYP2D6 substrate) metabolism by 40%. For that reason, we separated these two probes into two cocktails [FDA DDI guidance]. In this study, these two cocktail assays were regrouped and further validated to incorporate probe for CYP2E1 or CYP2A6. The new probe concentrations and cocktail combinations were selected based on those that generated the least amount of interactions between probes (<15%), without compromising detection sensitivity and metabolite formation (Figure 2.1). A new and more sensitive LC-MS/MS method was also developed to allow the use of lower amount of hepatocyte microsomal proteins (0.10 mg/mL). Together, these results confirmed that the DDIs between probes in the cocktail assays were minimal and statistically insignificant (p-value > 0.05, Student's paired T-test), and allowed accurate quantification and analysis of the individual enzyme activity.

In addition, CYP activity determinations in both the cocktail validation assays and hepatocyte induction studies were performed using isolated microsomes from either human livers or primary hepatocytes after induction treatments. By isolating microsomes from hepatocytes, we further eliminated any residual PIs that may not be removed after the 3 h wash-out period at the end of the 72 h induction treatment. This is important given most of the PIs are known MBIs, and their presence could diminish the magnitude of induction. It is also important to note that by performing microsomal incubations, we removed potential complications from phase-II conjugation of the probe metabolites and/or transport of the probe substrates or metabolites that could be present in in-cell incubations.

2.4.2 Induction of CYP mRNA Expression and Activity by the PIs

Except for NFV or TPV, no toxicity was observed in the hepatocytes after they were incubated for 72 h with the PIs at 10 μM, the incubation concentration of NFV or TPV was reduced to 1 μM.

Of the nine enzymes studied, > 2-fold induction was observed for CYP3As, 2B6, or 2C8 transcripts (Figure 2.2A). CYP3As demonstrated the highest magnitude of induction at the transcript level, with CYP3A4 mRNA expression (2-20 fold) being more inducible than that of CYP3A5 (2-4 fold). At the activity level, except for RTV, SQV, LPV, NFV or TPV, all PIs induced CYP3As (> 2-fold) (Figure 2.2B). In addition, following the recommendation from the FDA DDI draft guideline, we normalized the induction of CYP3A activity by the PIs with that produced by RIF, and found that 40%-79% of RIF fold-induction was observed for all PIs, except for RTV, SQV, TPV, or NFV (Figure 2.2C). CYP2B6 activity was induced by the greatest number of PIs. The magnitude of CYP2B6 activity induction ranged from 2-4 fold for all PIs except for TPV or IDV. Of the three CYP2C isoforms studied, CYP2C8 was the only one that demonstrated induction at both the mRNA and activity level by some PIs (APV and TPV), but of lesser magnitude compared to those observed for CYP3As and CYP2B6. CYP2C9 was induced at the mRNA level (~2-fold), but not at the activity level (< 2-fold). The remaining CYPs (CYP2C19, 2A6, 1As, 2D6, and 2E1) were not induced (< 2-fold, data not shown). Amongst the eight PIs tested, APV consistently ranked as the most potent inducer.

2.4.3 Induction of Transporter mRNA

For the hepatic transporters, only mRNA transcripts were evaluated (Figure 2.3). Of the transporters examined (OATP1B1, OATP1B3, OATP1A2, MDR1, MRP2, and MRP4), only

OATP1B1 and MDR1 were induced by the PIs (> 2-fold), and OATP1A2 was not detectable (data not shown). Except for ATV, all the PIs induced OATP1B1 (2-8 fold), and APV, RTV, or NFV induced MDR1. APV also ranked highest amongst the PIs in induction of the transporters.

2.5 Discussion and Conclusions

Validation assays are often not performed in previously published cocktail or n-in-1 assays, and when conducted, they mainly employed CYP inhibitors or monoclonal antibodies to confirm the lack of interactions between probes. However, such conclusions are highly dependent on the specificity of the inhibitors and antibodies used. The validations performed in this study directly compared the microsomal CYP activities measured from the two cocktail assays to those from individual probe incubations. Even though our investigation does not require a complete lack of interaction between probes within the two cocktails for our data analysis, since we are comparing the induced CYP activity relative to the control CYP activity based on metabolite formation, our validated assays were developed by selecting probe concentrations and cocktail combinations that generated minimum (<15%) and statistically insignificant interactions between probes (p-value > 0.05, Student's paired T-test). We did so using a lower amount of hepatocyte microsomal proteins (0.10 mg/mL), and without compromising metabolite formation and detection sensitivity. In addition to the validated cocktail assays, another advantage of our study design is that we utilized isolated microsomes to determine CYP activity. Doing so not only removed residual PIs that may be present to inactivate and diminish the CYP activity that we want to quantify, but also eliminated other factors that could confound the interpretation of our data using the cocktail assays, such as

phase-II metabolism of the probe metabolites, and/or transport of the probe substrates and/or metabolites.

This is the first investigation conducted to provide the most comprehensive net induction profiling of hepatic CYPs and transporters by the PIs using human hepatocytes. All PIs were studied at 10 μM except for NFV or TPV due to cell-toxicity observed. As summarized in Table 2.3, 10 μM was chosen to uniformly reflect the total C_{max} for all PIs at steady state (with or without RTV booster dose) after oral administration to healthy volunteers (5.94 – 21.02 μM), except for SQV (2.12 μM) and TPV (137.57 μM). The majority of the PIs produced net, but modest induction at both the mRNA and/or activity level of selective CYPs and transporters, with APV being the most potent. Consistent with our previously published data [Dixit et al., 2007a; Mugundu et al., 2010], RIF, RTV, or NFV produced net induction of CYP2B6 (2-5 fold) and CYP2C8 (~2-fold) activity. However, as potent CYP3A inactivator, RTV or NFV produced net decrease in CYP3A activity. It is not surprising that the mRNA induction of CYP3A by most of these PIs is greater than their ability to induce CYP3A activity, since many of these drugs with the exception of IDV, have been shown to be potent MBIs of CYP3As [Earnest et al., 2005]. However, whether TPV inactivates CYP3A enzymes is not known but our data would suggest that it does. For all other CYPs, little to no net induction at the activity level was observed. The modest level of induction was also observed for the hepatocyte transporters, in which only MDR1 and OATP1B1 transcript expressions were found to be inducible. Induction of transporter activity was not analyzed, but it is likely to be even lesser than the modest induction observed at the mRNA expression level. BCRP and OATP2B1 were previously studied to be not inducible by PIs [Dixit et al., 2007a], and therefore were not investigated further in this study.

APV has been shown to be one of the most potent CYP3A inactivator amongst the PIs, demonstrating potency that is comparable to that of RTV, and much greater than that of SQV, LPV, NFV or ATV in HLM [Earnest et al., 2005; www.accessdata.fda.gov]. Interestingly, our results showed that such ranking order is not reflected in the net CYP3A activity modulation produced by these PIs in hepatocytes, a system that enables us to quantify the net result of CYP3A induction and inactivation. While RTV's potency in inactivating CYP3A activity was reproduced in hepatocytes, APV was found to be the most potent net CYP3A activity inducer amongst the PIs, suggesting that significantly greater induction of CYP3A at the mRNA and protein level was likely achieved by APV to overcome its potent CYP3A inactivation. This is supported by our observed ~20 fold induction in CYP3A4 mRNA produced by APV, compared to ~4 fold induction produced by RTV. Therefore, if our hepatocyte results were reflective of the *in vivo* phenomenon, then we would expect chronic treatment of APV to produce modest net CYP3A induction that could lead to a net decrease or a lack of change in the AUC of the coadministered drugs that are predominantly eliminated via the CYP3A pathway, especially when compared to effects of other PIs (e.g., RTV). Indeed, this is observed clinically with a lack of change in clarithromycin AUC (primarily eliminated via CYP3As) after chronic treatment with APV, yet a significant increase (~77%) after chronic treatment with RTV [Brophy et al., 2000].

For other CYP enzymes, our *in vitro* results are in general agreement with the clinical PI-based DDIs. Drugs (e.g., methadone, bupropion, or loperamide) that demonstrated the largest AUC decrease (32-63%) after chronic PI treatments (e.g., RTV, LPV/RTV, or TPV/RTV) are typically substrates of CYPs (CYP2B6 and/or CYP2C8) that were found to be significantly induced by PIs in our hepatocyte induction studies [Hsyu et al., 2006; Hogeland et al., 2007;

Mukwaya et al., 2005]. On the other hand, object drugs that are substrates of CYPs where net activity increase was not observed in our hepatocyte studies, generated smaller and insignificant AUC changes (<30%) *in vivo* (e.g. phenytoin for CYP2C9) after chronic administration of LPV/RTV [Lim et al., 2004].

For the hepatic transporters, only OATP1B1 and MDR1 were induced by the PIs (> 2-fold), and again, APV ranked highest amongst the PIs in its induction of the transporters. These findings are in agreement with our review of the clinically significant PI-based DDIs, which showed that drugs (e.g., pravastatin, fexofenadine, and digoxin) that are substrates of the most inducible transporters in our hepatocyte induction studies (OATP1B1 and MDR1) also demonstrated clinically significant AUC decreases (50-384%) after chronic administration of PIs, (e.g., RTV/SQV, LPV/RTV, or RTV/IDV) [Fichtenbaum et al., 2002; Wyen et al., 2008; Kharasch et al., 2009]. APV's greater induction potential for OATP1B1 and MDR1 is also consistent with the clinical observations that rosuvastatin AUC (minimal metabolism, and OATP1B1 and MDR1 substrates) was increased (110-213%) after chronic treatment of ATV/RTV or LPV/RTV, yet unchanged after chronic administration of fosamprenavir/RTV (FPV, a pro-drug of APV), presumably due to net induction of its hepatic transporters by APV [Busti et al., 2008; Kiser et al., 2008]. Amongst the PIs, APV has been studied *in vitro* to be the least potent OATP1B1 inhibitor, and the most potent MDR1 inhibitor [Annaert et al., 2010; Hsiao et al., 2008]. Therefore, if transporter inhibition were the only mechanism involved, APV/RTV is expected to increase rosuvastatin AUC, and to a greater magnitude than LPV/RTV or ATV/RTV. Instead, to result in a lack of rosuvastatin AUC change after chronic administration of FPV/RTV, net induction of OATP1B1 and/or MDR1 by APV likely occurred to balance out the transporter inhibition in the presence of APV/RTV.

Overall, a qualitative correlation was demonstrated between our *in vitro* hepatocyte results and those observed *in vivo*. This confirms human hepatocytes as a useful prediction system for PI-based DDIs. However, to utilize human hepatocytes as a quantitative prediction model, the ability of the PIs to inhibit, inactivate, and/or induce CYP enzymes must be characterized over a range of concentrations. It is noteworthy that our results cannot fully explain other PI-based DDIs, such as the 2.1-fold increase in paraxanthine formation clearance (CYP1A2 probe) [Kirby et al., 2011b] after chronic administration of RTV, and many other paradoxical DDIs amongst the PIs themselves. All of which seems to suggest the ability of PIs to significantly induce CYP enzymes other than CYP3A, 2B6 and 2C8, as well as transporters that were either not induced or only moderately induced by the PIs in our hepatocyte induction studies. One likely reason is that the 2D-hepatocytes used in this investigation do not fully represent the hepatocytes *in vivo*, and that an even more sophisticated *in vitro* model such as the human sandwich-cultured hepatocytes (SCHH) are needed to provide an improved and more physiologically relevant representation of the hepatocytes *in vivo*. Thus, a similar evaluation of the PIs' induction potential towards CYPs and transporters using SCHH is currently being conducted by our group.

In conclusion, our validated cocktail assays should be of great utility for accurate quantification of CYP activities in both human liver and hepatocyte derived microsomes for a variety of experimental settings. Results from this study provide the most comprehensive data in profiling the net induction potential of PIs for CYPs and transporters, and demonstrate that PIs are net, but modest inducers of the CYPs and transporters. Overall, a qualitative correlation was demonstrated between our *in vitro* hepatocyte results and those observed *in vivo*. To better and quantitatively predict these DDIs, future investigations are needed to characterize the ability of

the PIs to inhibit, inactivate, and/or induce CYP enzymes using a range of PI concentrations and a more physiologically relevant model such as the SCHH.

Table 2.1: CYPs, probe substrate concentrations and literature Km values, metabolite ions and mass spectrometry conditions measured in the two cocktail assays[1].

CYPs	Substrates	Concentrations (µM)	Km (µM)	Metabolites	Parent Metabolites m/z	Metabolite m/z	CV	CE	RT (min)
Cocktail 1:									
3As	Testosterone	100	53-128	6-OH-testosterone	305.2	305.2	30	15	8.82
2C9	Tolbutamide	75	97-171	4-OH-tolbutamide	287.2	287	20	10	8.32
1As	Phenacetin	50	34	Acetaminophen	152.1	109.9	25	25	4.36
2D6	Dextromethorphan	5	2.8-15	Dextrorphan	258.2	156.9	45	50	6.46
2A6	Coumarin	0.5	0.4-1	7-OH-coumarin	163.1	107	35	30	7.26
Cocktail 2:									
2B6	Bupropion	100	109-162	OH-bupropion	238.1	130	35	50	6.68
2C8	Amodiaquine	4	2	N-desmethylamodiaquine	328.1	238	30	30	5.2
2C19	Omeprazole	20	10	5-OH-omeprazole	362.1	213.9	5	20	6.26
2E1	Chlorzoxazone	25	53-74	6-OH-chlorzoxazone	186	186	NA	NA	7.8

1. **LC-MS/MS Instrumentation:** Analysis of the cocktail validation results using HLM was conducted on LC-MS/MS using Waters Alliance 2690 equipped with an autosampler and interphased with a Micromass Quattro Ultima triple quadrupole mass spectrometer (Micromass, Beverly, MA). LC-MS/MS conditions are specified above. CV: cone voltage; CE: collision energy; RT: retention time.

Table 2.2: Demographic characteristics of the liver donors. NA, not available.

Donor	Age	Sex	Race	Medication	Cause of Death	Source
1	32	M	Caucasian	chemotherapy	NA	Organ donor
2	60	F	Caucasian	NA	Subarachnoidal hemorrhage	Organ donor
3	25	F	Caucasian	NA	Anoxia	Organ donor
4	65	M	Caucasian	NA	NA	Transplant
5	14	F	Caucasian	NA	NA	Organ donor

Table 2.3: Steady-state plasma concentrations of HIV PIs (plus or minus booster-RTV dose) in healthy volunteers.

		Cmax (µM)	Cavg (µM)	Plasma Protein Binding	Cmax,u (µM)	Cavg,u (µM)	References
APV	1200 mg b.i.d	13.55	2.80	90%	1.35	0.28	Wood et al., 2004
	1200/200 mg RTV q.d.	15.33	5.62		1.53	0.56	
ATV	400 mg q.d.	7.38	1.66	86%	1.03	0.23	Atazanavir drug label
	300/100 mg RTV q.d.	8.70	3.37		1.22	0.47	
IDV	800 mg t.i.d.	11.89	10.77	60%	4.76	4.31	Saah et al., 2001
	800/200 mg RTV b.i.d.	21.02	25.46		8.41	10.18	
NFV	750 mg t.i.d.	5.94	3.96	98%	0.12	0.08	Amsden et al., 2000
	1875/200 mg RTV q.d.	8.81	3.64		0.18	0.07	La Porte et al., 2004
SQV	1200 mg t.i.d.	2.12	0.78	97%	0.06	0.02	Saquinavir drug label
	1000/100 mg RTV b.i.d.	1.49	1.45		0.04	0.04	Kurowski et al., 2003
RTV	600 mg b.i.d.	15.54	7.91	99%	0.16	0.08	Hardman et al., 2001
LPV	400/100 mg RTV b.i.d.	15.59	12.25	99%	0.16	0.12	Klein et al., 2008
TPV	500/200 mg RTV b.i.d.	137.57	98.46	99%	1.38	0.98	Mathias et al., 2008
DRV	600/100 mg RTV b.i.d.	13.06	8.58	95%	0.65	0.43	Mathias et al., 2008

q.d. = once daily; b.i.d. = twice daily; t.i.d. = three times daily
Cmax,u = unbound Cmax ; Cavg,u = unbound Cavg

A)

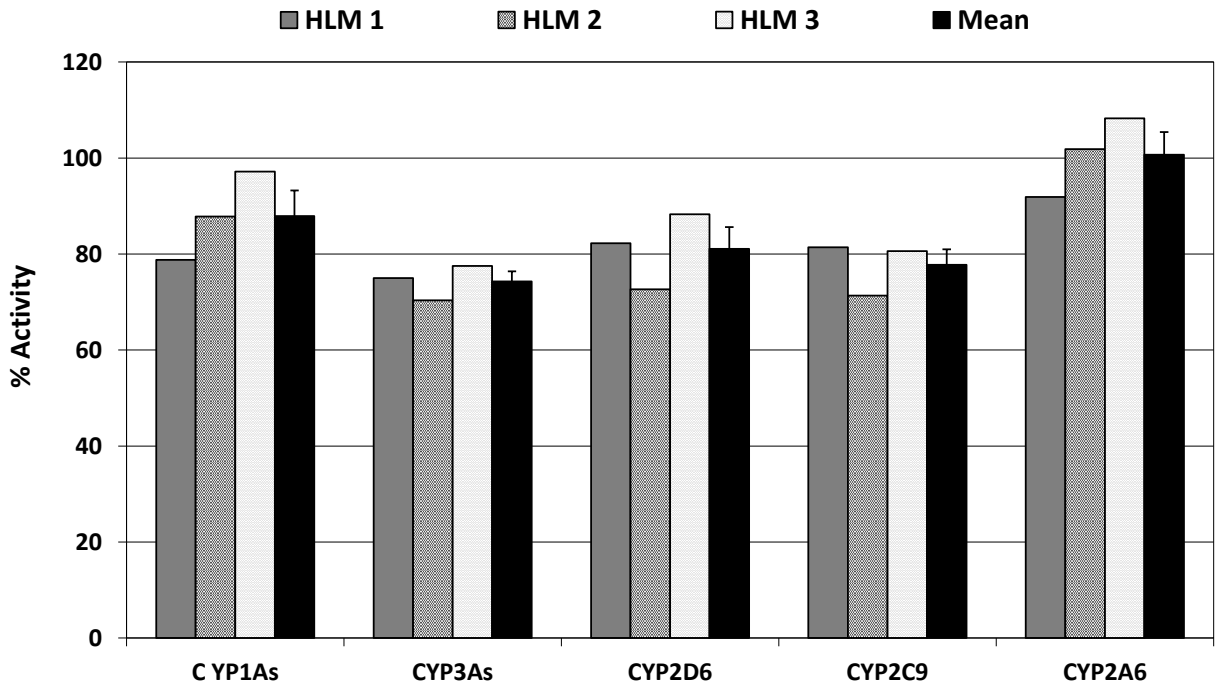
HLM 1
HLM 2
HLM 3
Mean
120
100
80
60
40
20
0
% Activity
C YP1As
CYP3As
CYP2D6
CYP2C9
CYP2A6

B)

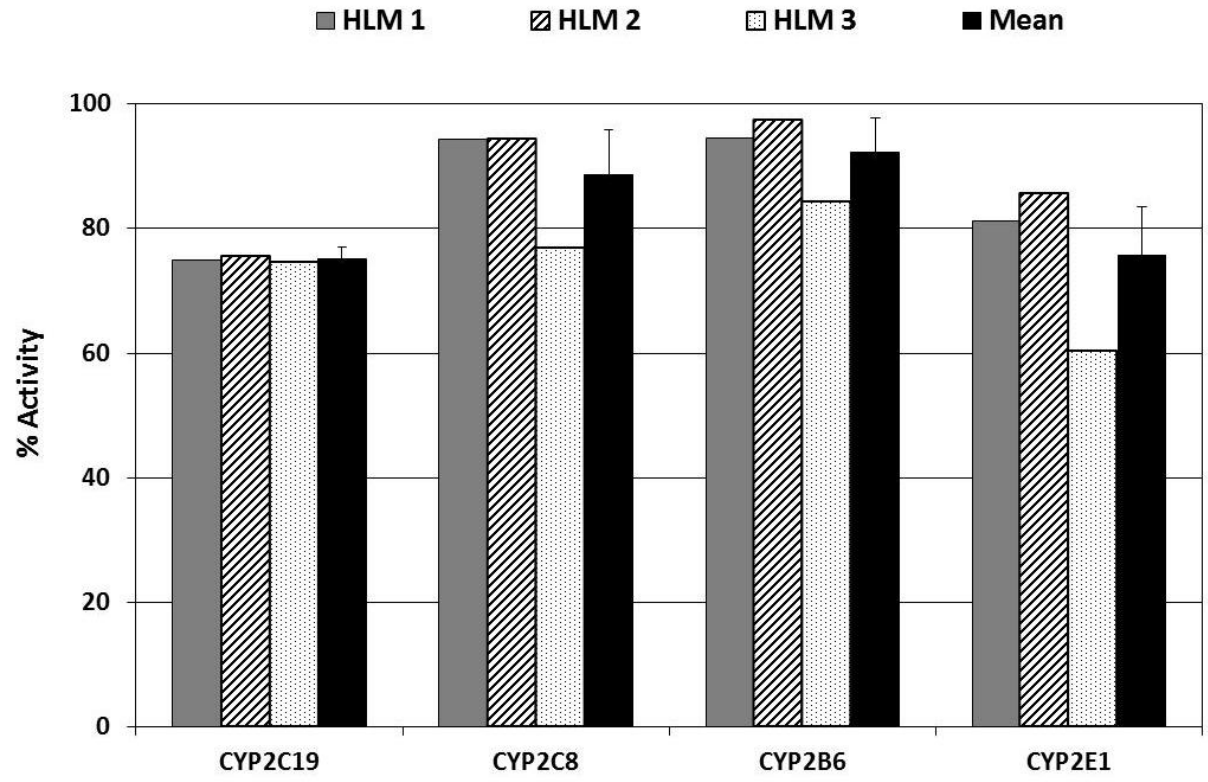
HLM 1
HLM 2
HLM 3
Mean
100
80
60
40
20
0
% Activity
CYP2C19
CYP2C8
CYP2B6
CYP2E1

Figure 2.1: CYP activity in human liver microsomes (HLMs) (n=3 livers, mean ± SEM.) using cocktail assays 1 **(A)** and 2 **(B)**. CYP activities in the cocktails are expressed as a % of the individual probe incubations, and demonstrated no statistically significant effect when incubated as a cocktail vs. individual probes (*p*-value >0.05).

A)

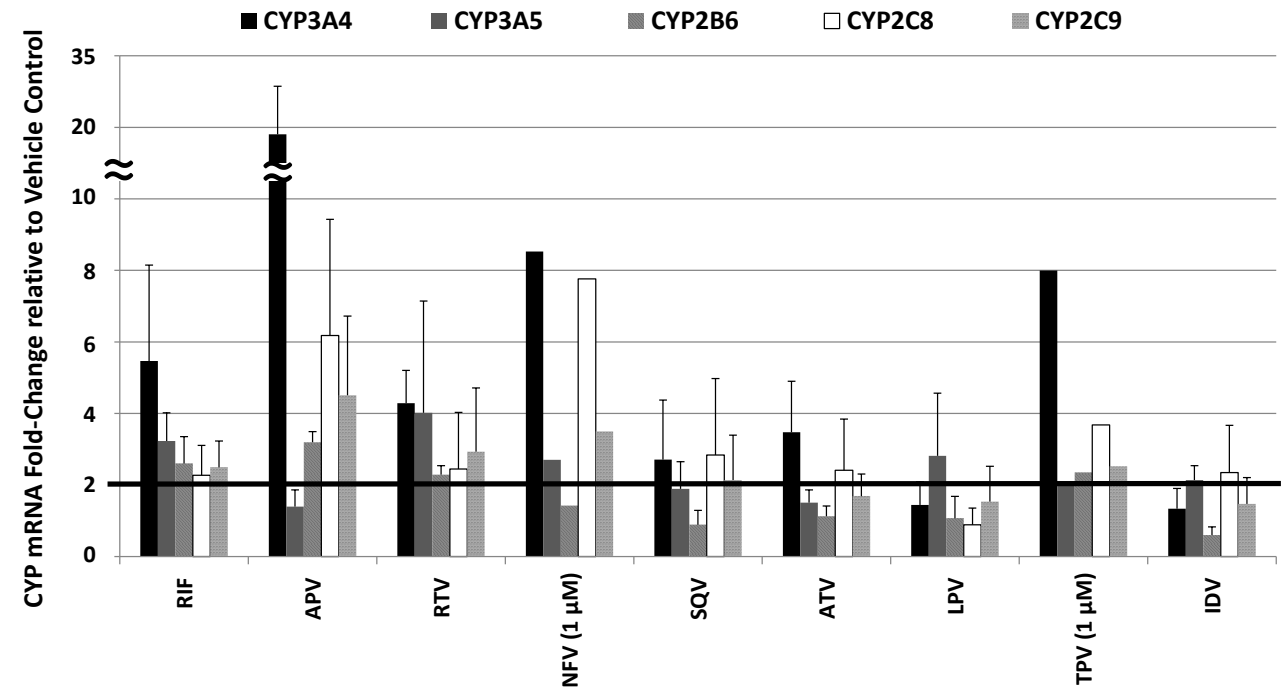
CYP3A4
CYP3A5
CYP2B6
CYP2C8
CYP2C9
CYP mRNA Fold-Change relative to Vehicle Control
35
20
10
8
6
4
2
0
RIF
APV
RTV
NFV (1 µM)
SQV
ATV
LPV
TPV (1 µM)
IDV

B)

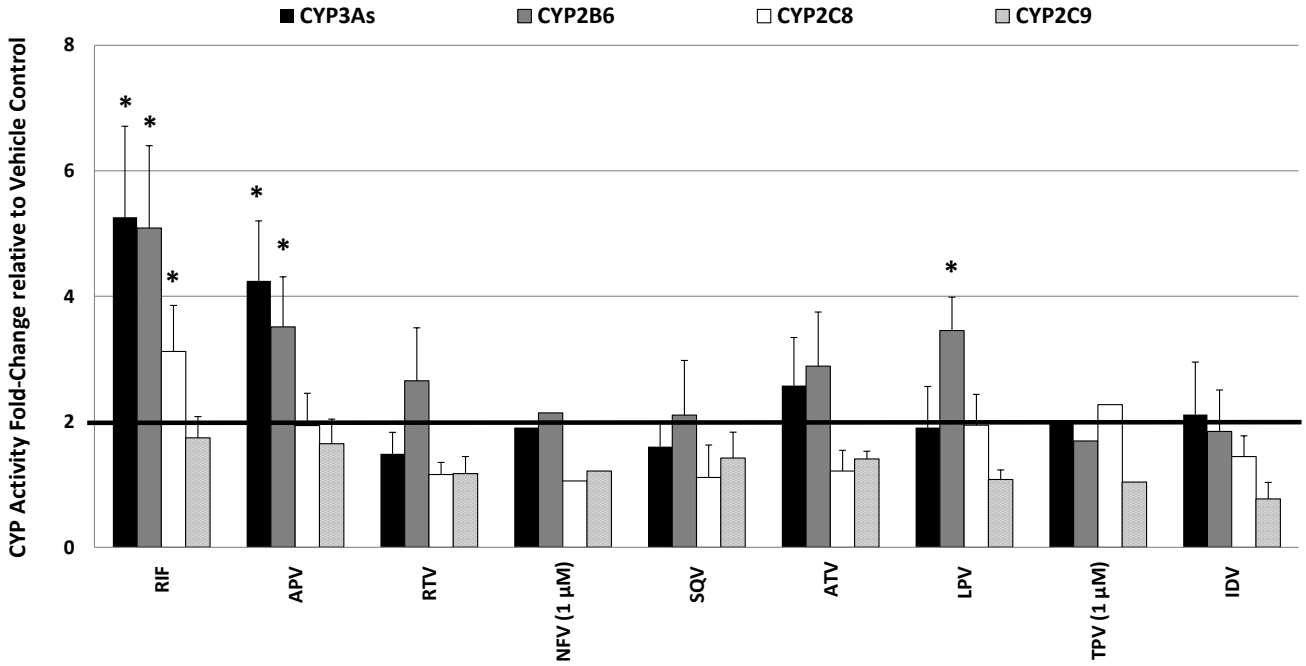
CYP3As
CYP2B6
CYP2C8
CYP2C9
CYP Activity Fold-Change relative to Vehicle Control
8
6
4
2
0
*
RIF
APV
RTV
NFV (1 µM)
SQV
ATV
LPV
TPV (1 µM)
IDV

C)

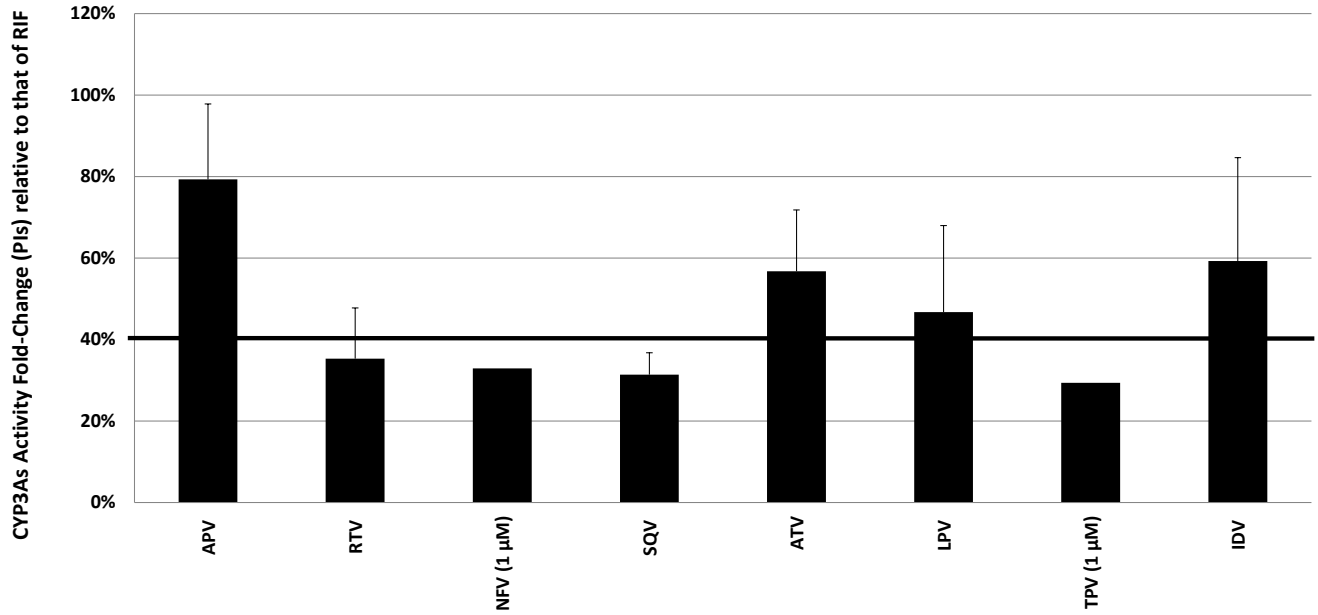

Figure 2.2: Induction of CYP mRNA expression **(A)**, or activity **(B)** when hepatocytes were incubated with rifampin (RIF, n=5 donors), amprenavir (APV, n=5 donors), ritonavir (RTV, n=5 donors), nelfinavir (NFV, n=2 donors), saquinavir (SQV, n=4 donors), atazanavir (ATV, n=4 donors), lopinavir (LPV, n=4 donors), tipranavir (TPV, n=2 donors), or indinavir (IDV, n=4 donors). Induction was expressed as a fold-change relative to vehicle control. Our primary index of significant induction was >2 fold-change, while the secondary index was significance ($p < 0.05$*) after paired t-test. Percent CYP3A activity induction is expressed as fold-induction relative to the positive control, RIF **(C)**. Data are expressed as mean ± SEM.

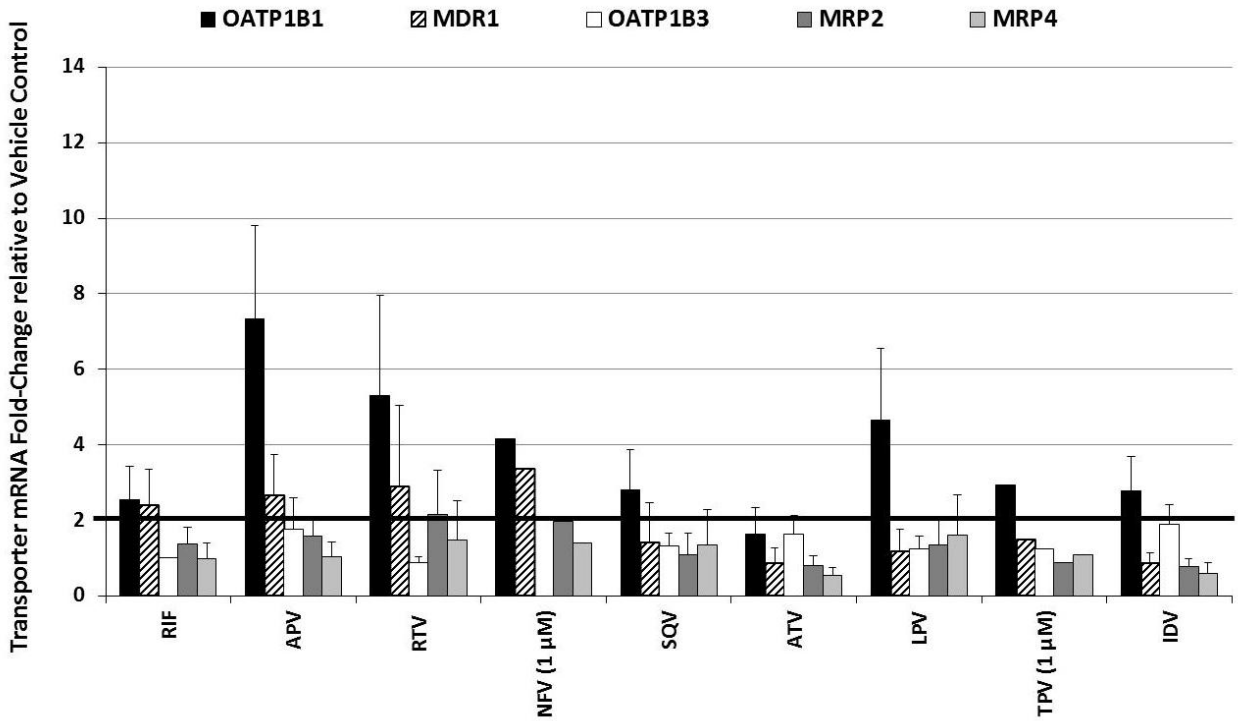

Figure 2.3: Induction of transporter mRNA expression after the hepatocytes were incubated with the with rifampin (RIF, n=5 donors), amprenavir (APV, n=5 donors), ritonavir (RTV, n=5 donors), nelfinavir (NFV, n=2 donors), saquinavir (SQV, n=4 donors), atazanavir (ATV, n=4 donors), lopinavir (LPV, n=4 donors), tipranavir (TPV, n=2 donors), or indinavir (IDV, n=4 donors). OATP1A2 was not detectable. Induction was expressed as a fold-change relative to vehicle control with significant induction was >2 fold-change. Data are expressed as mean ± SEM.

Chapter 3: Interaction between HIV Protease Inhibitors (PIs) and Hepatic Transporters in Sandwich Cultured Human Hepatocytes: Implication for PI-based DDIs

The data presented in this chapter has been submitted to the journal Biopharmaceutics and Drug Disposition.

3.1 Abstract

Although HIV protease inhibitors (PIs) produce profound metabolic interactions through inactivation/inhibition of CYP3A enzymes, their role as victims of transporter-based drug-drug interactions (DDIs) is less well understood. Therefore, we investigated if the PIs, nelfinavir (NFV), ritonavir (RTV), lopinavir (LPV), or amprenavir (APV) were transported into sandwich-cultured human hepatocytes (SCHH), and whether OATPs contributed to this transport. Our findings showed that except for ^{3}H-APV, no significant decrease in the total hepatocyte accumulation of the ^{3}H-PIs was detected in the presence of the corresponding unlabeled PI, indicating that the uptake of the other PIs was not mediated. Further, hepatocyte biliary efflux studies using ^{3}H-APV and unlabeled APV confirmed this decrease to be due to inhibition of sinusoidal influx transporter(s) and not the canalicular efflux transporters. Moreover, this sinusoidal transport of APV was not OATP-mediated. Our results indicate the hepatic uptake of NFV, RTV, or LPV was primarily mediated by passive diffusion. APV's hepatic uptake was mediated by an unidentified sinusoidal transporter(s). Therefore, NFV, RTV or LPV will not be

victims of DDIs involving inhibition of hepatic influx transporters; however, the disposition of APV may be affected if its sinusoidal transport is inhibited.

3.2 Introduction

HIV protease inhibitors (PIs) are a class of antiretroviral agents that are a critical component in the management of HIV infection and Highly Active Antiretroviral Therapy (HAART). Their use in the clinic is associated with profound drug-drug interactions (DDIs) where the PIs are both victims and precipitants. To date, the study of the PI-based DDIs has been focused on CYP3A-mediated mechanisms as many of the PIs are substrates (DDI victims), inducers and potent inactivators (DDI precipitants) of these enzymes [Dixit et al., 2007a; Liu et al., 2012]. Many of the PI-based DDIs may also be transporter-based as the PIs are inhibitors (DDI precipitants) of ABC transporters (e.g., P-gp, MRPs, BCRP), as well as OATPs [Hsiao et al., 2008; Ye et al., 2010; Annaert et al., 2010; Gupta et al., 2004]. In addition, the PIs may be victims of transporter-based DDI as they are substrates of several transporters such as P-gp and MRP2 [van der Sandt et al., 2001; Huisman et al., 2002]. For example, in humans, after oral administration of a **single dose** of radiolabeled PIs, these drugs are found to be cleared from the body via extensive hepatic elimination (>80%), of which 88% is accounted by CYP3A metabolism, and ~12% by biliary excretion [Denissen et al., 1997; Kumar et al., 2004; Sadler et al., 2001]. However, on **chronic administration** of the PIs, which are now almost always co-administered with ritonavir (RTV), the role of biliary excretion of the PIs may be even greater due to CYP3A inactivation [Hill et al., 2009]. Indeed, this is observed with tipranavir (TPV) after chronic administration of TPV/RTV [Chen et al., 2007]. Therefore, the role of hepatic

transporters could become more significant in the hepatic disposition of PIs under chronic administration of PIs and/or RTV-boosted PI regimen.

While PIs' interactions with the canalicular efflux transporters (e.g., P-gp, MRP2, BCRP) as substrates and/or inhibitors have been previously studied, very little is known about their interactions with the sinusoidal influx transporters. Such characterization is important since in order for the PIs to be metabolized in the hepatocytes or be excreted into the bile, they must either diffuse or be transported across the sinusoidal membrane. If transported, DDIs at the level of the sinusoidal uptake transporters could affect the disposition of the PIs. To date, the PIs have been shown to be inhibitors of OATPs, *in vitro* [Anneart et al., 2010], and possibly *in vivo* [Busti et al., 2008; Kiser et al., 2008]. However, whether they are substrates of OATPs is controversial. Some studies using primarily oocyte expression systems [Hartkoorn et al., 2010], HepG2 cells [Su et al., 2004], or rat hepatocytes [Parker et al., 2008], have shown that selective PIs may be transported by OATPs. Others, using MDCKII cells transfected with OATP2B1 and caco2 cells [Kis et al., 2010], have concluded that they are not transported by OATPs. In addition, whether PIs are transported into **human** hepatocytes has not been investigated. It is important to note that when a drug is found to be a low affinity substrate of a transporter in an over-expressing system, the contribution of that transporter *in vivo* or in primary culture of human tissues (e.g., hepatocytes) in the disposition of the drug may be negligible. This is because the expression of that transporter *in vivo* or in the cells will likely be lower than that in the over-expressing cells, and, other processes may contribute to the disposition of the drug (e.g., passive diffusion or other transporters). Therefore, it is critical to determine the contribution of the transporter(s) *in vivo* or a representative cell culture model. Thus, we evaluated the uptake of PIs in a physiologically relevant system (e.g., sandwich-cultured human hepatocytes [SCHH]) that exhibits *in vivo*-like

canalicular network and transporters (sinusoidal and canalicular). Addressing these questions is important in delineating the role of hepatic influx transporters in the hepatic disposition of the PIs and in understanding PI-based DDIs, where PIs are the victim drugs.

Therefore, the goals of this investigation were to conduct radioactive transport studies to determine: 1) whether the hepatic uptake of the PIs is transporter-mediated in the most physiologically relevant *in vitro* model, the sandwich-cultured human hepatocytes (SCHH), 2) whether the sinusoidal influx transport (if any) is contributed by OATPs. We focused our evaluation on the PIs, RTV, nelfinavir (NFV), lopinavir (LPV), and amprenavir (APV), based on their clinical relevance and/or commercial availability of the radiolabeled compound.

3.3 Materials and Methods

3.3.1 Materials

^{3}H-RTV (37 GBq/mmol), ^{3}H-LPV (37 GBq/mmol), and ^{3}H-APV (18.5 GBq/mmol) were purchased from Moravek Biochemicals and Radiochemicals (Brea, CA). ^{3}H-NFV (37 GBq/mmol), ^{3}H-estrone-3-sulfate (ES; 2.22 TBq/mmol), and ^{3}H-estradiol-beta-17-glucuronide (EG; 2.22 TBq/mmol) were purchased from American Radiolabeled Chemicals, Inc. (St. Louis, MO). ^{14}C-mannitol (1.66 GBq/mmol) was purchased from PerkinElmer Life and Analytical Sciences (Boston, MA). Unlabeled PIs were obtained from the National Institutes of Health AIDS Research and Reference Reagent Program. Unlabeled ES, EG, bromosulfophthalein (BSP), 1-aminobenzotrizole (ABT) and sodium butyrate were purchased from Sigma-Aldrich (St. Louis, MO). N-(4-(2-(1,2,3,4-Tetra-hydro-6,7-dimethoxy-2-isoquinolinyl)ethyl)phenyl)-

9,10-dihydro-5-methoxy-9-oxo-4-acridine carboxamide (elacridar, GF120918) was a generous gift from GlaxoSmithKline (King of Prussia, PA). 24-well BioCoated culture plates and Matrigel [high concentration (HC)] were from BD Biosciences (San Jose, CA). Hepatocyte plating and maintenance supplement packs, and **CHRM® Medium,** Williams E medium (WEM), Hanks balanced salt solution (HBSS) containing 10 mM Hepes and adjusted to pH 7.4, either with or without $CaCl_2$ and $MgCl_2$ (Ca^{2+} plus or Ca^{2+} minus buffer, respectively), and fetal bovine serum (FBS) were from GIBCO, Invitrogen (Carlsbad, CA). BCA protein assay reagent was from Pierce Chemical (Rockford, IL). Cell lysis buffer was prepared with 10 mM Tris-HCL, pH 8.0, 0.5% Triton X-100, and 1 mM EDTA). Freshly isolated human hepatocytes in a 24-well BioCoat plate with Matrigel overlay were purchased from Celsis (Baltimore, MD), and cryopreserved human hepatocytes were purchased from CellzDirect (Durham, NC). MDCKII cells expressing human OATP1B1 (MDCKII-OATP1B1) were kindly provided by Dr. Yuichi Sugiyama (University of Tokyo, Japan).

3.3.2 SCHH and MDCKII-OATP1B1 Tissue Culture

Cryopreserved hepatocytes (0.325×10^6 viable cells/well) were thawed and plated in 24-well BioCoat culture plates overlaid with Matrigel following manufacture's protocol (Invitrogen Life Technologies). Both freshly isolated and cryopreserved SCHH were maintained in serum-free supplemented WEM and were replenished with fresh media every day until transport studies were conducted on day 6 post-plating. MDCKII-OATP1B1 cells were cultured in low glucose Dulbecco's modified Eagle's medium (DMEM; Invitrogen, Carlsbad, CA) with 10% FBS and 1% antibiotic-antimycotic solution (Sigma-Aldrich). The transfected MDCKII cells were selected with Zeocin (700 µg/ml; Invitrogen) before further sub-culturing. Both the hepatocytes

and transfected cells were cultured and maintained at 37°C in a humidified incubator with 95% atmospheric air and 5% CO_2.

3.3.3 SCHH Transport Studies

Due to solubility and non-specific binding issues associated with PIs, 2% FBS and 0.8% DMSO were added to all transport buffers. Positive control transport studies using OATP model substrates, 1 µM ^{3}H-ES (uptake transport studies) with or without BSP, OATP pan-inhibitor or 1 µM ^{3}H-EG (biliary excretion studies) with or without elacridar (P-gp, BCRP and OATP inhibitors) were performed to confirm OATP expression, the formation of canalicular network and the expression of the canalicular efflux transporters in SCHH, respectively [Oostendorp et al., 2009; Hagenbuch et al., 2008; Yanni et al., 2010; Hewitt et al., 2001]. All SCHH transport experiments were performed in three independent batches of hepatocytes.

3.3.3.1 SCHH Pretreatment with ABT

To prevent significant metabolic depletion of PIs during transport studies, SCHH were pre-incubated with 5 mM ABT (pan-inactivator for CYPs) for 1 h and washed twice using Ca^{2+} plus buffer to eliminate residual ABT before initiation of all transport studies. The efficacy of ABT in preventing metabolism of 0.1 µM ^{3}H-NFV, ^{3}H-RTV, ^{3}H-LPV, and ^{3}H-APV during the transport experiments was confirmed by determining the recovery of the unchanged drug in both the transport buffer and cell lysates by LC/UV coupled with fraction collection. To confirm that ABT does not affect the OATP-mediated transport of ^{3}H-ES, transport studies using 1 µM ^{3}H-ES were also conducted after 1 h pre-incubation with or without 5 mM ABT.

3.3.3.2 SCHH Uptake Studies

Unlike transport experiments performed using hepatocytes in suspension format, where a greater cellular surface area allows rapid uptake and thus shorter incubation period to evaluate initial uptake, transport studies performed using plated cell systems (e.g., SCHH, or cell lines) require longer incubation times [Ye et al., 2010; Yanni et al., 2010; Ye et al., 2010, Govindarajan et al., 2008]. Indeed, after evaluating the hepatic uptake of ^{3}H-PIs at 2, 5, 15, and 25 min of transport in our pilot studies, we found that a minimum of 10 min incubation period was required to provide sufficient intracellular accumulation and dynamic range of ^{3}H-PIs radioactivity for downstream inhibition studies to evaluate potential uptake transport mechanisms. Additionally, our pilot studies demonstrated that the uptake of ^{3}H-PIs was linear up to the first 25 min of transport studies. To determine if the uptake of the ^{3}H-PIs into the SCHH was temperature-dependent we first pre-incubated SCHH with Ca^{2+} plus buffer for 10 min at either 4°C or 37°C, followed by replacing the pre-incubation buffer with transport buffer (Ca^{2+} plus buffer) containing 0.1 µM ^{3}H-NFV, ^{3}H-RTV, ^{3}H-LPV, or ^{3}H-APV, and then incubating the SCHH for 0, 10 or 20 min at 4°C or 37°C. To determine if this uptake was transporter-mediated, we pre-incubated the SCHH at 37°C for 20 min with Ca^{2+} plus buffer containing unlabeled NFV, RTV, LPV, APV (20 or 100 µM; self-inhibition studies), or the OATP inhibitor, BSP (20 or 100 µM), followed by a 20 min incubation with transport buffers (Ca^{2+} plus buffer containing 0.1 µM ^{3}H-NFV, ^{3}H-RTV, ^{3}H-LPV, or ^{3}H-APV and the corresponding unlabeled PIs, or BSP). At the end of the incubation, the transport buffer was harvested; cells were washed twice with ice-cold PBS buffer, and then lysed with the lysis buffer (0.5 mL/well). 50 µL aliquots of the cell lysates were saved for protein quantification using the BCA assay as per manufacturer's instructions. Radioactivity was measured in both the transport buffer and cell lysates. The cell-to-media

radioactivity ratio was normalized to the protein content of the hepatocytes and used as the uptake index.

3.3.3.3 SCHH Biliary Excretion Studies

To measure the biliary efflux of ^{3}H-APV, SCHH were first pre-incubated for 10 min with either Ca^{2+} plus buffer or Ca^{2+} minus buffer at 37°C, followed by a second pre-incubation (20 min) with Ca^{2+} plus or Ca^{2+} minus buffer containing elacridar or unlabeled APV at 20 or 100 µM. Then, the SCHH were incubated for another 20 min with Ca^{2+} plus or Ca^{2+} minus buffer containing 0.1 µM ^{3}H-APV, with or without the inhibitors. The Ca^{2+} plus buffer maintains tight junction integrity and bile canalicular network, allowing measurement of drug efflux across the sinusoidal and canalicular membranes and total accumulation in the cell and bile. However, the Ca^{2+} minus buffer disrupts the tight junctions and opens bile canalicular networks, and therefore measures uptake across the sinusoidal membrane only [Yanni et al., 2010]. Accumulation of the radioactivity was measured at the end of the transport period, and the protein content normalized cell-to-media radioactivity ratio was determined. Biliary excretion of the ^{3}H-APV was calculated using the following equation:

$$\text{Biliary Excretion (\%)} = \frac{\left(\frac{^{3}\text{H in cell lysate}}{^{3}\text{H in media}}\right)\text{in } Ca^{2+} \text{ plus buffer} - \left(\frac{^{3}\text{H in cell lysate}}{^{3}\text{H in media}}\right)\text{in } Ca^{2+} \text{ minus buffer}}{\left(\frac{^{3}\text{H in cell lysate}}{^{3}\text{H in media}}\right)\text{in } Ca^{2+} \text{ plus buffer}} \text{ x } 100\%$$

3.3.4 MDCKII-OATP1B1 Transcellular Transport studies

Cells (0.1 x 10^{6} cells/well) within the first twelve passages were grown on Transwell membrane inserts (6.5 mm diameter, 0.4 µm pore size; Corning Costar, Bodenheim, Germany) for 3 days until confluence, and the transporter expression level was induced with 10 mM sodium butyrate for 24 h before the transport study [Matsushima et al., 2005]. The trans-

epithelial electrical resistance (TEER; $\Omega \cdot cm^2$) value was measured for each monolayer, and was ~300 $\Omega \cdot cm^2$ (monolayers < 100 $\Omega \cdot cm^2$ were not used). Cell monolayers were first equilibrated in transport buffer (HBSS buffer) for 30 min at 37°C, followed by 20 min pre-incubation with transport buffer containing unlabeled NFV, RTV, LPV, APV, or BSP (20 or 100 μM). Both the basolateral to apical (B→A) and apical to basolateral (A→B) transport were determined by incubating the cells for 3 h with transport buffers (HBSS buffer containing 0.1 μM ^{3}H-NFV, ^{3}H-RTV, ^{3}H-LPV, ^{3}H-APV, or 1 μM ^{3}H-ES and the corresponding unlabeled PIs or BSP) added to the donor chamber (basolateral: 0.6 mL; apical: 0.1 mL), and blank plus buffer added to the recipient chamber (basolateral: 0.6 mL; apical: 0.1 mL). The B→A transport studies using ^{14}C-mannitol (2.5 μM) were also performed to assess paracellular transport and monitor cell monolayer and membrane integrity. At the end of the transport studies, radioactivity in the transport buffer from A and B chambers were determined. Transcellular transport was calculated as the % of radiolabeled drug transferred from the donor to the recipient chamber.

3.3.5 Statistical and Data Analysis

Statistical assessments were performed using a paired two-tailed Student's T-test, with significance level defined as $p \leq 0.05$.

3.4 Results

3.4.1 SCHH Transport Studies

After 1 h pre-treatment with 5 mM ABT, at the end of the uptake experiments, all ^{3}H-PIs were recovered as unchanged drug (>98%) from both the transport buffer and hepatocyte lysate. This was confirmed by LC-UV analysis coupled with radioactivity fractionation of ^{3}H-PIs or metabolites. This indicates that the metabolism of the PIs, which can potentially confound the interpretation of uptake experiments, was eliminated. The uptake of ^{3}H-ES, an OATP positive control substrate, was not affected by the 1 h pre-treatment of the SCHH with 5 mM ABT (Figure 3.1).

During the first 20 min of transport studies, SCHH uptake of ^{3}H-ES or ^{3}H-PIs was within the linear range. The SCHH showed robust hepatic OATP activity as demonstrated by the significant decrease in the hepatic uptake of ^{3}H-ES in the presence of 20 or 100 μM BSP (Figure 3.1). Of the four PIs, only ^{3}H-APV and ^{3}H-LPV demonstrated significant increase in 20 min SCHH uptake at 37°C vs. 4°C (Figure 3.2A-D). The uptake of ^{3}H-PIs was not affected by the presence of the OATP inhibitor, BSP (20 or 100 μM). Likewise, the uptake of the ^{3}H-NFV, ^{3}H-RTV, or ^{3}H-LPV was unaffected by the corresponding unlabeled PI (Figure 3.3A-C). However, the uptake of ^{3}H-APV was significantly decreased by unlabeled APV (Figure 3.3D).

Of the four PIs, only ^{3}H-APV demonstrated both temperature-dependent uptake and self-inhibition (by the unlabeled APV) uptake in SCHH. Since our uptake data are based on radioactivity in the cell lysate plus canalicular space, these observations could be a result of potential inhibition of ^{3}H-APV transport into the SCHH and/or inhibition of ^{3}H-APV efflux at the canalicular membrane. To examine the contribution of biliary efflux in the hepatocyte

uptake of APV, we evaluated the biliary excretion of ^{3}H-APV in the absence or presence of elacridar (a P-gp and BCRP dual inhibitor). The hepatocyte uptake of ^{3}H-APV in the Ca^{2+} plus buffer was significantly different from that in the Ca^{2+} minus buffer and remained so in the presence of 20 μM elacridar (Figure 3.4A). However, this difference was ablated in the presence of 100 μM elacridar due to a decrease in ^{3}H-APV uptake in the presence of Ca^{2+} with no effect on ^{3}H-APV uptake in the absence of Ca^{2+}. As a result, the biliary excretion of ^{3}H-APV was significantly decreased. Furthermore, in the presence of unlabeled APV (20 or 100 μM), the hepatocyte uptake of ^{3}H-APV remained significantly different between the Ca^{2+} plus and Ca^{2+} minus conditions, and the biliary excretion of ^{3}H-APV was unaffected and remained at ~35% (Figure 3.4B). In the presence of 20 or 100 μM APV, the hepatocyte uptake of ^{3}H-APV under the Ca^{2+} plus or Ca^{2+} minus condition was significantly decreased and by similar magnitudes. To confirm the integrity of the canalicular membrane and the expression of the canalicular efflux transporters in the SCHH used for these biliary excretion studies, we measured the biliary excretion of ^{3}H-EG (a positive control for biliary excretion). Biliary excretion of ^{3}H-EG decreased from 35% in the absence of elacridar to < 5% in the presence of 100 μM elacridar (Figure 3.4C).

3.4.2 MDCKII-OATP1B1 Transcellular Transport Studies

To provide further support to our findings from the SCHH transport studies, we investigated the transport of the PIs using an additional *in vitro* system, MDCKII cells stably transfected with OATP1B1. OATP1B1 was chosen because it is the predominant OATP isoform expressed in human livers [Hagenbuch et al., 2008] and previous studies have shown that PIs (e.g. RTV, atazanavir, LPV, or darunavir) are not OATP2B1 or OATP1B3 substrates [Kis et al.,

2010; Hartkoorn et al., 2010]. While both B→A and A→B transport were evaluated, since OATPs are expressed on the basolateral membrane in kidney epithelial cells, the B→A transport provides a more direct and sensitive quantification of OATP inhibition because the A→B was confounded by expression of endogenous P-gp, which can transport PIs. Indeed, the B→A transport of the OATP1B1 positive control substrate (^{3}H-ES) was decreased significantly from 27% to 8% in the presence of the OATP inhibitor, 100 μM BSP, which confirmed the expression of OATP1B1 in the transfected MDCKII cells. However, the B→A transport of all four ^{3}H-PIs (NFV, RTV, LPV or APV) was not affected in the presence of BSP or the corresponding unlabeled drug (20 or 100 μM) (Figure 3.5). To confirm that the lack of inhibition by BSP was not due to paracellular transport or poor monolayer integrity, we confirmed that the bidirectional transport of ^{14}C-mannitol (paracellular transport marker) was < 0.5% (% transfer from donor to recipient chamber).

3.5 Discussion and Conclusions

Many of the PI-based DDIs can be explained by CYP3A-mediated mechanisms (inhibition, inactivation and/or induction). However, as presently used in the clinic (usually chronic RTV-boosted PI regimen), where CYP3A-mediated metabolism is minimized, biliary excretion is likely the predominant route of hepatic elimination for the PIs. In addition, for the PIs to be metabolized and excreted in the bile, they must first enter the hepatocytes by transport or by diffusion. To better understand PIs hepatic transport *in vivo*, and the potential role of the sinusoidal influx transporters in the transporter-based DDIs, where PIs are potential victim drugs, we investigated the hepatic transport of PIs in the SCHH model.

SCHH offers a superior and more comprehensive *in vitro* model system than other alternatives (e.g., transfected cell lines, HepG2 cells, oocyte expression systems), because they express, as *in vivo*, both the sinusoidal and canalicular membrane transporters [Hewitt et al., 2001]. By confirming that the hepatic uptake of ^{3}H-PIs is within the linear range and that the activity of known sinusoidal influx transporters (e.g., OATPs) is robust during the 10-20 min of SCHH transport studies, we were able to evaluate PIs hepatic uptake in a most *in vivo*-like model, and study the importance of the potential sinusoidal influx transporters relative to other competing processes present *in vivo* (e.g., diffusion, sinusoidal and/or canalicular efflux). However, the presence of the canalicular membrane transporters can complicate interpretation of transport data from cell lysates as the lysate measurements include the ^{3}H-substrate (e.g., PIs) in both the bile as well as in the hepatocytes. In addition, biliary efflux of the unchanged ^{3}H-substrate into the canalicular space can operate as a sink and driving force that can seemingly "accumulate" a drug in the SCHH, which includes the bile. Similarly, when the ^{3}H-substrate is extensively metabolized in the hepatocytes, such "accumulation" will also be observed in the absence of any sinusoidal uptake transport when only total drug radioactivity (parent plus metabolites) is monitored. Under both circumstances, this "accumulation" of the ^{3}H-substrate can be erroneously interpreted as hepatic transport even when no sinusoidal transport is present. Therefore, when using the SCHH to study hepatic drug uptake, two guiding principles must be followed. First, the parent ^{3}H-substrate concentration must be monitored or its hepatic metabolism must be minimized. Second, sinusoidal transport must be distinguished from canalicular membrane transport. In this communication we followed these two guiding principles.

To eliminate hepatocyte metabolism of the PIs, we pre-incubated all SCHH with 5 mM ABT for 1 h before conducting our transport studies, and confirmed the lack of hepatocyte metabolism of the ^{3}H-PIs via LC/UV coupled with radioactivity fractionation. Previous studies conducted in human liver microsomes and hepatocytes showed that pre-incubation with ABT (>2 mM), a potent CYP inactivator, can effectively abolish the activities of multiple CYPs [Kent et al., 1997; Parker et al., 2008]. In addition, ABT does not appear to be an inhibitor of the transporters expressed in the human hepatocytes, as Kimoto et al. (2012), found ABT (1 mM) does not inhibit the hepatocyte transport of rosuvastatin or atorvastatin, which is known to be mediated by OATPs, MRP2, BCRP, and P-gp [Kimoto et al., 2012]. To distinguish between biliary efflux and sinusoidal transport, we determined the hepatocyte uptake of the ^{3}H-PIs in the presence and absence of the canalicular network.

Of the PIs studied, only ^{3}H-APV and ^{3}H-LPV demonstrated significantly greater hepatocyte accumulation at 37ºC vs. 4ºC, suggesting that only these two PIs appear to be transported into the hepatocytes. However, temperature-sensitive hepatic accumulation of ^{3}H-LPV can be an experimental artifact, potentially due to the temperature dependent changes in diffusion, membrane fluidity and permeability. We conducted self-inhibition studies using up to 100 µM of unlabeled PIs as inhibitors to determine whether the hepatic accumulation of these two PIs was due to transporter-mediated process. These studies showed that the hepatic accumulation of ^{3}H-APV was self-inhibited while that of ^{3}H-LPV was not. Unless LPV is a very low affinity substrate of hepatic influx transport, our results indicate that only the hepatic accumulation of ^{3}H-APV was transporter-mediated.

As discussed above, hepatic accumulation of ^{3}H-APV could be a result of canalicular efflux transporters and/or sinusoidal influx transporters. Therefore, to identify the site of

transport, we determined the uptake of ^{3}H-APV in the presence and absence of the canalicular network. As expected, our results demonstrate that in the absence of metabolism, ^{3}H-APV underwent extensive biliary excretion (~40%), which was significantly decreased to ~11% in the presence of 100 μM elacridar, a P-gp/BCRP inhibitor that does not inhibit MRP2. Since APV is not a BCRP substrate [Gupta et al., 2004], but a P-gp substrate [van der Sandt et al., 2001], these data indicate that the biliary excretion of APV is likely mediated by P-gp. In contrast, the biliary excretion of ^{3}H-APV was unaffected in the presence of unlabeled APV. Furthermore, the uptake of ^{3}H-APV in SCHH with intact canalicular network (Ca^{2+} plus condition) and disrupted canalicular network (Ca^{2+} minus condition) was decreased by similar magnitudes (~8-fold in the presence of 100 μM APV). Together, these results indicate that the significant decrease in the hepatocyte uptake of ^{3}H-APV (Ca^{2+} plus condition) in the presence of unlabeled APV is due to inhibition of the sinusoidal uptake transporters and not due to inhibition of the biliary efflux of ^{3}H-APV. We speculate that APV may have higher affinity for the sinusoidal transporter(s) than for P-gp and that the intracellular concentrations of APV may not have reached the concentration sufficient to inhibit P-gp.

Based on prior studies that indicate that the PIs can be transported by OATPs, we investigated if the sinusoidal transport of APV was mediated by hepatic OATPs. It is not. Several lines of evidence indicate that sinusoidal OATPs are not involved in the uptake of APV or any of the other PIs studied. First, the hepatic uptake of all four ^{3}H-PIs, including ^{3}H-APV, was not inhibited by BSP, a classical pan-OATP inhibitor. Second, neither BSP nor the corresponding unlabeled PIs inhibited the B→A transport of the four ^{3}H-PIs in MDCKII-OATP1B1 cells. Third, the ^{3}H-APV hepatic uptake in the absence of Ca^{2+} was not inhibited by elacridar. Elacridar, besides inhibiting P-gp/BCRP, also inhibits OATPs [Oostendorp et al.,

2009]. This is consistent with our own finding that showed elacridar inhibited the uptake of ^{3}H-EG into the hepatocytes in the absence of Ca^{2+} (Fig. 4C). The fact that both elacridar and BSP did not inhibit the sinusoidal influx transport of APV suggests that allosterism of OATPs [Kindla et al., 2011; Grube et al., 2006], is not a likely explanation for the observed lack of inhibition. This is further supported by the fact that we did not observe self-inhibition of ^{3}H-PI transport in the presence of the corresponding unlabeled PIs.

The lack of transport of the PIs by OATPs is not inconsistent with data from others who have studied human OATP-mediated transport of the PIs. For example, Kis et al. (2010) confirmed that RTV is not a substrate of OATP2B1 (also expressed hepatically) using both MDCKII cells transfected with OATP2B1 and Caco-2 cells [Kis et al., 2010]. In the same study, atazanavir (ATV) was also shown to not be an OATP2B1 substrate, and both RTV and ATV were transported into Caco-2 cells by an unknown pH-dependent active influx transporter. However, a previous study that did report OATP-mediated transport of PIs (lopinavir, saquinavir or darunavir) found low or marginal affinity transport of the PIs, based on results of <2 fold difference between the ^{3}H-PIs accumulation in OATP overexpressing and control oocytes, compared to ~10 fold difference observed in the accumulation of ^{3}H-ES (standard OATP substrate) [Hartkoorn et al., 2010]. Kinetic analysis of saquinavir uptake into OATP1A2 overexpressing oocytes reported a high Km of 36.4±21.8 μM, and this value increased to 94.6±22.8 μM in HepG2 cells [Su et al., 2004]. OATP1B1 genetic polymorphism (521T>C, V174A) has been reported to be associated with slightly higher LPV plasma concentration [Hartkoorn et al., 2010]. Indeed, the evaluation in LPV plasma C_{min} concentration (10-14 h postdose) was marginal (TT homozygotes: 8.5 ng/mL, TC heterozygotes: 8.7 ng/mL, and CC heterozygotes [6 out of 400 patients]: 9 ng/mL), suggesting that the contribution of OATPs (if

any) to the disposition of LPV is small. Therefore, we propose that except for APV (which is transported into the SCHH by as yet unknown transporter), the PIs are unlikely to be significantly transported by OATPs *in vivo*. If they were transported, this contribution is minimal. Furthermore, due to the lower, but more *in vivo*-like OATPs expression levels in human hepatocytes than in the overexpression systems, diffusion across the cell membrane is likely the dominant mechanism for the *in vivo* hepatic uptake of the PIs studied here.

In conclusion, our results indicate that NFV, RTV, LPV and APV are not substrates (or poor substrates) of human hepatic OATPs. However APV may be transported into SCHH by an unidentified sinusoidal active uptake mechanism(s). In contrast to APV that exhibits a xlogP value of 1.8, NFV, RTV, and LPV have higher xlogP values (4.6, 3.9, and 3.9). Therefore, the hepatocyte uptake of NFV, RTV or LPV is likely to be primarily mediated by passive diffusion, and the contribution of sinusoidal active uptake may only be significant in the hepatic uptake of APV. Further studies are needed to identify this transporter(s). It would also be interesting to determine if PIs not studied here (e.g., darunavir) are substrates of this unidentified transporter(s). Based on our results, we propose that inhibitors and/or inducers of hepatic uptake transporters (including OATPs) will not affect the hepatic disposition of NFV, RTV or LPV. However, all four PIs are OATP inhibitors in both SCHH and OATP-transfected cell lines, and therefore have the potential to produce, and in some cases do produce, clinically significant OATP-based DDI (e.g., with statins) [Busti et al., 2008; Kiser et al., 2008].

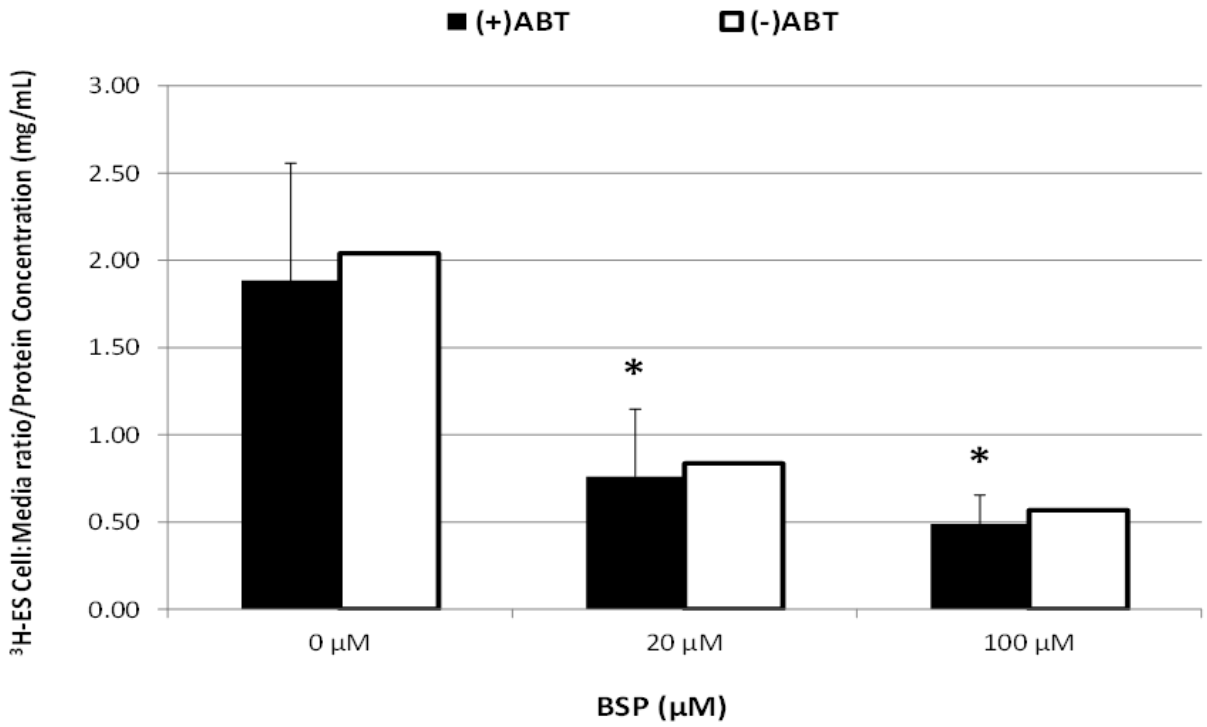

Figure 3.1: The hepatic uptake of ^{3}H-ES (1 µM), an OATP positive control transport substrate, was not affected by 1 h pre-treatment of 5 mM ABT (N=3 donor sources; N=2 donor sources in the absence of ABT). However, the uptake of ^{3}H-ES, in the presence of ABT was decreased by 2.67 or 3.84-fold in the presence of 20 or 100 µM BSP, respectively, confirming robust OATP expression in SCHH (*p<0.05; mean ± SD, N=3 donor sources).

A)

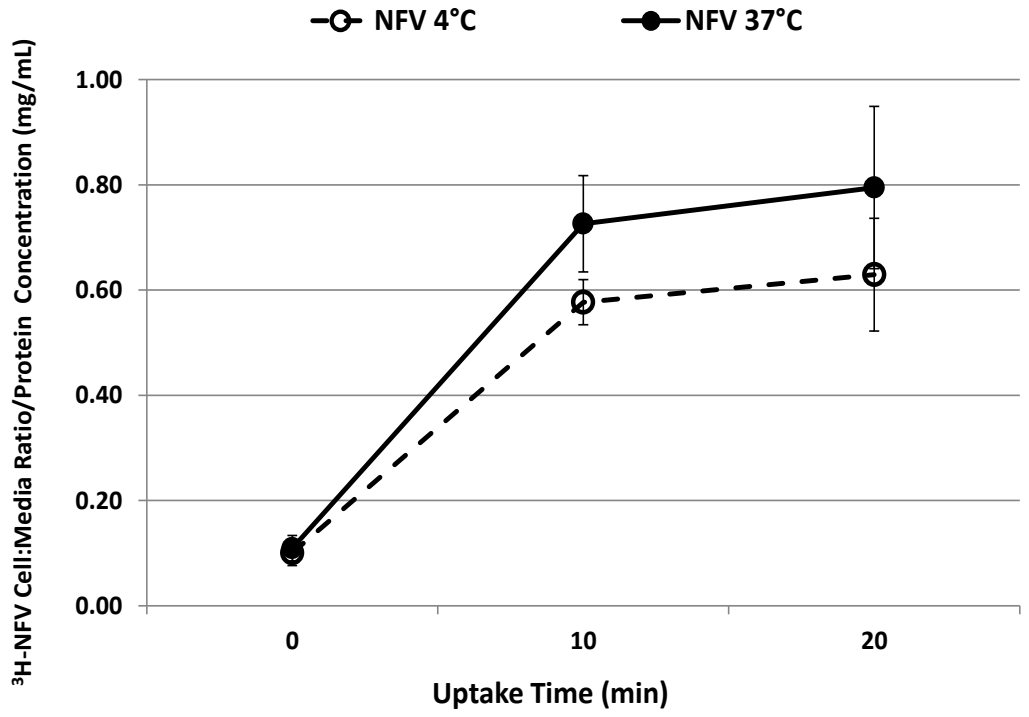
NFV 4°C
NFV 37°C
1.00
0.80
0.60
0.40
0.20
0.00
^{3}H-NFV Cell:Media Ratio/Protein Concentration (mg/mL)
0
10
20
Uptake Time (min)

B)

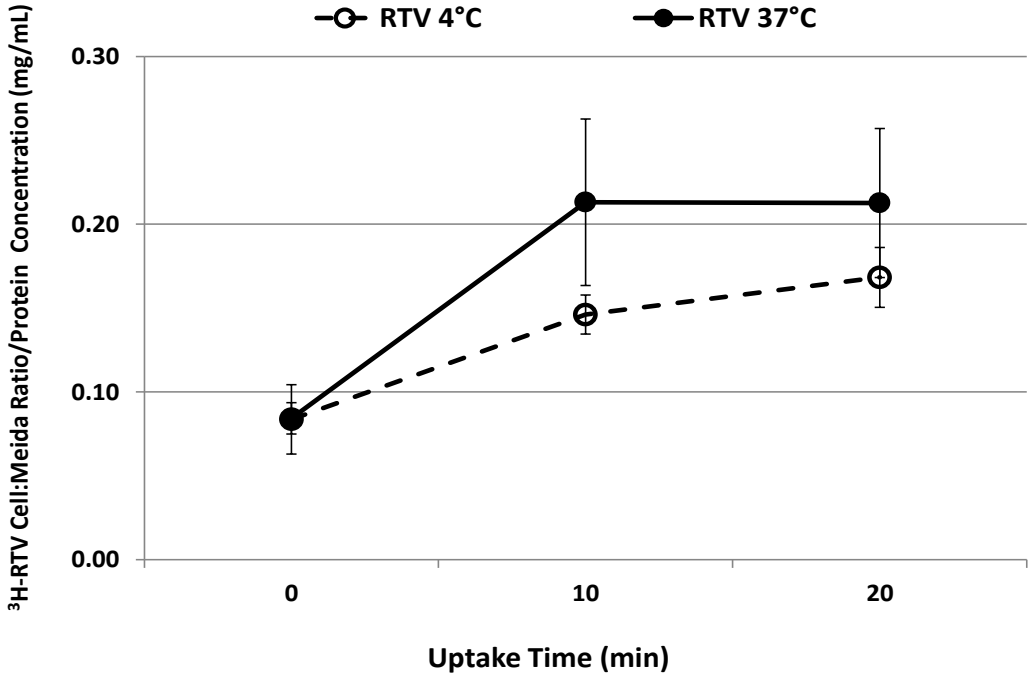
RTV 4°C
RTV 37°C
0.30
0.20
0.10
0.00
^{3}H-RTV Cell:Meida Ratio/Protein Concentration (mg/mL)
0
10
20
Uptake Time (min)

C)

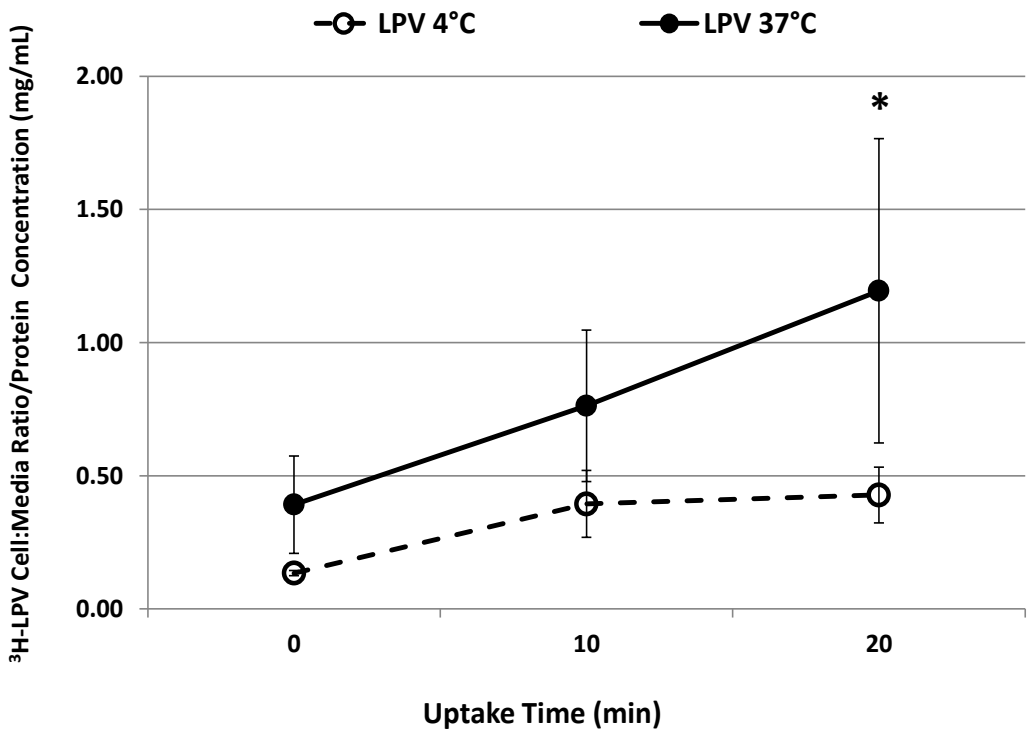
LPV 4°C
LPV 37°C
2.00
1.50
1.00
0.50
0.00
*
0
10
20
Uptake Time (min)
³H-LPV Cell:Media Ratio/Protein Concentration (mg/mL)

D)

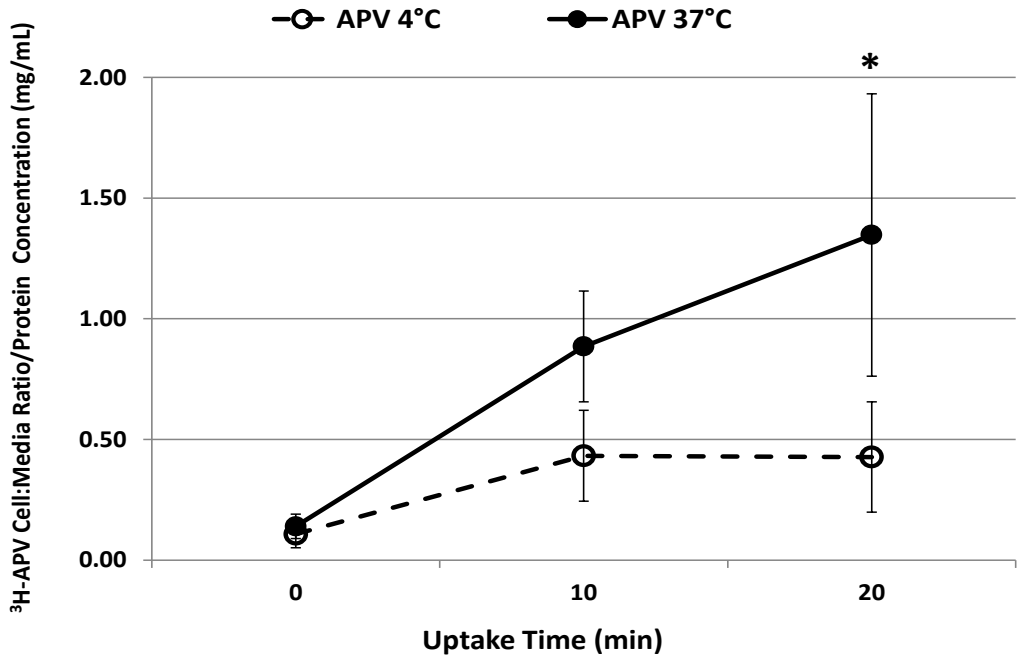
APV 4°C
APV 37°C
2.00
1.50
1.00
0.50
0.00
*
0
10
20
Uptake Time (min)
³H-APV Cell:Media Ratio/Protein Concentration (mg/mL)

Figure 3.2: Of the four PIs, only ^{3}H-APV **(D)** and ^{3}H-LPV **(C)** demonstrated statistically significant decrease in their 20 min SCHH uptake at 4°C vs. 37°C. These results indicate that ^{3}H-NFV **(A)** and ^{3}H-RTV **(B)** are not transported into SCHH. Data are expressed as mean ± SD, N=3 donor sources. *p=0.05

A)

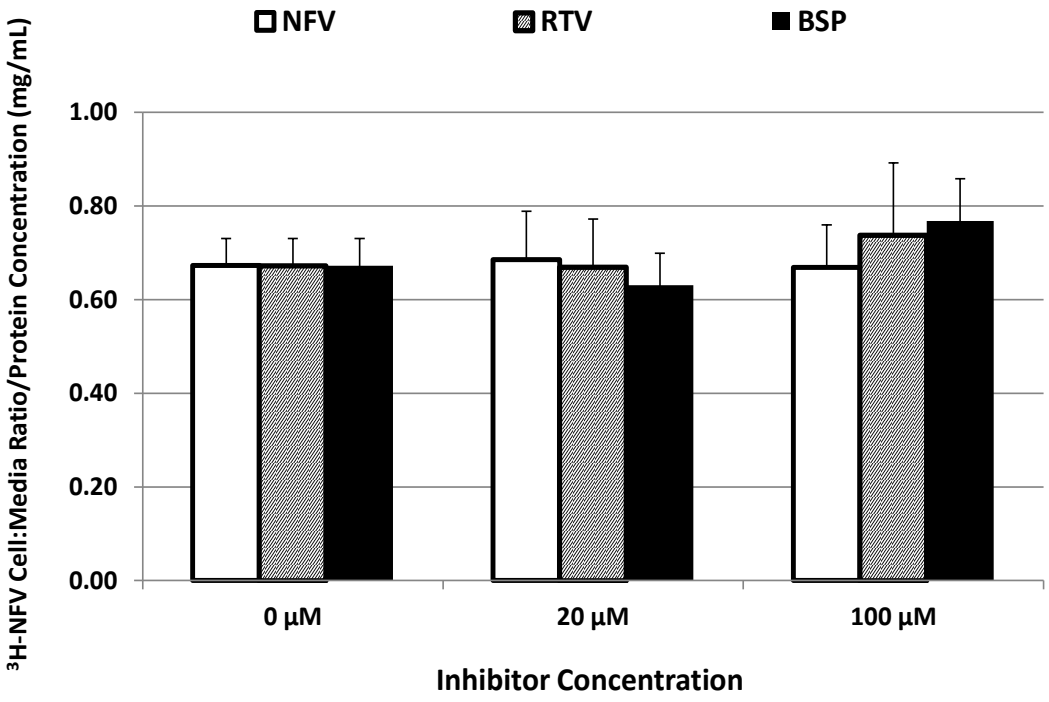
NFV
RTV
BSP
1.00
0.80
0.60
0.40
0.20
0.00
^{3}H-NFV Cell:Media Ratio/Protein Concentration (mg/mL)
0 µM
20 µM
100 µM
Inhibitor Concentration

B)

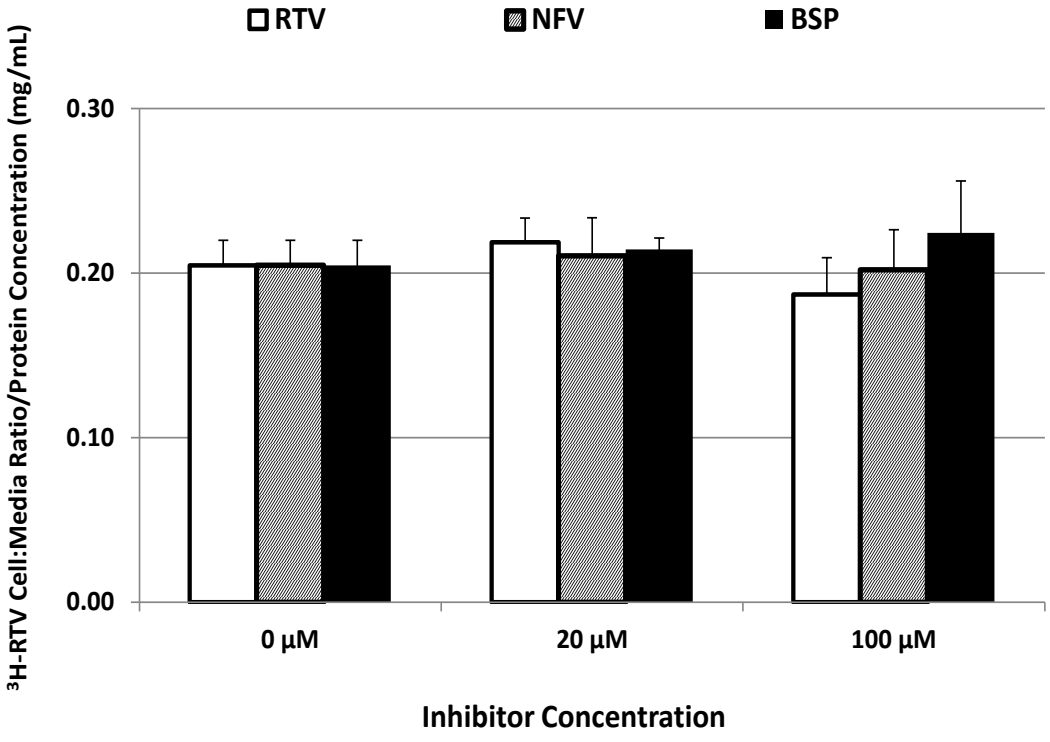
RTV
NFV
BSP
0.30
0.20
0.10
0.00
^{3}H-RTV Cell:Media Ratio/Protein Concentration (mg/mL)
0 µM
20 µM
100 µM
Inhibitor Concentration

C)

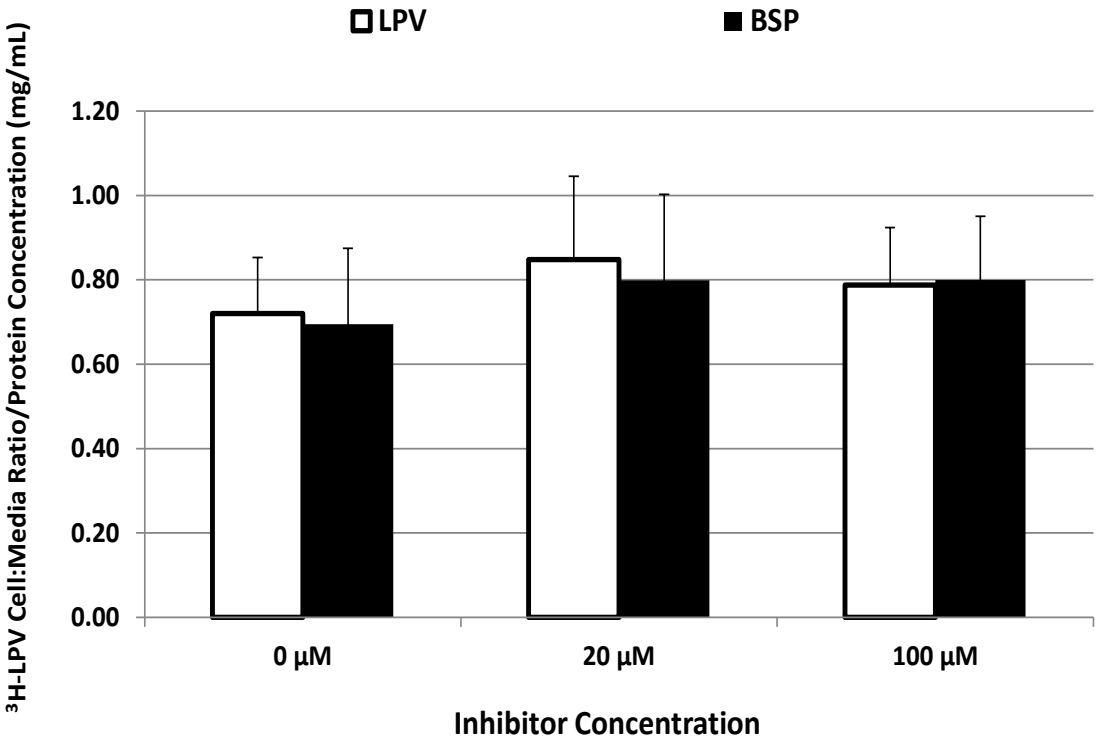
LPV
BSP
1.20
1.00
0.80
0.60
0.40
0.20
0.00
^{3}H-LPV Cell:Media Ratio/Protein Concentration (mg/mL)
0 µM
20 µM
100 µM
Inhibitor Concentration

D)

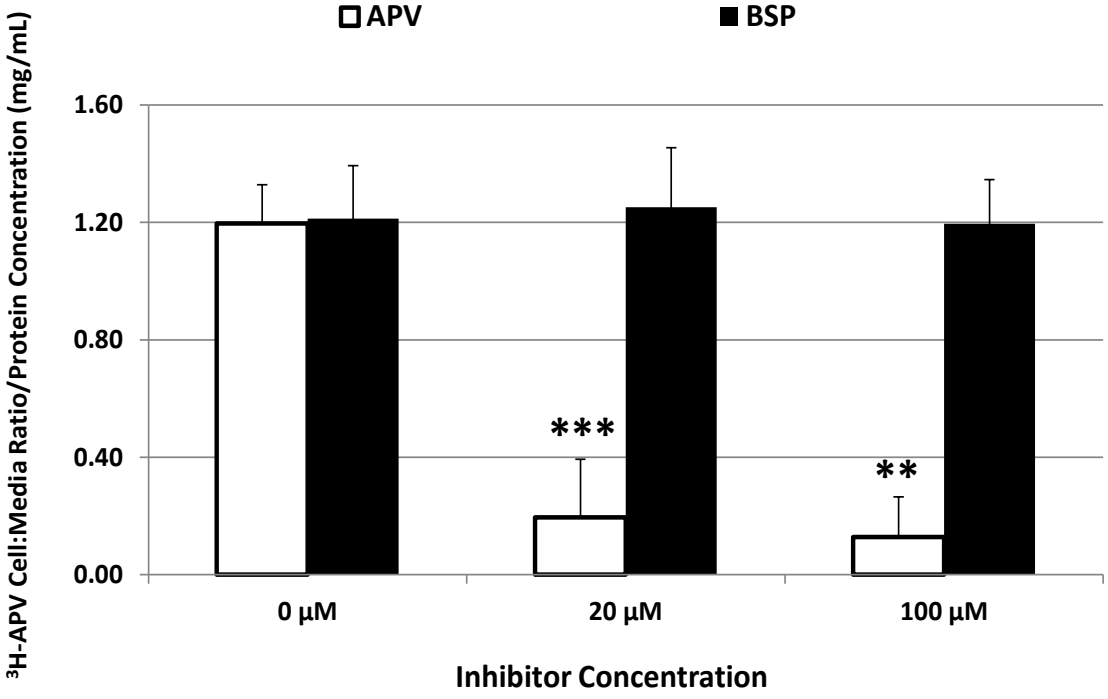
APV
BSP
1.60
1.20
0.80
0.40
0.00
^{3}H-APV Cell:Media Ratio/Protein Concentration (mg/mL)
***
**
0 µM
20 µM
100 µM
Inhibitor Concentration

Figure 3.3: The SCHH uptake of all of the ^{3}H-PIs, **(A)** ^{3}H-NFV, **(B)** ^{3}H-RTV, **(C)** ^{3}H-LPV, **(D)** ^{3}H-APV, was not affected by BSP (20 or 100 µM). Likewise, except for ^{3}H-APV, the uptake of the ^{3}H-PIs was unaffected in self-inhibition studies (in the presence of unlabeled PIs). The uptake of ^{3}H-APV **(D)**, was significantly decreased (6.04±1.52 fold, ***p<0.001 and 9.39±1.20 fold, **p<0.01) by unlabeled APV (20 or 100 µM, respectively). Data are expressed as mean ± SD, N=3 donor sources.

A)

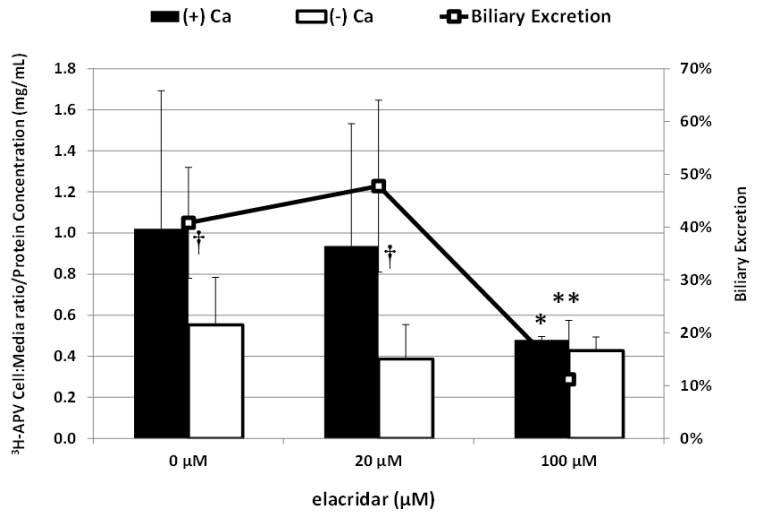
(+) Ca
(-) Ca
Biliary Excretion
^{3}H-APV Cell:Media ratio/Protein Concentration (mg/mL)
Biliary Excretion
1.8
1.6
1.4
1.2
1.0
0.8
0.6
0.4
0.2
0.0
70%
60%
50%
40%
30%
20%
10%
0%
†
†
*
**
0 µM
20 µM
100 µM
elacridar (µM)

B)

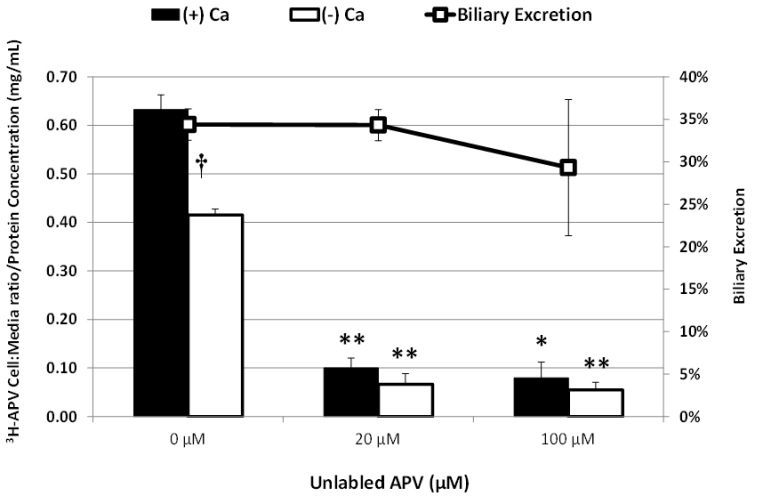
(+) Ca
(-) Ca
Biliary Excretion
^{3}H-APV Cell:Media ratio/Protein Concentration (mg/mL)
Biliary Excretion
0.70
0.60
0.50
0.40
0.30
0.20
0.10
0.00
40%
35%
30%
25%
20%
15%
10%
5%
0%
†
**
**
*
**
0 µM
20 µM
100 µM
Unlabled APV (µM)

C)

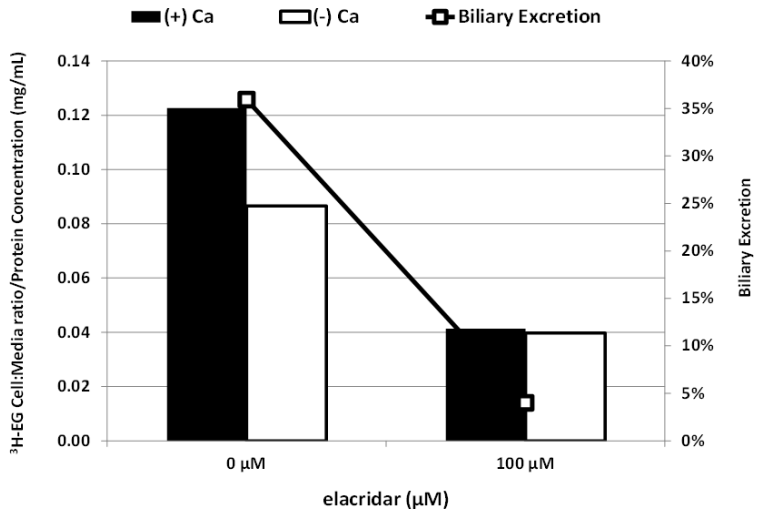
(+) Ca
(-) Ca
Biliary Excretion
^{3}H-EG Cell:Media ratio/Protein Concentration (mg/mL)
Biliary Excretion
0.14
0.12
0.10
0.08
0.06
0.04
0.02
0.00
40%
35%
30%
25%
20%
15%
10%
5%
0%
0 µM
100 µM
elacridar (µM)

Figure 3.4: (A) SCHH uptake of ^{3}H-APV in the presence of Ca^{2+} was significantly greater than that in the absence of Ca^{2+} under all conditions (†: $p<0.05$), except when elacridar was present at 100 µM concentration. As a result, biliary efflux of ^{3}H-APV remained unchanged in the presence of 20 µM elacridar, but was decreased from ~40% to 11% (~3.9-fold, **$p<0.01$) in the presence of 100 µM elacridar. Data are expressed as mean ± SD, N=4 donor sources. **(B)** In the presence of unlabeled APV (20 or 100 µM), the biliary excretion of ^{3}H-APV was unaffected and remained at ~35%. The hepatocyte uptake of ^{3}H-APV under the Ca^{2+} plus or Ca^{2+} minus condition was significantly decreased in the presence of 20 µM APV (Ca^{2+} plus or Ca^{2+} minus: ~6-fold; **$p < 0.01$), or 100 µM APV (~8-fold; Ca^{2+} plus: *$p < 0.05$, or Ca^{2+} minus: **$p < 0.01$). Data are expressed as mean ± SD, N=3 donor sources. **(C)** Biliary efflux of ^{3}H-EG (positive control) in the absence and presence of elacridar confirmed intact canalicular network and the expression of the canalicular efflux transporters in the SCHH. In the presence of elacridar and under the Ca^{2+} minus condition, the decrease in SCHH uptake of ^{3}H-EG was likely due to inhibition of OATPs. Data are expressed as mean, N=2.

A)

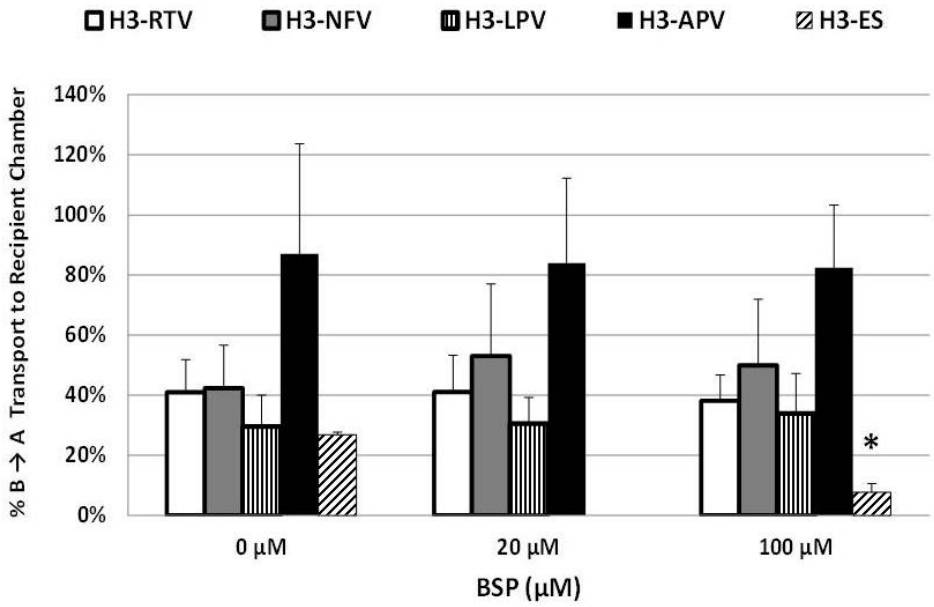

B)

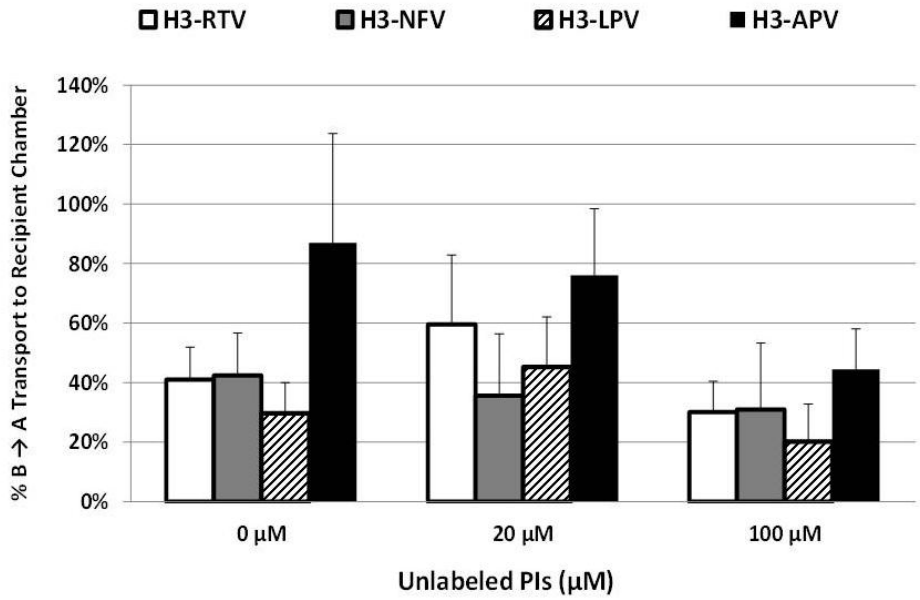

Figure 3.5. ^{3}H-PIs B→A was unaffected by the presence (20 or 100 µM) of BSP **(A)**, or unlabeled PIs **(B)**. The B→A transport of ^{3}H-ES **(A)** across the MDCKII-OATP1B1 Transwell monolayer was significantly decreased in the presence of BSP, confirming robust OATP1B1 expression. Data are expressed as mean ± SD; N=7 in the absence of BSP, N=3 in the presence of BSP, N=4 in the presence of unlabeled PI.

Chapter 4: Quinidine Inhibition of P-glycoprotein at the Human Blood-Brain Barrier as Measured by Positron Emission Tomography Imaging

4.1 Abstract

Permeability-glycoprotein (P-glycoprotein, P-gp), an efflux transporter at the human blood-brain barrier (BBB), is believed to be a significant obstacle in the central nervous system (CNS) delivery of P-gp substrate drugs. Using Positron Emission Tomography (PET) imaging, we have shown that the brain extraction ratio (ER) or cerebral blood flow (CBF)-normalized distribution clearance (K1) of ^{11}C-verapamil radioactivity into the brain can be modestly increased (by 40%) in the presence of the P-gp inhibitor, cyclosporine-A (CsA). In this study, we determined if this inhibition (as measured by ER) could be greater with an approved P-gp inhibitor, quinidine, and whether it could be predicted from preclinical experimental models. Healthy volunteers were administered ^{15}O-water and ^{11}C-verapamil, in the absence or presence of quinidine, to assess CBF and BBB P-gp activity, respectively. We used three different data analysis approaches (noncompartmental, compartmental and parametric maps) and accounted for potential confounders that could influence the interpretation of our data (e.g., changes in CBF, ^{11}C-verapamil metabolism, and verapamil plasma protein binding). At clinically relevant plasma concentrations, quinidine can inhibit P-gp at the human BBB to a greater extent than CsA (~90% vs. 40% increase in ER). In agreement with previous findings from us and others, we found that when BBB P-gp is inhibited, K1 and ER of ^{11}C-verapamil radioactivity were increased while the

efflux rate of ^{11}C-verapamil radioactivity out of the brain (k_2) remained unchanged. Additionally, the magnitude of BBB P-gp inhibition by quinidine was successfully predicted by a combination of *in vitro* and *in vivo* macaque data, but not rat data. Although quinidine did not completely inhibit P-gp, it has the potential to produce clinically significant CNS drug-drug interactions with P-gp substrate drugs with a narrow therapeutic window that are significantly excluded from the brain by P-gp. Finally, to determine the utility of inhibiting P-gp to improve CNS delivery of drugs, more potent and selective P-gp inhibitors that are clinically approved are needed.

4.2 Introduction

The poor brain delivery of many central nervous system (CNS) drugs has been widely attributed to the ATP-binding cassette efflux transporter, permeability-glycoprotein (P-gp), expressed at the blood-brain barrier (BBB). The functional importance of P-gp at the BBB was first confirmed in P-gp chemical inhibition and knockout studies in rodents [Kim et al., 1998; Kemper et al., 2004], suggesting that when P-gp activity at the human BBB is inhibited, drastic increase in the CNS distribution of P-gp substrate drugs may occur, resulting in significant drug-drug interactions (DDI) that could lead to increased CNS toxicity and/or enhanced efficacy of these drugs.

We provided the first **direct** evidence of P-gp's importance at the **human** BBB in a clinical study using Positron Emission Tomography (PET) imaging [Sasongko et al., 2005], where the brain uptake of the P-gp radiolabeled substrate, ^{11}C-verapamil radioactivity, was increased by 88% (ratio of AUC_{brain}: AUC_{blood} [AUCR]) or 40% (extraction ratio [ER] or

cerebral blood flow [CBF]-normalized distribution clearance, K1) in the presence of the P-gp inhibitor, cyclosporine-A (CsA). Since then, the largest magnitude of P-gp inhibition at the human BBB has been observed in the brain uptake of (R)-^{11}C-verapamil radioactivity (~3.4-fold increase in K1), after administration of an experimental P-gp inhibitor, tariquidar [Bauer et al., 2012]. Since tariquidar is not approved for human administration, an approved drug that could more potently inhibit P-gp at the human BBB than CsA is needed. This is not only important in quantifying the maximum potential for unintended P-gp based DDIs at the human BBB, but is also essential for further investigation of the utility of P-gp inhibition to increase CNS delivery of P-gp substrate drugs (e.g., treatment of brain tumors). Amongst the clinically approved drugs that can potently inhibit P-gp, quinidine, based on its ability to inhibit P-gp *in vitro* (EC_{50}: 0.9 μM) and its unbound therapeutic plasma concentration (C_u: 1.3 μM; C_u/EC_{50}: 1.4) is predicted to produce significantly greater inhibition of P-gp at the human BBB (by ~4 fold) than CsA (EC_{50}: 0.6 μM; C_u: 0.2 μM; C_u/EC_{50}: 0.3) [Hsiao et al., 2008]. Interestingly, in humans, quinidine produces a significant CNS DDI (increased respiratory depression) with loperamide, a peripheral opiate and P-gp substrate that normally does not produce any CNS effects because it is excluded from the CNS by BBB P-gp [Sadeque et al., 2000]. However, this DDI remains controversial, as it has not been reproduced by others [Vandenbossche et al., 2010], perhaps because measurement of the CNS pharmacological effect of loperamide is indirect and therefore may not have the required sensitivity. PET imaging, however, can provide superior quantification of quinidine's ability to inhibit human BBB P-gp, as it is quantitative, non-invasive and exquisitely sensitive.

In the drug development process, it is important to predict the "liability" of a new chemical entity to produce P-gp based DDI at the human BBB and also, its susceptibility to be a victim of such a DDI. Therefore, it is important to develop and validate preclinical models (*in*

vitro and animal models) to predict P-gp based DDIs at the human BBB. We have previously shown that the rat, in combination with *in vitro* studies in cells expressing MDR1 (human P-gp), successfully predicted the CsA-^{11}C-verapamil DDI at the human BBB [Hsiao et al., 2006]. However, confirmation studies with other P-gp inhibitors are needed. This is especially important for P-gp since it is known to exhibit multiple binding sites and demonstrate allosteric interactions [Martin et al., 2000; Zolnerciks et al., 2011].

Previously, when we evaluated the inhibition by CsA of P-gp activity at the human BBB by compartmental modeling of the ^{11}C-verapamil PET imaging data [Muzi et al., 2009], we showed that it was the distribution clearance of ^{11}C-verapamil radioactivity into the brain (K1) that was increased rather than the efflux rate constant out of the brain (k_2). This is consistent with the concept that P-gp is a gatekeeper at the BBB, preventing entry of drugs into the brain parenchyma [Aller et al., 2009]. Indeed others, using the same or different P-gp PET ligands have confirmed this finding [Bauer et al., 2012; Kreisl et al., 2010; Bankstahl et al., 2008; Liow et al., 2009]. However, some have claimed that when P-gp is inhibited at the BBB, K1 is not affected, instead k_2 is decreased [Bart et al., 2003; Lubberink et al., 2007]. Therefore, the study presented here provided another an opportunity to re-examine whether our previous finding that inhibition of P-gp at the BBB results in an increase in K1 or a decrease in k_2.

In summary, the objectives of this study in healthy human volunteers using PET-imaging and ^{11}C-verapamil were to: 1) quantify quinidine's ability to inhibit P-gp at the BBB at therapeutic plasma concentrations of the drug; 2) predict the resulting quinidine-^{11}C-verapamil DDI from preclinical experimental models; and 3) confirm that inhibitory DDIs at the human BBB result in an increase in the K1 and ER (K1/CBF) of ^{11}C -verapamil radioactivity, rather than a decrease in k_2.

4.3 Materials and Methods

4.3.1 Subjects

Nine healthy volunteers (5 men and 4 women; 20-42 years old; 61-98 kg body weight) completed the study. Subjects were excluded if they had chronic medical conditions or were breast-feeding, pregnant, smokers, taking long-term medications (except for stable doses of oral contraceptives for women), or had a history of substance abuse. No short-term medication (other than acetaminophen) was allowed for 24 hr before the imaging visit. Caffeine-containing beverages were not allowed on the day of study imaging. Potential subjects underwent a screening visit with medical history review, physical examination, EKG, complete blood-cell count, hepatic and renal function tests, and pregnancy tests for women. Those with normal evaluations were recruited for the study. The study was approved by the University of Washington's Human Subjects Review Committee, Radiation Safety Committee, and Radioactive Drug Research Committee (Seattle, Washington). Informed consent was obtained from each subject.

4.3.2 Chemicals and Reagents

Racemic verapamil and verapamil metabolites (norverapamil, D-617, D-717) were obtained from the sources described previously [Sasongko et al., 2005]. SPE C_8 cartridges (1 mL, 100 mg) were purchased from Varian (Lake Forest, CA, USA). Ultrafiltration devices were purchased from Amicon Centrifree Micropartition Device (Bedford, MA, USA). All other reagents were of the highest grade available from commercial sources.

4.3.3 Radiopharmaceuticals

The radiosynthesis of ^{15}O-water and ^{11}C-verapamil was as previously described [Sasongko et al., 2005]. All PET tracers were greater than 99% radiochemically and chemically pure, with a specific activity of approximately 62.6 TBq /mmol at the end of radiosynthesis. ^{3}H-verapamil (verapamil [N-methyl ^{3}H] hydrochloride; 2.2 TBq/mmol) was purchased from American Radiolabeled Chemicals, Inc. (St. Louis, MO, USA).

4.3.4 Experimental Study Design

This substudy was part of a larger study to evaluate inhibition and induction of P-gp activity at the human BBB by quinidine and rifampin, respectively. The study was divided into two arms with subjects assigned to Arms A or B. Subjects in Arm A were first imaged in the absence or presence of quinidine (consecutive studies on the same day). Then, they were imaged again after 10-21 days of rifampin (600 mg QD) treatment. Subjects in Arm B were studied in the reverse order, e.g., first imaged after 10-21 days of rifampin treatment followed by 20-42 days of washout, and then imaged in the absence or presence of quinidine. Here we present the results from the quinidine substudy; the rifampin study will be the focus of another manuscript.

On the imaging days, a negative pregnancy test was performed to confirm the eligibility of women volunteers. Each subject had catheters inserted in both arms (antecubital veins), one with two separate lines for PET tracer injections and quinidine venous blood sampling, and the other catheter for quinidine infusion. In the arm used for quinidine infusion, the radial artery was catheterized for arterial blood sampling during PET-imaging. Each subject's head was immobilized during the PET imaging studies using a custom-made thermoplastic mask and head-holder.

The PET imaging experimental design and image acquisition followed the study sequence described previously with the modifications illustrated in Figure 4.1 [Sasongko et al., 2005]. Within 1 week of the PET studies, the subjects underwent magnetic resonance (MR) imaging of their brain (T1- and T2-weighted images) to provide anatomic information for the construction of region-of-interest (ROI) PET analysis. Subjects were evaluated post-study (1 to 2 weeks after the imaging session), with all tests performed at the screening visit, except for the EKG and the pregnancy test.

4.3.5 Blood Sample Collection and Processing

Arterial blood samples (1 mL) during both PET imaging sessions (baseline and quinidine treatment) were collected as follows, ^{15}O-water (first 1 min: every 5 sec; 1-2 min: every 15 sec; 2-4 min: ever 30 sec; and then at 5 min), and ^{11}C-verapamil (first 1 min: every 15 sec; 1-2 min: every 20 sec; 2-3 min: every 30 sec; 3-8 min: every 1 min; 8-12 min: every 2 min; and then at 15 and 20 min). ^{15}O-water blood radioactivity in pre-weighed gamma-counting tubes, and ^{11}C-verapamil blood and plasma radioactivity were determined using a gamma counter (Cobra Counter; Packard Corporation, Meriden, CT).

In addition, arterial blood samples (2 mL) were collected during both sets of ^{11}C-verapamil PET imaging at 5, 10, and 20 min to quantify the radioactivity content of ^{11}C-verapamil and its known ^{11}C-dealkylated metabolites (D-617, D-717) and ^{11}C-N-demethylated metabolites (polar species) in the plasma at baseline or in the presence of quinidine via solid-phase extraction (SPE) and HPLC methods described previously [Sasongko et al., 2005; Unadkat et al., 2008].

4.3.6 Quantification of Quinidine Plasma Concentration

To measure quinidine plasma concentrations, venous blood samples (2 mL) were drawn at 0, 15, 30, 45, 60, and 80 min after the start of quinidine infusion (or the last sample was taken at the end of the second ^{11}C-verapamil PET imaging). The calibrators were prepared in human plasma (quinidine concentration range: 1 – 15 µM). For each subject, the quality control samples (QCs; quinidine concentrations: 1 µM, 4 µM, and 15 µM) were prepared using their plasma, and processed along with the venous plasma samples collected during the PET-imaging studies. All plasma samples (800 µL) were spiked with equal volume of acetonitrile containing 1 µg/mL Hoechst 33258 (internal standard), and processed in duplicate as previously described [Reece et al., 1980]. The supernatants were then reconstituted in the HPLC mobile phase (initial elution gradient condition), and 50 µL were injected onto the HPLC. HPLC separation was achieved using Agilent XDB C18 2.1 x 50 mm, 5 µm column, and the analytes (quinidine at 250 nm, retention time 3.5 min; internal standard: Hoechst 33258 at 350 nm, retention time 5 min) were eluted with 1% formic acid 0.1 M potassium phosphate in water at pH=3.30 (solvent A), and 1% formic acid in acetonitrile (solvent B). For the first 3 min, the gradient was maintained at 90% solvent A, then a linear decrease to 60% solvent A until 8 min, and then cycled back to initial conditions.

4.3.7 Verapamil Plasma Protein Binding

The unbound verapamil fraction in pooled plasma samples (n=3 subjects), collected before (baseline) or after 1 hr of quinidine infusion during the PET-imaging studies, was measured by ultrafiltration in triplicates as described before [Sasongko et al., 2005].

4.3.8 Image Processing

Both the PET image acquisition and reconstruction were conducted as described previously [Sasongko et al., 2005]. Regions of interest (ROIs) for three tissue types/brain regions (whole brain, gray matter, or white matter) were identified on the coregistered PET-MR images manually, and extended continuously to an average of 18 slices (~6 cm) to create volumes of interest (VOIs) for each tissue type. VOIs were applied to both the ^{15}O-water and ^{11}C-verapamil dynamic images to determine decay corrected radioactivity concentration in each brain region.

4.3.9 Noncompartmental Analysis

After decay correction, the area under the ^{11}C-verapamil radioactivity concentration-time curve in the brain region ($AUC_{brain\ region}$; whole brain, gray matter or white matter) or blood (AUC_{blood}) was calculated from ^{11}C-verapamil PET imaging at baseline or in the presence of quinidine using the trapezoidal rule. The percent increase in the ratio of $AUC_{brain\ region}$: AUC_{blood} (AUCR) produced by quinidine was computed.

4.3.10 Compartmental Analysis

Regional CBF for the whole brain, gray matter or white matter was estimated for each subject by fitting a flow-dispersion model to the first 2 min of the ^{15}O-water tissue time-activity curves in the respective brain tissue using the PKIN module in PMOD (PMOD Technologies).

A 1-tissue compartment (1-TC) compartment model has been shown to be the best model to estimate the distribution clearance of ^{11}C-vearpamil radioactivity into the brain (K1) at baseline and in the presence of CsA [Muzi et al., 2009]. To confirm this finding, we analyzed

our data with a 1-TC model with different duration of data sets (10 min or 20 min) and input functions (total plasma radioactivity; ^{11}C-verapamil plus ^{11}C-verapamil metabolites that are P-gp substrates [^{11}C-dealkylated metabolites]; or a dual input function that modeled simultaneously and separately the ^{11}C-radioactivity contributed by P-gp substrates and non P-gp substrates [^{11}C-polar metabolites]) using PKIN software (PMOD Technologies). An average value of human brain tissue blood volume (V_b: 0.044 mL/g) determined previously [Sasongko et al., 2005], was incorporated as a fixed constant when estimating CBF and $K1_p$ (based on plasma data). Weights were set at $1/Y^2$. The model that best estimated the $K1_p$ of ^{11}C-verapamil radioactivity was determined by evaluating the Akaike information criterion (AIC), runs test, visual inspection of the residuals and model fits, and % coefficient of variation (COV) of the $K1_p$ estimates. To determine the brain extraction ratio of ^{11}C-verapamil radioactivity (ER; based on blood data), the ratio of $K1_b$ ($K1_p$ corrected for the individual blood-to-plasma ratio) and CBF was computed.

4.3.11 Parametric Map Analysis

For each subject, parametric maps (PMAPs) of $K1_b$ of ^{11}C-verapamil radioactivity or CBF were generated using a 1-TC compartmental model in PXMOD software (PMOD Technologies) with ^{11}C-verapamil or ^{15}O-water PET dynamic images and the corresponding arterial blood input functions. After coregistering the $K1_b$ or CBF PMAPs to the individual MR images from each subject, the PMAP-MR fused images were then coregistered to the standard brain atlas from FMRIB Software Library (FSL). ER of ^{11}C-verapamil radioactivity was determined using FSL software fslmaths and pixel-by-pixel division of the $K1_b$ PMAPs by the CBF PMAPs. The final $K1_b$ and ER results were then evaluated using a non-parametric voxel-by-voxel paired t-test with multiple comparison correction using the Threshold-Free Cluster

Enhancement option from Software randomise. The multiple comparison correction was performed based on cluster statistical characteristics such as extent of cluster size.

4.3.12 Statistical and Data Analysis

Data are expressed as mean ± SD, and analyzed using a Student paired *t* test, with the significance level set at $p < 0.05$.

4.4 Results

These 9 volunteers successfully completed both the PET (baseline and quinidine) and MR imaging protocol without any unexpected side effects.

The accuracy and precision of the quinidine assay based on the three QC samples were acceptable (< 12% error and < 5% COV). Using this method, the mean ± SD quinidine total pseudo steady-state plasma concentration during the second ^{11}C-verapamil PET-imaging session was 8.3 ± 1.4 µM (1.3 ± 0.3 µM unbound). The quinidine concentrations achieved for all subjects were below or within the therapeutic range (9 – 15 µM) [Brunton et al., 2011].

The blood-to-plasma ratio of ^{11}C-verapamil radioactivity during PET imaging was not significantly affected by quinidine (baseline 0.77 ± 0.06 vs. in the presence of quinidine 0.81 ± 0.08; $p > 0.05$). Verapamil fraction unbound in plasma did not differ significantly between baseline and in the presence of quinidine (7.6% ± 0.7% vs. 9.1% ± 0.9%; $p > 0.05$), and was consistent with literature reported value of 10% [Brunton et al., 2011].

Quinidine did not significantly affect the average CBF (e.g., gray matter: baseline= 0.47 ± 0.17 mL/min/g vs. quinidine= 0.43 ± 0.18 mL/min/g; $p > 0.05$), or the difference in CBF

between white matter and gray matter (Figure 4.2). The average white matter or gray matter CBF values at baseline estimated in this study were in agreement with the historical data compiled from multiple sources [Aslan et al., 2011; Reich et al., 1989]. However, the individual CBF did vary, and therefore were used for all subsequent data analysis.

As expected, quinidine (a potent CYP2D6 inhibitor) treatment had no significant ($p > 0.05$) effect on ^{11}C-verapamil metabolism, which is primarily mediated by CYP2Cs and CYP3A4 to form the ^{11}C-dealkylated metabolites (P-gp substrates) and ^{11}C-N-demethylated metabolites (polar species and non P-gp substrates), respectively (Figure 4.3) [Tracy et al., 1999; Pauli-Magnus et al., 2000]. Similar to our previous findings, at 5 min and 10 min of the PET imaging sessions, ~85% of the total plasma radioactivity was attributed to P-gp substrates, with little contribution from non-P-gp substrates.

Quinidine significantly increased, by ~60-70% ($p < 0.001$; Figure 4.4A; Table 4.1), the distribution of ^{11}C-verapamil radioactivity (as measured by the AUCR) into the whole brain (baseline: 0.25 ± 0.06; quinidine: 0.40 ± 0.08), gray matter (baseline: 0.28 ± 0.06; quinidine: 0.45 ± 0.09) or white matter (baseline: 0.18 ± 0.04; quinidine: 0.30 ± 0.07). The AUCR was significantly greater for gray matter than for white matter at baseline and in the presence of quinidine.

Consistent with our previous finding [Muzi et al., 2009], a 1-TC model using the single input function consisting of total plasma radioactivity (AIC values for 10 and 20 min data of 19 and 20, respectively) for estimating $K1_p$ and k_2 of ^{11}C-verapamil radioactivity at baseline and in the presence of quinidine, was equivalent or better than using other input functions (^{11}C-verapamil radioactivity contributed by P-gp substrates [AIC values for 10 and 20 min data of 24 and 23, respectively]; or dual input function of ^{11}C-verapamil radioactivity contributed by P-gp

substrates or non P-gp substrates [AIC values for 10 and 20 min data of 21 and 19, respectively]). To minimize the ^{11}C-verapamil metabolites from confounding our results, we limited our data analysis to the first 10 min. Quinidine significantly increased the mean $K1_b$ of ^{11}C-verapamil radioactivity into the gray matter by ~40-50% (e.g., gray matter, baseline: 0.06 ± 0.01 mL/min/g; quinidine: 0.09 ± 0.01 mL/min/g) ($p < 0.001$; Figure 4.4B; Table 4.1), but did not affect k_2 (e.g., gray matter, baseline: 0.1 ± 0.01 min^{-1}; quinidine: 0.1 ± 0.02 min^{-1}). Quinidine significantly increased the ER of ^{11}C-verapamil radioactivity by ~70-90% ($p < 0.05$; Figure 4.4C; Table 4.1), in the whole brain (baseline: 0.15 ± 0.04; quinidine: 0.25 ± 0.14), gray matter (baseline: 0.15 ± 0.04; quinidine: 0.25 ± 0.13), and white matter (baseline: 0.13 ± 0.04; quinidine: 0.25 ± 0.15). After CBF normalization, the significant regional difference observed in the $K1_b$ of ^{11}C-verapamil radioactivity between gray matter and white matter at baseline and in the presence of quinidine was eliminated (Figure 4.4C). The $K1_b$ and AUCR of ^{11}C-verapamil radioactivity were significantly correlated for the whole brain, gray matter, and white matter with correlation coefficients of 0.82, 0.84, and 0.85, respectively.

Results from both the noncompartmental and compartmental analyses were further confirmed through the parametric maps, which illustrate the brain regions where statistically significant increases in $K1_b$ ($p < 0.02$) or ER ($p < 0.05$) of ^{11}C-verapamil radioactivity were observed (Figure 4.5). The significant increases observed were uniform across the prefrontal, frontal, temporal, parietal, and occipital lobes.

We evaluated the ability of two animal models, the rat and the macaque, in combination with *in vitro* data in MDR1-expressing cells, to predict the magnitude of P-gp inhibition by quinidine at the human BBB. Based on the maximal increase in the distribution of ^{11}C-verapamil radioactivity into the animal brains [Hsiao et al., 2006; Eyal et al., 2009] when P-gp was

completely inhibited (macaque: 3.4-fold, rat: 11.6-fold), the fractional contribution by P-gp were computed (macaque: 0.92; rat: 0.79). Then, we assumed that the inhibitory properties of quinidine (*in vitro* EC_{50}: 0.9 μM and γ: 0.8) determined using LLCPK-cells stably transfected with MDR1 [Hsiao et al., 2008] applies to the *in vivo* inhibition of P-gp at the human BBB. Based on these data and assumptions, the macaque and rat models predicted ~112% and ~554% increase in the brain distribution of ^{11}C-verapamil radioactivity in human at the average plasma quinidine unbound concentration (C_u = 1.3 μM) observed in our study.

4.5 Discussion and Conclusions

To evaluate P-gp inhibition by quinidine, we adopted three different approaches in analyzing our data, noncompartmental, compartmental and parametric map analyses. Each approach provided a unique perspective on our data. The advantage of using the noncompartmental or the AUCR approach is that it is nonparametric and therefore free of any compartmental model assumptions. It provides an *in vivo* assessment of the ^{11}C-verapamil radioactivity partition coefficient into the brain with reference to the ^{11}C-verapamil radioactivity in the systemic circulation. However, this nonparametric approach cannot discern the influence of CBF or ^{11}C-verapamil metabolites on the brain distribution of ^{11}C-verapamil radioactivity. In contrast, compartmental analysis can. In addition, this approach allows one to dissect which parameter, K1 or k_2, is affected when P-gp is inhibited. Parametric map analysis provides a third, although qualitative perspective by producing a pictorial map of the brain regions where P-gp is inhibited by quinidine as measured by K1 or ER. These different approaches strengthened our conclusions.

In our data analysis, we took into consideration factors that could potentially alter our data interpretation, such as changes in CBF, ^{11}C-verapamil plasma protein binding or ^{11}C-verapamil metabolism. Plasma protein binding of ^{11}C-verapamil was unaffected by quinidine. This ensures that our interpretation of quinidine's inhibition of P-gp at the human BBB was not confounded by potential transient increase in ^{11}C-verapamil unbound plasma concentration that could result from plasma protein displacement interaction between quinidine and verapamil. Quinidine also did not affect ^{11}C-verapamil metabolism during the first 10 min of PET imaging, thus, we limited all of our data analysis to the 10 min. period.

At the average plasma quinidine unbound concentration achieved during the second ^{11}C-verapamil PET imaging session, the AUCR, increased by ~60-70% for all brain regions studied (Table 4.1). Though variable in magnitude, this increase was observed in all subjects studied. The AUCR was larger for gray matter than white matter (baseline and in the presence of quinidine), which is likely due to differences in CBF to these regions. This AUCR reflects the increased $K1_b$ of ^{11}C-verapamil radioactivity into the brain as shown by the excellent correlation between the two parameters.

Consistent with our findings from the previous CsA PET study, analysis of our data by compartmental modeling showed that the 1-TC compartment model using the single input function of total plasma radioactivity was the best fit to the first 10 min of ^{11}C-verapamil PET imaging data. The goodness of fit of the 1-TC model to the data was not improved with other input functions when the ^{11}C- radioactivity contributed by the ^{11}C-polar metabolites was separated from those contributed by P-gp substrates (^{11}C-verapamil and ^{11}C-dealkylated metabolites). As we hypothesized, these data suggest that the ^{11}C-dealkylated metabolites behaved like ^{11}C-verapamil with respect to their distribution into the brain, and the ^{11}C-polar

metabolites exerted minimal impact on the estimation of $K1_p$. The statistically significant increase in both $K1_b$ and ER of ^{11}C-verapamil radioactivity in the presence of quinidine was confirmed and illustrated by the parametric map analysis, which showed that significant P-gp inhibition was observed virtually across all brain regions protected by the BBB.

Mechanistically, P-gp substrates can be efficiently extracted by P-gp from the membrane bilayer while in transit through the membrane, and/or effluxed out by P-gp after entering the intracellular compartment [Aller et al., 2009]. Both mechanisms should result in increased K1 of P-gp substrates into the brain when P-gp is inhibited. While we and others have previously confirmed this hypothesis, some have found that it is the rate constant k_2 that is affected. Therefore, we reinvestigated this issue with quinidine as the P-gp inhibitor. Indeed, quinidine inhibition of P-gp significantly increased $K1_b$ into the brain (e.g., 36 ± 17% for gray matter) with no significant change in k_2 (3 ± 17% for gray matter).

Conceptually, K1 is the product of tissue extraction (ER; net effect of tissue uptake and P-gp mediated efflux) and blood flow (CBF). For a lipophilic and highly permeable drug, when P-gp is completely inhibited, the extraction of the drug by the brain may be so efficient as to be limited by CBF. In that case, under maximum P-gp inhibition, the brain ER of the drug will reach an upper boundary of unity. Indeed, as we have shown previously [Eyal et al., 2010], we confirmed that the ER of ^{11}C-verapamil radioactivity by the pituitary gland, which resides outside the BBB and therefore lacks tight junctions and P-gp [Nussey et al., 2001], was close to unity (1.13 ± 0.02). Therefore, we propose that the ER of P-gp substrates, rather than K1, be used as a measure of P-gp activity and its modulation at the BBB. Doing so will take into consideration intra-individual variability in CBF (either due to the P-gp inhibitor or a change

with time) when P-gp inhibition is measured using a highly permeable and lipophilic PET ligand such as verapamil.

Another advantage of using the ER as a measure of P-gp inhibition is that it provides a means to predict the maximum possible DDI at the human BBB when only the baseline ER is available through PET studies. This allows an estimation of the maximum liability from such a DDI and determination of the maximum possible magnitude of increase in the CNS delivery of drugs when P-gp is completely inhibited. Currently, the maximum magnitude of P-gp based inhibition cannot be experimentally determined as approved drugs that are P-gp inhibitors (e.g., quinidine or CsA) cannot be safely administered at doses necessary to completely inhibit P-gp at the human BBB (tariquidar is not an approved drug). Based on our data, the maximum possible P-gp based DDI at the human BBB when the victim drug is verapamil (or a drug that is excluded from the brain to a similar degree as verapamil) will be approximately 6-fold. This estimate is in reasonable correspondence with the ~3 fold increase in the brain uptake of ^{11}C-verapamil observed in macaques or humans when P-gp is maximally inhibited by CsA or tariquidar respectively [Bauer et al., 2012; Eyal et al., 2009]. It is also important to note that this maximum level of P-gp inhibition may be considerably greater for substrates that are excluded from the brain by P-gp to an even greater extent than verapamil (e.g., lower baseline ER value. such as for N-desmethyl-loperamide or nelfinavir) [Seneca et al., 2009; Kaddoumi et al., 2007]

Since P-gp demonstrates allosterism with multiple ligand binding sites, the magnitude of P-gp based DDI may be dependent on both the inhibitor and substrate. Therefore, we investigated whether the quinidine-^{11}C-verapamil DDI at the human BBB could be equally well predicted from preclinical studies as the CsA-^{11}C-verapamil DDI. Our observed quinidine-^{11}C-verapamil DDI (~70-90% increase in ER) at the human BBB was well predicted based on the *in*

vivo macaque data (~112%), but was poorly predicted from the *in vivo* rat data (554%). This discrepancy between the two predictions could be due to either the MDR1 cells not accurately reporting the *in vivo* inhibitory characteristics (EC_{50} and gamma) of quinidine or that the dynamic range of P-gp inhibition in the rat over-predicts the corresponding dynamic range in humans. The latter is possible as the CBF in the rat is approximately twice that in humans and macaques [Yuen et al., 2008], and the P-gp protein expression at the macaque and human BBB is similar, but ~2 fold lower than that at the rat BBB [Shawahna et al., 2011; Ito et al., 2011; Uchida et al., 2011]. However, this explanation is not satisfactory as the CsA-^{11}C-verapamil DDI at the human BBB is well predicted by the rat data [Hsiao et al., 2006]. Additional studies are required to determine which animal model can serve as the best predictive model for P-gp based DDI at the human BBB.

In summary, in agreement with our previous conclusions and those of others, we propose that P-gp activity and its modulation at the human BBB should be characterized using the ER of the P-gp substrate. In addition, quinidine, at its therapeutic plasma concentrations, can inhibit P-gp activity at the human BBB to result in approximately ~70-90% increase in the brain ER of ^{11}C-verapamil radioactivity. As predicted from *in vitro* data, this inhibition was greater than the CsA-^{11}C-verapamil DDI, but not sufficient to completely inhibit P-gp. These findings provide the first quantitative support of the previous DDI observed between quinidine and loperamide [Sadeque et al., 2000]. Although this quinidine-^{11}C-verapamil DDI was quantitatively predicted by data from the macaque and cells expressing MDR1, additional data are required to determine if the macaque or the rat is the best preclinical model to predict P-gp based DDI at the human BBB. Finally, to determine the utility of inhibiting P-gp to improve CNS delivery of drugs, more potent and selective P-gp inhibitors that are clinically approved are needed.

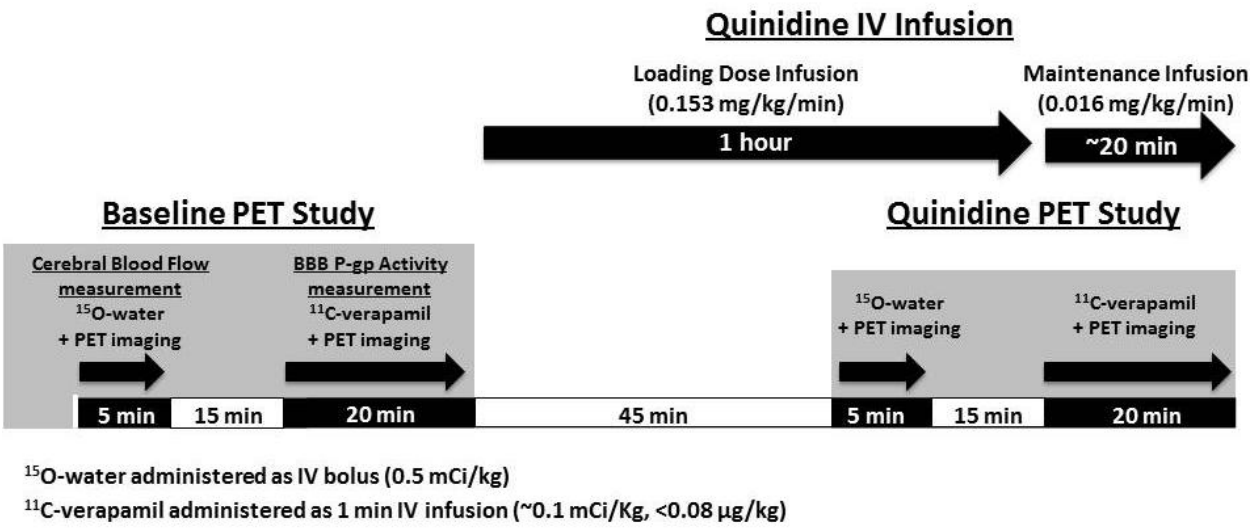

Figure 4.1: Timeline for administration of the PET tracers, ^{15}O-water and ^{11}C-verapamil, to respectively assess cerebral blood flow (CBF) and BBB P-gp activity in the absence or presence of the P-gp inhibitor, quinidine.

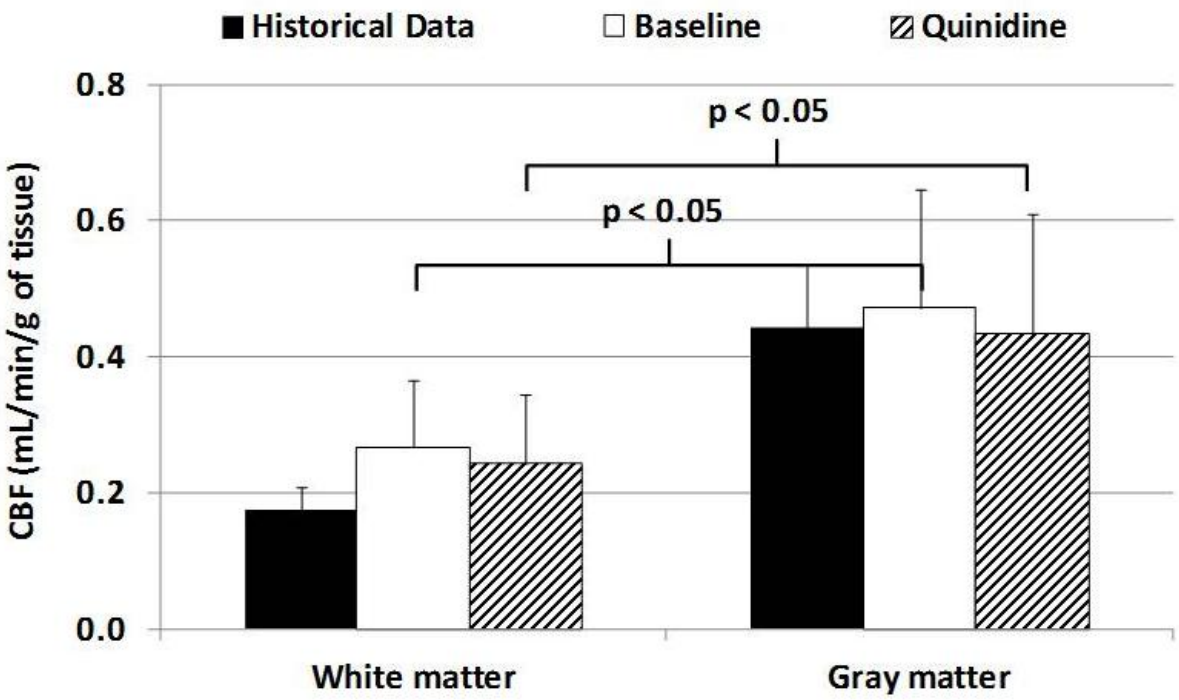

Figure 4.2: The cerebra blood flow (CBF) was unaffected by the presence of quinidine. However, the individual CBF did vary, and therefore were used for all subsequent data analysis. The average white matter or gray matter CBF values at baseline estimated in this study were in agreement with the historical data compiled from multiple sources. Data are expressed as mean ± SD (n=9).

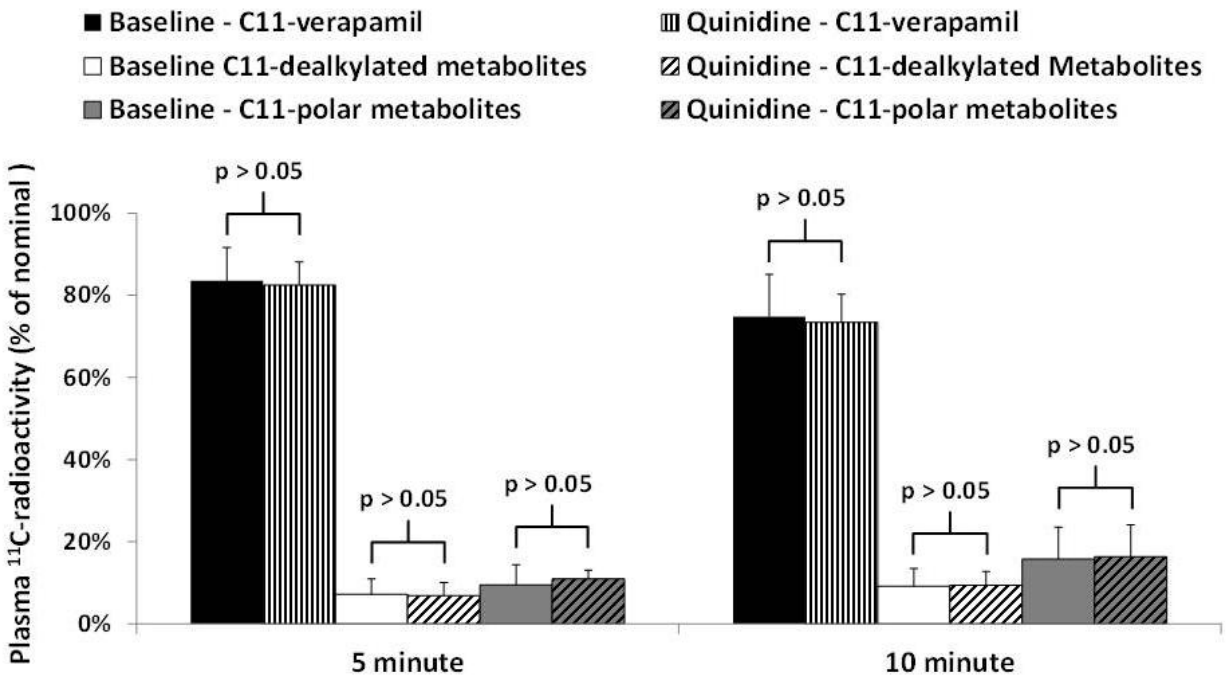

Figure 4.3: The plasma content of ^{11}C-verapamil and its circulating ^{11}C-dealkylated metabolites and ^{11}C-N-demethylated (polar species) metabolites at 5 or 10 min of the PET-imaging sessions was unaffected by the presence of quinidine. Nearly 100% of the ^{11}C-radioactivity in all samples was recovered after the SPE analysis, and confirmed by HPLC. Similar to our previous finding from the CsA-^{11}C-verapamil PET study, at 5 min and 10 min of the PET imaging sessions, ~85% of the total plasma radioactivity was attributed to P-gp substrates (^{11}C-verapamil, ~75%; its ^{11}C-dealkylated metabolites, ~10%), with little contribution from non-P-gp substrates (^{11}C-N-demethylated metabolites or polar metabolites, ~15%). Data are expressed as mean ± SD (n=9).

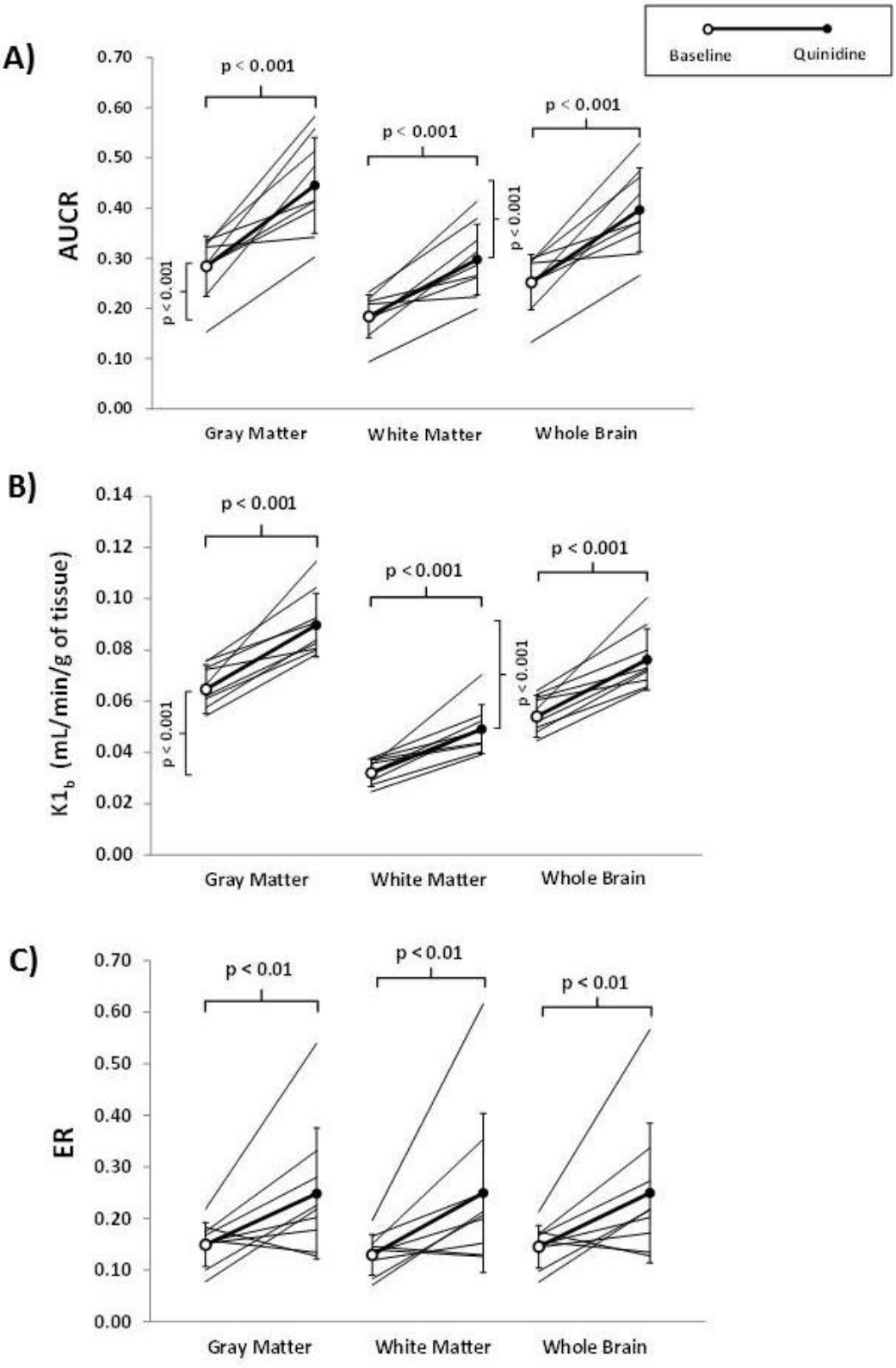
A)
Baseline
Quinidine
AUCR
0.70
0.60
0.50
0.40
0.30
0.20
0.10
0.00
p < 0.001
p < 0.001
p < 0.001
p < 0.001
p < 0.001
Gray Matter
White Matter
Whole Brain
B)
K1b (mL/min/g of tissue)
0.14
0.12
0.10
0.08
0.06
0.04
0.02
0.00
p < 0.001
p < 0.001
p < 0.001
p < 0.001
p < 0.001
Gray Matter
White Matter
Whole Brain
C)
ER
0.70
0.60
0.50
0.40
0.30
0.20
0.10
0.00
p < 0.01
p < 0.01
p < 0.01
Gray Matter
White Matter
Whole Brain

Figure 4.4: Quinidine significantly ($p<0.05$) increased the mean distribution of ^{11}C-verapamil radioactivity into the whole brain, gray matter, or white matter as measured by **(A)** the AUCR, **(B)** distribution clearance ($K1_b$) or **(C)** extraction ratio (ER). Of note, the AUCR and $K1_b$ of ^{11}C-verapamil radioactivity were significantly greater for the gray matter than the white matter (at baseline and in the presence of quinidine). These regional differences were eliminated when the ER for these regions was computed. Data are expressed as mean ± SD (n=9).

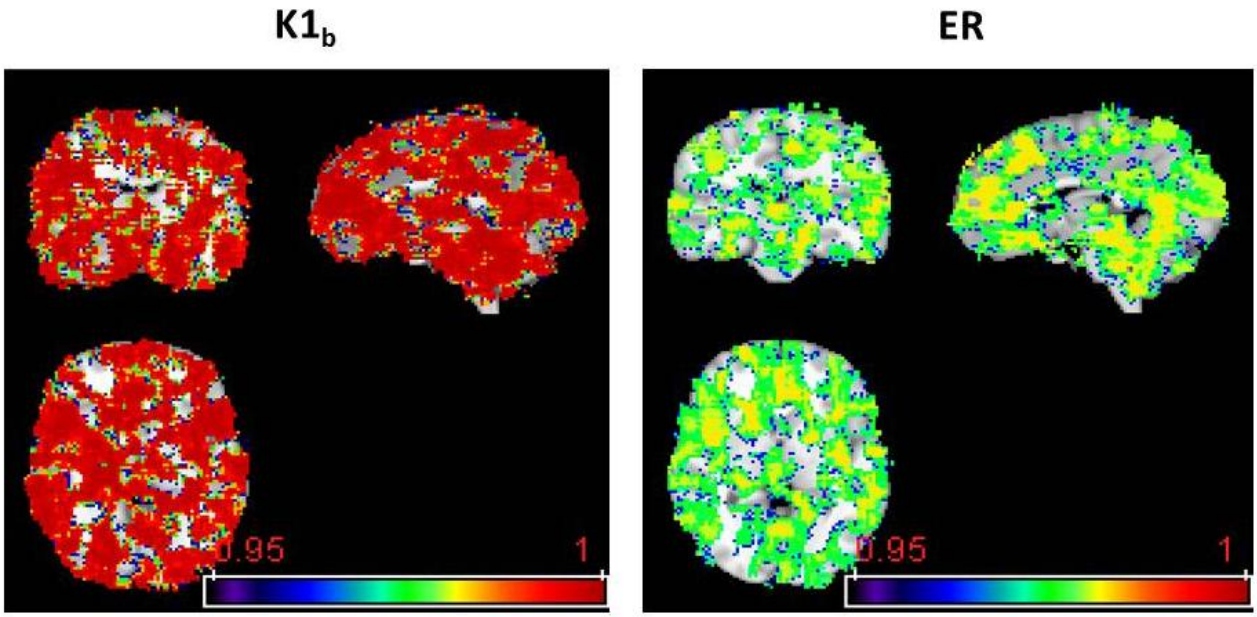

Figure 4.5: As indicated by the different views of the brain (coronal, sagittal, and axial), the parametric map analysis shows the significant increase in the $K1_b$ ($p < 0.02$) or ER ($p < 0.05$) of ^{11}C-verapamil radioactivity produced by quinidine across all brain regions protected by the BBB. The color scale corresponds to the level of statistical significance (1 – *p* value). The more intense the color (towards the right end of the color spectrum), the smaller the *p* value is.

Table 4.1: Quinidine induced change in brain distribution of ^{11}C-verapamil radioactivity in healthy volunteers as measured by three different parameters, AUCR, $K1_b$, and ER.

	% Change (Mean ± SD)		
	AUCR	**$K1_b$**	**ER**
Gray Matter	61% ± 36%	36% ± 18%	68% ± 73%
White Matter	67% ± 38%	50% ± 26%	90% ± 87%
Whole Brain	62% ± 37%	38% ± 19%	72% ± 76%

Chapter 5: Can P-glycoprotein at the Human Blood-Brain Barrier be Induced by Rifampin? A PET Imaging Study

5.1 Abstract

While we and others have shown that P-glycoprotein (P-gp) at the human blood-brain barrier (BBB) can be inhibited, it is not known whether it can be induced. P-gp induction at the human BBB could be clinically significant, as it may: 1) provide innovative treatment strategies for Alzheimer's Disease by increasing P-gp-mediated clearance of beta-amyloids from the brain, 2) further increase central nervous system (CNS) protection by decreasing the penetration of neurotoxins or drugs not targeted to the CNS, and 3) establish guidelines to prevent inadvertent drug-drug interaction with P-gp inducers that would decrease drug delivery to the brain, and hence the efficacy of CNS P-gp substrate drugs. Therefore, we investigated if P-gp at the human BBB in healthy human volunteers can be induced by a FDA-approved potent P-gp inducer (rifampin, 600 mg QD). To do so, we used Positron Emission Tomography (PET) imaging, and the P-gp PET tracer, ^{11}C-verapamil. We used two measures to assess P-gp activity at the BBB, namely, $AUC_{brain\ region}$: AUC_{blood} of ^{11}C-radioactivity and the brain distribution clearance ^{11}C-radioactivity, K1. Our findings showed that while rifampin induced systemic CYP3A-metabolism of ^{11}C-verapamil, it did not induce P-gp activity at the human BBB. The expression of nuclear receptors known to regulate P-gp is poorly studied in human brains, with one study reporting that the mRNA expression of pregnane X receptor (PXR) is not detectable in the human brain microvessels. However, since other nuclear receptors that can regulate P-gp

expression could be present in human brain endothelial cells (e.g., glucocorticoid receptor), their expression in the brain endothelial cells should be determined. Likewise, drugs that are ligands of these receptors should be tested to determine if they can induce *in vivo* P-gp activity at the human BBB. Based on these data, we predict that inadvertent inductive drug interactions with currently approved PXR ligand drugs are unlikely.

5.2 Introduction

Permeability-glycoprotein (P-gp), an ABC transporter that belongs to the multi-drug resistance (MDR) family, was one of the first xenobiotic transporters identified at the blood-brain barrier (BBB). [Kim et al., 2002] Due to its high expression at the BBB and wide substrate selectivity (>30% of approved drugs and endogenous compounds), P-gp is widely believed to be the most important transporter in modulating the entry of drugs into the central nervous system (CNS). [Sun et al., 2003] P-gp's functional importance at the **human** BBB has been **quantitatively confirmed** through positron emission tomography (PET) imaging using a combination of PET tracers that are P-gp substrates (e.g., ^{11}C-verapamil) and model P-gp inhibitors (e.g., cyclosporine-A, tariquidar, quinidine). [Sasongko et al., 2005; Bauer et al., 2012; Liu et al., 2012b] However, whether P-gp at the human BBB can be induced has never been investigated.

There are several compelling reasons to evaluate P-gp induction at the human BBB. First, P-gp at the BBB can decrease the brain penetration and efficacy of drugs targeted to the CNS (e.g., opioids, HIV protease inhibitors, and chemotherapeutics). [Kim et al., 1998; Kim et

al., 2002; Kemper et al., 2004] Therefore, induction of P-gp at the human BBB by chronic co-administration of known P-gp inducers (e.g., rifampin, St. John's wart, carbamazepine, selective HIV protease inhibitors) [Kim et al., 2002] could further reduce CNS penetration of these drugs. Second, beta-amyloid, an endogenous peptide that accumulates in Alzheimer's Disease (AD) brain and a causative factor of the disease, is a P-gp substrate. [Cirrito et al., 2005] Experimental evidence suggests that increased brain accumulation of beta-amyloid is due to its compromised elimination from the brain, and not because of its increased production. [Vogelgesang et al., 2002] Thus, inducing P-gp at the human BBB could potentially be a novel and innovative therapeutic strategy for the treatment of AD. Third, as demonstrated by the proof-of-concept studies conducted in mice [Hartz et al., 2010], P-gp induction (e.g., by rifampin, dexamethasone) could be used to "tighten" the human BBB to prevent the entry of neurotoxins or xenobiotics. [Bauer et al., 2006; Narang et al., 2008] The resulting increased protection of the brain could be advantageous to reduce CNS penetration and toxicity of drugs not targeted to the brain (e.g., loperamide or methadone). [Linnet et al., 2008]

The regulation of P-gp at the BBB has recently been extensively reviewed. [Miller et al., 2010] P-gp activity at the BBB can be influenced by various factors, including disease, pharmacotherapy and diet (e.g., seizure-induced signaling through COX-2, HIV-Tat protein signaling through RhoA, or proinflammatory signaling initiated by TNF-α and ET-1 pathways). [Miller et al., 2010] The expression of P-gp is generally thought to be regulated at the transcriptional level. Numerous nuclear receptors (e.g., pregnane X receptor, PXR; constitutive androstane receptor, CAR; glucocorticoid receptor, GR; vitamin D receptor, VDR; farnesoid X receptor, FXR) have been shown to transactivate P-gp expression, with PXR activation identified as the major mechanism for xenobiotic induction of *in vivo* and *in vitro* P-gp activity. [Reschly et

al., 2006; Aiba et al., 2005; Martin et al., 2008] However, whether these nuclear receptors are expressed at the human BBB remains controversial and poorly studied.

In the study presented here, we asked if P-gp activity at the human BBB can be induced, *in vivo*, by a FDA-approved drug and potent intestinal P-gp inducer, rifampin. To address this question, we quantified the ability of rifampin to induce P-gp at the human BBB, in healthy human volunteers using PET-imaging and ^{11}C-verapamil as the P-gp PET tracer.

5.3 Materials and Methods

5.3.1 Subjects

Nine healthy volunteers (5 men and 4 women; age, 22-42 years; weight, 61-98 kg) were enrolled in the study. Potential subjects underwent a screening visit with medical history review, physical examination, EKG, complete blood-cell count, hepatic and renal function tests, and pregnancy tests for women. Those with normal evaluations were recruited for the study. Subjects were excluded if they had chronic medical conditions or were breast-feeding, pregnant, smokers, taking long-term medications (except for stable doses of oral contraceptives for women), or had a history of substance abuse. No short-term medication (other than acetaminophen) was allowed for 24 hr before the PET imaging visit. Caffeine-containing beverages were not allowed on the day of study imaging. The study was approved by the University of Washington's Human Subjects Review Committee, Radiation Safety Committee, and Radioactive Drug Research Committee (Seattle, Washington). Informed consent was obtained from each subject.

5.3.2 Chemicals and Reagents

Racemic verapamil and verapamil metabolites (norverapamil, D-617, D-717) were obtained from sources previously described. [Sasongko et al., 2005] SPE C_8 cartridges (1 mL, 100 mg) were purchased from Varian (Lake Forest, CA, USA). Ultrafiltration devices were purchased from Amicon Centrifree Micropartition Device (Bedford, MA, USA). All other reagents were of the highest grade available from commercial sources.

5.3.3 Radiopharmaceuticals

^{11}C-verapamil and ^{15}O-water were synthesized as previously described [Sasongko et al., 2005], and were greater than 99% radiochemically and chemically pure, with a specific activity of approximately 63 TBq /mmol at the end of radiosynthesis. ^{3}H-verapamil (verapamil [N-methyl ^{3}H] hydrochloride; 2.2 TBq/mmol) for verapamil plasma protein binding assays was purchased from American Radiolabeled Chemicals, Inc. (St. Louis, MO, USA).

5.3.4 Experimental Study Design

This substudy was part of a larger study to evaluate induction and inhibition of P-gp activity at the human BBB by rifampin and quinidine, respectively. The study was divided into two arms with subjects assigned to Arms A or B of the study design illustrated in Figure 5.1A. Here, we present the results from the rifampin substudy; the quinidine study was the focus of another manuscript. [Liu et al., 2012b] The same baseline group was used to determine the effect of rifampin or quinidine (evaluated on the same day as the baseline study) on the BBB P-gp activity. Subjects received a daily dose of rifampin (600 mg QD) at night for at least 11-29 days (Figure 5.1A). On the PET study date, a pregnancy test was performed on female

volunteers. Each subject had catheters inserted in both arms; one (antecubital vein) for PET tracer injections, and the other (radial artery) for arterial blood sampling during PET-imaging. Each subject's head was immobilized during the PET imaging sessions using a custom-made thermoplastic mask and head-holder. We used the PET imaging protocol described previously [Sasongko et al., 2005] with the following minor modifications (Figure 5.1B). Briefly, during both PET-imaging sessions (baseline or post-rifampin treatment), the subjects were administered ^{15}O-water (~0.5 mCi/kg, IV bolus) and ^{11}C-verapamil (~0.1 mCi/kg, <0.08 μg/kg, 1 min IV infusion) consecutively separated by ~15 min and brain PET images were acquired to determine cerebral blood flow (CBF) and P-gp activity, respectively. Magnetic resonance (MR) imaging of the brain (T1- and T2-weighted images) was performed within 1 week of the PET-imaging sessionsto provide anatomic information for the construction of region-of-interest (ROI) PET analysis. After 1 to 2 weeks of the final imaging session, subjects were evaluated post-study with all tests performed at the screening visit, except for the EKG and the pregnancy test.

5.3.5 Blood Sample Collection and Processing

Arterial blood samples (1 mL) during both PET sessions were collected as follows, ^{15}O-water (first 1 min: every 5 sec; 1-2 min: every 15 sec; 2-4 min: ever 30 sec; and then at 5 min), and ^{11}C-verapamil (first 1 min: every 15 sec; 1-2 min: every 20 sec; 2-3 min: every 30 sec; 3-8 min: every 1 min; 8-12 min: every 2 min; and then at 15 and 20 min). ^{15}O-water blood radioactivity, in preweighed gamma-counting tubes, and ^{11}C-verapamil blood and plasma radioactivity were measured by a gamma counter (Cobra Counter; Packard Corporation, Meriden, CT). Arterial blood samples (2 mL) were collected during both sets of ^{11}C-verapamil PET imaging sessions at 5, 10, and 20 min to quantify the radioactivity content of ^{11}C-verapamil and

its known ^{11}C-dealkylated metabolites (D-617, D-717) and ^{11}C-N-demethylated metabolites (polar metabolites) in the plasma at baseline or after rifampin treatment via solid-phase extraction (SPE) and HPLC as described previously. [Sasangko et al., 2005; Unadkat et al., 2008]

5.3.6 Verapamil Plasma Protein Binding

To evaluate the effect of any potential residual rifampin (daily dose administered at night) on verapamil plasma protein binding, ultrafiltration was used to quantify and compare verapamil plasma protein binding in pooled plasma samples (n=3 subjects) collected during baseline or post-rifampin treatment PET-imaging sessions. 600 µL of the plasma was spiked with ^{3}H-verapamil (20 nCi/mL), and incubated at 37ºC for 20 min, in triplicates. At the end of the incubation, 500 µL of the plasma was transferred into the ultrafiltration device and centrifuged (2000*g*) at 37ºC for 10 min. Radioactivity in 100 µL of the plasma or ultrafiltrate was then determined by radioactivity scintillation counting. Verapamil plasma protein binding was calculated by the difference in plasma and the ultrafiltrate radioactivity expressed as a percent of plasma radioactivity [Sasongko et al., 2005].

5.3.7 Image Processing

Both the PET image acquisition and reconstruction were conducted as described previously. [Sasongko et al., 2005] A 20 min attenuation scan for attenuation correction was acquired before each set of PET imaging using a rotating germanium 68 source, and was repeated when there was any significant change in the position of the head noted between the phases of the PET-imaging sessions. For each subject, MR images (T1) were coregistered to the PET images based on mutual information criteria using PMOD (PMOD Technologies). ROIs for three tissue

types/brain regions (whole brain, gray matter, or white matter) were identified on the coregistered PET-MR images manually, and extended continuously to an average of 18 slices (~6 cm) to create volumes of interest (VOIs) for each tissue type. VOIs were applied to both the ^{15}O-water and ^{11}C-verapamil dynamic image sets to determine decay corrected radioactivity concentration in each brain region.

5.3.8 Noncompartmental Analysis

After radioactivity decay correction, the area under the ^{11}C-radioactivity-time curve (AUC) for the brain or brain region ($AUC_{brain\ region}$) and blood (AUC_{blood}) was calculated from 0-5 minutes of ^{11}C-verapamil PET imaging at baseline or post-rifampin treatment using the trapezoidal rule. The percent change in the ratio of $AUC_{brain\ region}$: AUC_{blood} (AUCR) was used to evaluate the magnitude of BBB P-gp modulation by rifampin treatment.

5.3.9 Compartmental Analysis

Regional CBF for the whole brain, gray matter or white matter was estimated for each subject by fitting a flow-dispersion model to the first 2 min of the ^{15}O-water tissue time-activity curves in the respective brain tissue using PKIN (PMOD Technologies) [Muzi et al., 2009]. Previously, a 1-tissue compartment (1-TC) compartment model was shown to be the best model to estimate the distribution clearance of ^{11}C-verapamil into the human brain (K1) [Muzi et al., 2009]. We and others have also confirmed that when P-gp activity at the human BBB is inhibited, it is the K1 of ^{11}C-verapamil radioactivity into the brain that is changed, rather than the efflux rate constant out of the brain (k2) [Liu et al., 2012b; Bauer et al., 2012; Kreisl et al., 2010; Bankstahl et al., 2008; Liow et al., 2009]. To confirm that the 1-TC model can also be extended

to characterize the brain distribution kinetics of ^{11}C-verapamil radioactivity post-rifampin treatment, we fitted the 1-TC model (PKIN software, PMOD Technologies) to data sets of different duration (5, 10, or 20 min), each with different input functions: total plasma radioactivity; ^{11}C-verapamil plus ^{11}C-verapamil metabolites that are P-gp substrates (^{11}C-dealkylated metabolites); or a dual input function that modeled simultaneously and separately the ^{11}C-radioactivity contributed by P-gp substrates and non P-gp substrates (^{11}C-polar metabolites). An average value of V_b (human brain tissue blood volume) determined previously (0.044 mL/g) [Sasongko et al., 2005], was incorporated as a constant when estimating CBF, $K1_p$ (based on plasma data) and k2. Weights were set at 1/(observed radioactivity)^2. The best model was determined by evaluating the Akaike information criterion (AIC), runs test, visual inspection of the residuals and model fits, and % coefficient of variation (COV) of the final estimates. To determine the brain extraction ratio of ^{11}C-verapamil radioactivity (ER; based on blood data), the ratio of $K1_b$ ($K1_p$ corrected for the individual blood-to-plasma ratio) and CBF was computed.

5.3.10 Parametric Map Analysis

For each subject, parametric maps (PMAPs) of $K1_b$ of ^{11}C-verapamil radioactivity or CBF were generated using a 1-TC compartmental model (PXMOD software, PMOD Technologies) with ^{11}C-verapamil or ^{15}O-water PET dynamic images and the corresponding arterial blood input functions. Each subject's $K1_b$ or CBF PMAPs were coregistered to their MR images, and the fused images were then coregistered to the standard brain atlas from FMRIB Software Library (FSL). $K1_b$ PMAPs were normalized to the CBF PMAPs (via pixel-by-pixel division using FSL software fslmaths) to determine ER of ^{11}C-verapamil radioactivity. The final $K1_b$ and ER results were then evaluated statistically to determine whether chronic rifampin

treatment significantly affected P-gp activity at the human BBB, by using a non-parametric voxel-by-voxel paired t-test with multiple comparison correction (Threshold-Free Cluster Enhancement option from Software randomize). The multiple comparison correction was performed based on cluster statistical characteristics such as extent of cluster size.

5.3.11 Statistical and Data Analysis

Data are expressed as mean ± SD, and analyzed using a Student paired *t* test, with the significance level set at $p < 0.05$.

5.4 Results

All volunteers successfully completed both the baseline and post-rifampin PET and MRI imaging protocol with no unexpected side effects.

Verapamil plasma protein binding was unaffected after rifampin treatment (baseline: 92% ± 0.7% vs. post-rifampin: 93% ± 0.9%, $p > 0.05$). The blood-to-plasma ratio of ^{11}C-verapamil radioactivity during the first 5 min of PET imaging did not differ significantly between baseline (0.76 ± 0.05) and post-rifampin treatment (0.77 ± 0.08).

As expected, rifampin, a selective PXR ligand and a potent inducer of PXR-regulated CYP genes (e.g., CYP3A), did induce ^{11}C-verapamil metabolism. This manifested as a significant increase (~2 fold compared with baseline, $p < 0.05$) in the 10 min plasma content of ^{11}C-polar metabolites of ^{11}C-verapamil formed by CYP3A (Figure 5.2). A corresponding decrease (from 77% at baseline to 60% post-rifampin; $p < 0.05$) was observed in the plasma content of unchanged ^{11}C-verapamil. However, after rifampin treatment, no significant change

was observed in the plasma content of the ^{11}C-dealkylated metabolites of ^{11}C-verapamil formed by CYP2Cs. During the first 5 min of ^{11}C-verapamil PET-imaging, the ^{11}C-radioactivity composition at baseline or post-rifampin treatment was not significantly different ($p > 0.05$), and was therefore chosen as the time frame for all subsequent data analysis.

Chronic rifampin treatment did not affect CBF, or the regional CBF difference between gray and white matter (Figure 5.3). The absolute CBF values estimated at baseline for the gray matter or white matter were also consistent with historical data compiled from multiple published studies [Aslan et al., 2011; Reich et al., 1989]. However, the individual CBF did vary, and therefore were used for all data analysis.

After rifampin treatment, no significant change ($p > 0.05$) was observed in the AUCR for whole brain (baseline: 0.12 ± 0.03; post-rifampin: 0.13 ± 0.02), white matter (baseline: 0.09 ± 0.03; post-rifampin: 0.09 ± 0.02), or gray matter (baseline: 0.14 ± 0.04; post-rifampin: 0.14 ± 0.02) during the first 5 min of ^{11}C-verapamil PET imaging (Figure 5.4A). Similar to the regional CBF differences, the distribution of ^{11}C-verapamil radioactivity (as measured by AUCR) into gray matter was significantly greater than that into white matter at baseline or after rifampin treatment ($p < 0.001$).

After evaluating the goodness of fit of the 1-TC model, using different plasma radioactivity input functions and data of different imaging durations (5, 10 or 20 min), the best model for the data was when the total plasma ^{11}C-verapamil radioactivity was used as the input function (AIC values for baseline and post-rifampin treatment of 19 and 13, respectively, vs. AIC values of >23 and >17 using other input functions). This is consistent with our previous findings for both the CsA-^{11}C-verapamil, and quinidine-^{11}C-verapamil PET studies [Sasongko et al., 2005; Liu et al., 2012b]. Using this input function, we found that the $K1_p$ estimates were

similar irrespective of the duration of data used (5, 10, or 20 min). However, since the ^{11}C-verapamil plasma metabolite content at 5 min was the least and not significantly affected by rifampin treatment, to minimize the contribution of these metabolites from confounding our data interpretation, we limited all our modeling analysis to the first 5 min of the ^{11}C-verapamil PET imaging. Our results showed that chronic rifampin treatment did not significantly change the mean $K1_b$ of ^{11}C-verapamil radioactivity into the brain (e.g., gray matter; baseline: 0.07 ± 0.01 mL/min/g; post-rifampin: 0.07 ± 0.01 mL/min/g; Figure 5.4B), the mean ER of ^{11}C-verapamil radioactivity (e.g., gray matter; baseline: 0.16 ± 0.05; post-rifampin: 0.16 ± 0.08; Figure 5.4C), or the mean k2 (e.g., gray matter; baseline: 0.14 ± 0.04 min^{-1}; post-rifampin: 0.15 ± 0.03 min^{-1}; data not shown). After normalizing $K1_b$ to CBF, the significant regional difference (gray matter vs. white matter) observed for $K1_b$ was eliminated as shown by the equivalent ER values at baseline (gray matter: 0.09 ± 0.03, white matter: 0.07 ± 0.03) or post-rifampin treatment (gray matter: 0.09 ± 0.05, white matter: 0.08 ± 0.04). Results from the parametric mapping analysis of $K1_b$ and ER of ^{11}C-verapamil radioactivity showed no significant difference ($p > 0.05$) between pre and post-rifampin treatments in any of the brain regions (data not shown because of this lack of difference). This confirmed the findings from both the noncompartmental and compartmental analysis.

5.5 Discussion and Conclusions

In order to observe P-gp induction at the BBB, a PET tracer that is specific for P-gp and has significant brain distribution at baseline must be used. For this reason, we chose ^{11}C-verapamil as our PET ligand. At baseline, the distribution of ^{11}C-verapamil into the brain (ER:

~0.2) is larger than other validated P-gp PET ligands (e.g., ^{11}C-N-desmethyl-lopearmide, ER: ~0.03) [Kreisl et al., 2010]. In addition, we chose rifampin as our prototypic P-gp inducing agent because it is the most potent FDA-approved P-gp inducer. Numerous healthy volunteer studies have shown that rifampin (600 mg QD for as little as 6 days) induces intestinal and/or hepatic P-gp *in vivo*, as measured by the increased oral clearance and decreased plasma AUC of digoxin, fexofenadine, or talinolol [Niemi et al., 2003; Gurley et al., 2008; Hamman et al., 2001]. Therefore, we followed this standard P-gp induction protocol and instructed all human volunteers to take rifampin once a day (600 mg nightly) for 11 to 29 days to determine if P-gp activity at the human BBB can be induced. Significant increase in the CYP3A-mediated metabolism of ^{11}C-verapamil to ^{11}C-polar metabolites was observed in all subjects, and confirmed that our subjects were compliant and that the rifampin plasma concentrations achieved were sufficient to induce CYP3A. However, rifampin did not induce P-gp activity at the human BBB as indicated by the lack of significant change observed in the AUCR, $K1_b$, or ER of ^{11}C-verapamil radioactivity for whole brain, gray matter, or white matter (Figure 5.4), as well as the lack of any significant change in $K1_b$ or ER for any of the brain regions analyzed by parametric maps (data not shown).

We confirmed that the lack of P-gp induction at the human BBB by rifampin was not due to potential confounders such as rifampin-induced changes in verapamil plasma protein binding, CBF, or ^{11}C-verapamil metabolism. Any changes in CBF between the baseline and post-rifampin treatment PET-imaging sessions were accounted for by ER (CBF normalized $K1_b$) of ^{11}C-verapamil radioactivity. As elaborated previously [Eyal et al., 2010; Liu et al., 2012b], ER provides an estimate of the intrinsic *in vivo* P-gp activity not confounded by changes in CBF, and we propose that it be used as the preferred index to characterize P-gp activity and its modulation

at the human BBB. Interestingly, rifampin (PXR-selective ligand is not a CAR ligand) selectively induced CYP3A-mediated metabolism to ^{11}C-polar metabolites (primarily regulated by PXR), and not CYP2C-mediated metabolism to ^{11}C –dealkylated metabolites (regulated by both CAR and PXR) [Hewitt et al., 2006]. This is consistent with published *in vivo* and human hepatocyte induction studies, where CYP3A activity is induced by rifampin to a greater extent than CYP2C [Dixit et al., 2007; Kirby et al., 2011a; 2011b]. Passive distribution of ^{11}C-polar species (non P-gp substrates that can freely diffusible across the rodent BBB) into the brain could diminish the magnitude of P-gp induction at the BBB when measured by PET imaging, because PET imaging cannot distinguish between unchanged ^{11}C-verapamil and its ^{11}C- polar metabolites. We accounted for this potential confounder by limiting our data analysis and modeling to a time frame (5 min) when ^{11}C-verapamil metabolism was minimal. This assumes that ^{11}C-verapamil metabolism in the human brain is insignificant, an assumption supported by the negligible CYP3A and CYP2Cs expression in the human brain [Shawahna et al., 2011]. Furthermore, because rifampin is also a P-gp substrate and inhibitor [Kim et al, 2002], to prevent it from confounding the interpretation of our data, subjects were instructed to take rifampin nightly, so that during the PET imaging study on the following day (~17 hr or ~8 rifampin plasma half-lives after the last rifampin dose), no or little rifampin remained in the systemic circulation.

To date, the *in vivo* induction of P-gp at the human BBB has never been studied. Promising results from Bauer et al. (2006) using the transgenic mouse over-expressing the human PXR (hPXR), showed that *in vivo* P-gp activity at the mouse BBB can be induced by rifampin (70% decrease in methadone CNS effect compared to transgenic controls not exposed to rifampin). However, because PXR was artificially over-expressed in all mouse tissues,

including the BBB, this result cannot be extrapolated to humans. But their subsequent study, using the transgenic mouse model expressing the human amyloid precursor protein did show that the BBB P-gp activity could be induced by the PXR ligand, pregnenolone 16α-carbonitrile, to significantly increase the brain efflux clearance of beta-amyloid [Ott et al., 2009]. However, our data indicate that P-gp at the human BBB was not induced by rifampin at the usual doses used to induce intestinal/hepatic P-gp activity. This difference might be due to species difference or the concentration of the inducer exposed to the brain endothelial cells (see below).

Why was P-gp at the human BBB not induced by rifampin? There are several possible explanations. First, PXR expression at the human BBB may be too low (or absent) to induce P-gp activity despite sufficient rifampin exposure. The mRNA expression of PXR, CAR and AhR has been previously evaluated in human brain microvessels (isolated from epilepsy patients). Transcripts of PXR or CAR were not detected, but that of AhR were [Dauchy et al., 2008]. Second, rifampin concentration achieved within the brain microvessel endothelial cells may not be high enough to induce P-gp. After daily oral rifampin administration, the unbound intestinal and portal vein plasma rifampin concentrations will be much higher than those in the systemic circulation, and therefore it is not surprising that intestinal P-gp expression and activity is induced by rifampin. Rifampin exposure to the intracellular milieu of the brain endothelial cells will be further reduced by P-gp efflux from these cells.

In conclusion, rifampin, at the dose used in the clinic, did not induce P-gp at the human BBB, most likely due to the low (or negligible) expression of PXR in the endothelial cells. However, since other nuclear receptors that can regulate P-gp expression could be present in human brain endothelial cells (e.g. GR), their expression in the brain endothelial cells should be

determined. Then, drugs that are ligands of these receptors should be tested to determine if they can induce *in vivo* P-gp activity at the human BBB.

A)

		11-29 days		
Arm A (n=5)	Baseline PET Study Quinidine PET Study	Rifampin treatment (600 mg QD at night)		Post-rifampin PET Study
	11-29 days		21-42 days	
Arm B (n=4)	Rifampin treatment (600 mg QD at night)	Post-rifampin PET Study	Rifampin washout	Baseline PET Study Quinidine PET Study

B)

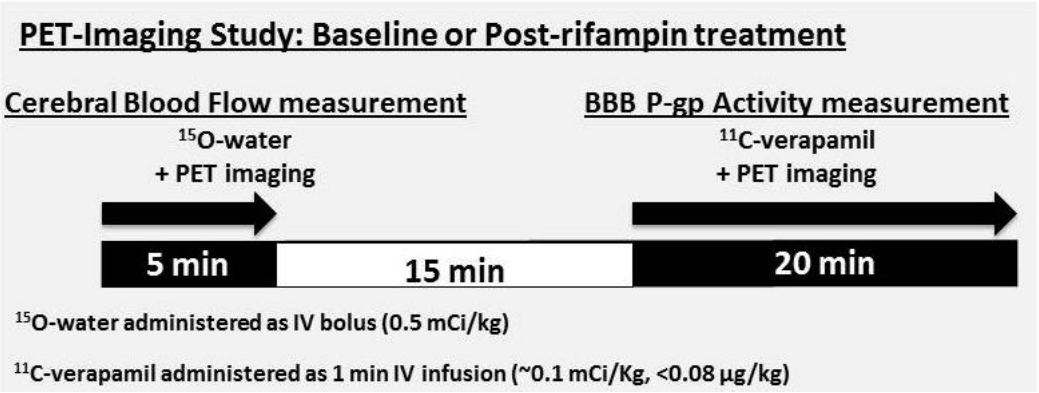

Figure 5.1: (A) PET study design. Baseline and quindine PET imaging sessions were conducted on the same day. **(B)** PET-imaging timeline after ^{15}O-water or ^{11}C-verapamil administration to respectively assess cerebral blood flow (CBF) and P-gp activity at the human BBB.

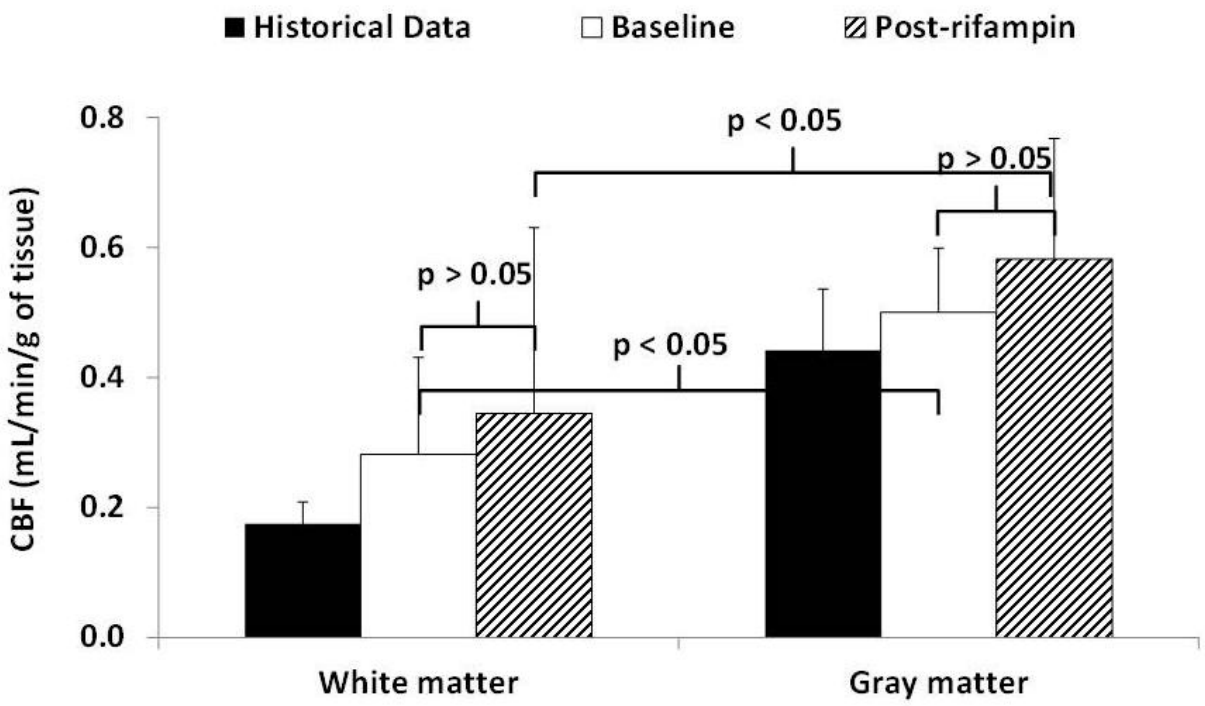

Figure 5.2: Regional cerebra Blood Flow (rCBF) was estimated by fitting a flow-dispersion model to 2 min of the ^{15}O-water plasma and tissue time-activity curves. While significant inter-individual variability in rCBF was observed across different subjects (data not shown), the average rCBF was not significantly altered after rifampin treatment. Data are expressed as mean±SD (n=9).

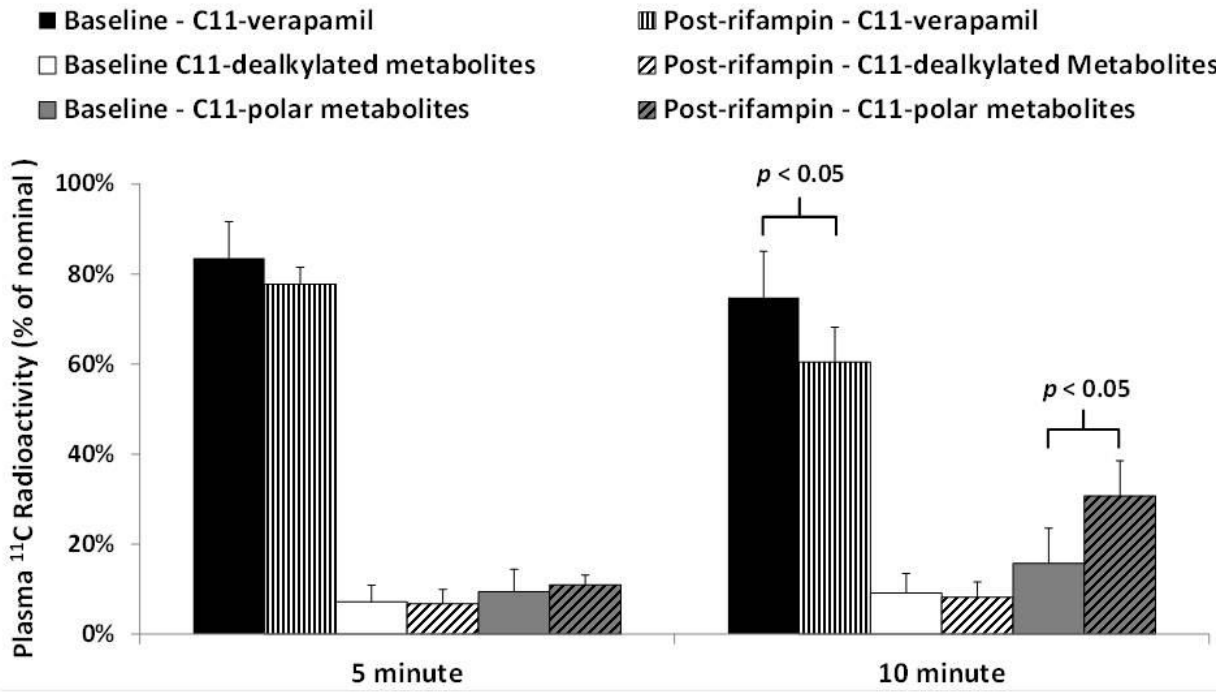

Figure 5.3: Plasma ^{11}C-verapmil polar metabolite (formed by CYP3A) contents at 5 min after ^{11}C-verapamil administration during baseline and post-rifampin PET-imaging sessions were not significantly different while those at 10 min were. In contrast, the plasma content of ^{11}C-dealkylated metabolites (formed by CYP2Cs) during baseline and post-rifampin PET imaging session were not significantly different at 5 or 10 min, Data are expressed as mean ± SD (n=9).

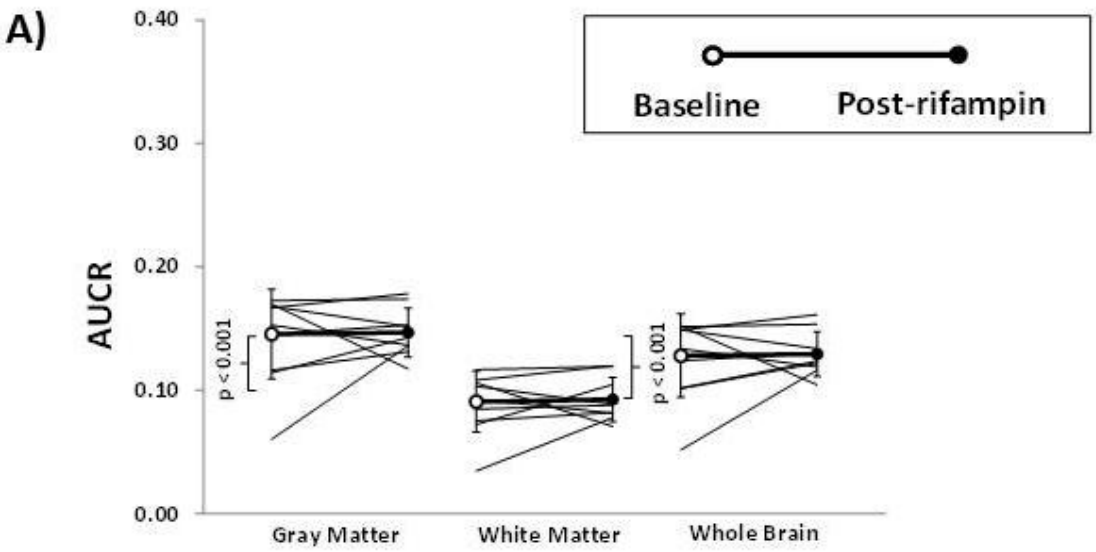
A)
Baseline
Post-rifampin
AUCR
0.40
0.30
0.20
0.10
0.00
p < 0.001
p < 0.001
Gray Matter
White Matter
Whole Brain

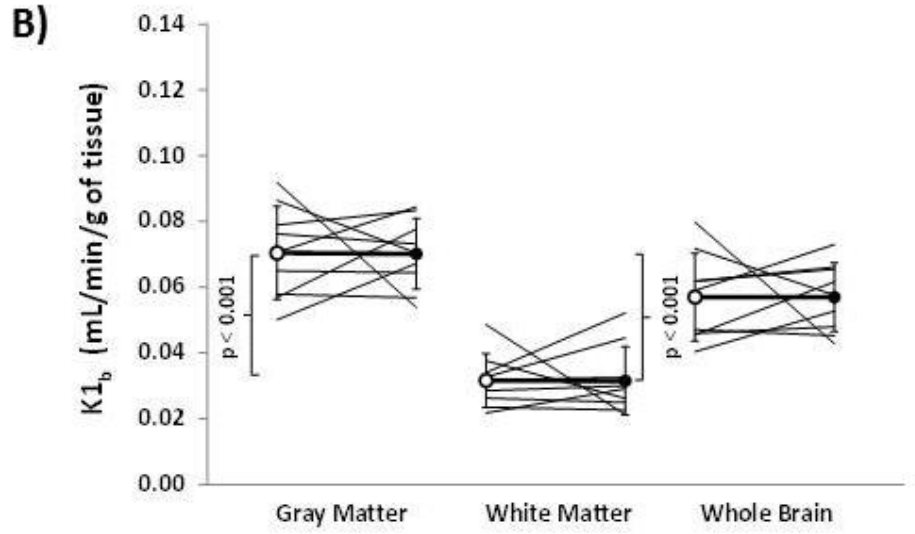
B)
$K1_b$ (mL/min/g of tissue)
0.14
0.12
0.10
0.08
0.06
0.04
0.02
0.00
p < 0.001
p < 0.001
Gray Matter
White Matter
Whole Brain

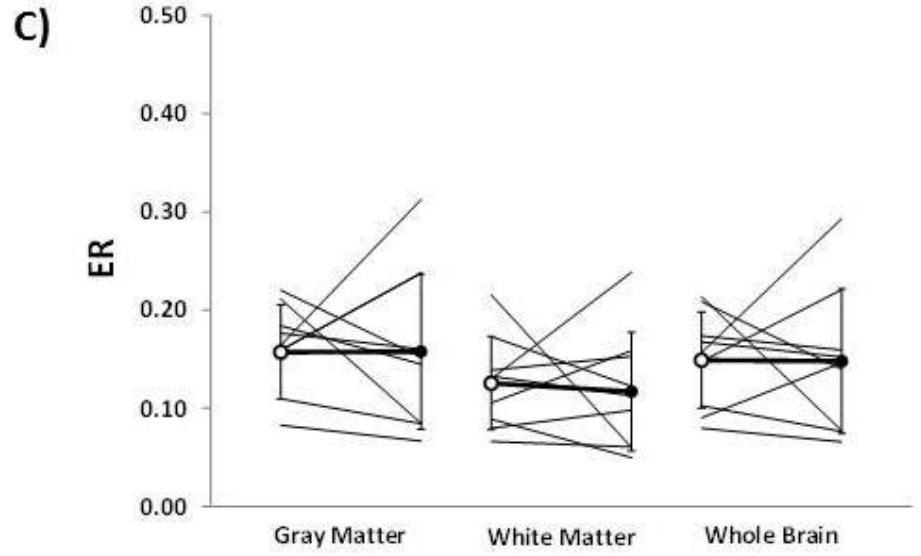
C)
ER
0.50
0.40
0.30
0.20
0.10
0.00
Gray Matter
White Matter
Whole Brain

Figure 5.4: The initial 5 min plasma and tissue time-activity data were used to determine ^{11}C-verapamil radioactivity **(A)** $AUC_{brain\ region}$: AUC_{blood},(AUCR); **(B)** distributional clearance, $K1_b$; or **(C)** ER for the whole brain, gray matter, or white matter. After rifampin treatment (600 mg QD), no significant change was observed in the AUCR, $K1_b$, and ER, indicating that P-gp activity at the human BBB was not induced. Data are expressed as mean ± SD (n=9).

Chapter 6: General Conclusions and Future Directions

In summary, this thesis has presented a series of studies that aim to enhance the understanding and prediction of complex transporter and metabolic-based DDIs. These studies are divided into two parts. In the first part, our main objectives were to better understand the transporter and metabolic-based DDIs associated with the HIV protease inhibitors at the hepatic level, so to better prevent their occurrence and improve PIs' safety in PIs-based HAART regimen. In the second part, our major goals were to determine the clinical significance of P-gp mediated DDIs at the human BBB, and to evaluate the utility of BBB P-gp modulation in the development of novel treatment strategies for CNS diseases.

6.1 HIV protease inhibitor DDIs

PI-based DDIs are complex, unpredictable and often paradoxical. *In vivo* DDIs suggest that PIs are capable of both inhibiting the activity, and inducing the expression of metabolic enzymes (CYP3A, 2B6, 1A2, 2C9) and drug transporters (P-gp, MRP2, OATPs). The potential for PIs to elicit their multifaceted effects is further increased, because they are almost always co-administered with a low dose of RTV, which is used to inactivate CYP3A (major metabolic enzyme and elimination pathway for PIs) to increase their systemic exposure, and likely their intracellular concentrations. Much advancement has been made in our understanding of PIs' ability to inhibit CYPs and drug transporters. However, investigations dedicated to evaluating PIs' potential as inducers of the CYPs and drug transporter, and PIs' as substrates of hepatic uptake transporters haven been scarce, especially those using human hepatocytes, an advanced *in vitro* systems that provides the most comprehensive and *in vivo*-like hepatocyte cellular

characteristics. These investigations are much needed to better understand and predict the *in vivo* DDIs with PIs as precipitant and/or object drugs.

Therefore, as described in **Chapter 2**, we used human hepatocytes and performed comprehensive quantification of the net induction potential of the eight PIs (RTV, NFV, SQV, APV, LPV, TPV, IDV, ATV) for nine major hepatic CYPs (CYP3A, 2B6, 1A, 2C8, 2C9, 2C19, 2D6, 2E1, 2A6) at the activity level, as well as their induction of the mRNA transcripts of the same CYPs, and the hepatic drug transporters (P-gp, OATPs, MRPs). We showed that the majority of PIs (particularly APV) produced significant induction in CYP3A4 mRNA expression, and net increase in CYP3A activity, although the magnitude of the activity increase was low (≤ 2-fold). Most of PIs were also net and modest inducers of CYP2B6 (mRNA and activity), and OATP1B1 and P-gp (mRNA). Based on these findings, we were able to establish qualitative agreement between our *in vitro* results and those observed *in vivo*. In extension, we confirmed and recommend that human hepatocyte be used for future evaluation of PIs' induction potential for CYPs and transporters. We also recommend the usage of our newly validated CYP cocktail assays to simultaneously quantify multiple CYP activities in various experimental systems (e.g., human hepatocytes, human liver microsomes), especially those with precious and low sample yields (e.g., microsomes isolated from human hepatocytes). Lastly, our findings provide an important foundation for future efforts to improve the quantitative prediction of PI-based DDIs, as our screening highlighted the PIs that would warrant additional investigation (e.g., APV, LPV, ATV), such as the determination of their net induction EC_{50} for the hepatic CYPs and transporters.

Similarly, using human hepatocytes (e.g., SCHH), we performed transport studies detailed in **Chapter 3** to show that in the absence of CYP metabolism, but in the presence of

biliary excretion, the hepatic uptake of RTV, NFV, or LPV (LogP 4-6) was dominated by passive diffusion. Although it is possible that RTV, NFV, or LPV could be substrates of sinusoidal influx transporters, contribution from such uptake transporters *in vivo* or in *in vivo*-like *in vitro* systems (e.g., human hepatocytes) is likely marginal and masked by passive diffusion. However, we did find that APV (LogP of 2) was transported into the human hepatocytes, but that sinusoidal transport was not OATP-mediated. These findings are critical since sinusoidal uptake of PIs has never been evaluated in human hepatocytes, and the previous investigations studying the role of OATPs in mediated PIs uptake have been conflicting and inconclusive. Therefore, based on our transport evaluation performed in SCHH, we believe that modulation of sinusoidal uptake transporters is unlikely to affect the disposition of RTV, NFV, or LPV, but could produce significant DDIs with APV. Future studies should be conducted to identify the sinusoidal uptake transporter(s) responsible for APV hepatic uptake. In addition, future evaluation of the hepatic uptake of other PIs, particularly those are used most clinically (e.g., ATV, DRV), should be performed to comprehensively address the significance of modulating sinusoidal uptake transporter(s) in PIs-based DDIs, and PIs' hepatic disposition. Once completed, results from the studies presented and those proposed here, in conjunction with PBPK simulations, could be used to test whether the complex DDIs of the PIs can be predicted from in vitro studies.

6.2 PET Imaging: P-gp Mediated DDIs at the Human BBB

P-gp is functionally important at the human BBB; however the clinical significance of P-gp and its modulation at the human BBB is unknown. Studying P-gp mediated DDIs at the

human BBB is important to better understand how P-gp at the BBB protects the CNS, and to evaluate whether this mechanism can be manipulated (decreasing or increasing P-gp activity) to our advantage to prevent neurotoxicity, and develop novel treatment for CNS disease with unmet medical needs. Therefore, when investigating the utility of P-gp modulation at the human BBB as potential treatments for CNS diseases, it is equally important to look for and use clinically approved drugs (e.g., quinidine as model P-gp inhibitor, and rifampin as model P-gp inducer) to facilitate the translation of these P-gp modulators into future clinical use. PET-imaging, a non-invasive and exquisitely sensitive technique, enabled us to study P-gp, and quantify its modulation at the human BBB in real time and *in vivo*.

Therefore, in **Chapter 4**, we described our quantification of P-gp inhibition at the human BBB by clinically relevant concentrations of quinidine, in healthy human volunteers, using PET imaging and ^{11}C-verapamil as our P-gp PET tracer. We showed that quinidine significantly inhibited P-gp activity at the human BBB by ~2-fold, which is about two times greater than the magnitude observed previously with supertherapeutic concentrations of CsA. The maximum P-gp inhibition at the human BBB (estimated to be ~5-fold) was not achieved by quinidine's clinical concentrations, therefore, in general, quinidine is not likely to be a useful P-gp inhibitor that can significantly increase the CNS delivery and efficacy of P-gp substrate drugs targeted for the CNS. However, this does not discount the possibility of significant DDIs with quinidine. These are likely when the P-gp substrate drug exhibits a narrow therapeutic index (e.g., digoxin, loperamide), and where P-gp is a major component in mediating the drug's transport across the BBB (e.g., nelfinavir). We also showed that the quinidine-^{11}C-verapamil DDI mediated by BBB P-gp observed in this study was well predicted using a combination of preclinical data from macaque BBB and *in vitro* MDR1 overexpressing cell line studies. But discrepancy was

observed when the rodent BBB data was used, confirming the species-dependent differences previously reported for BBB P-gp expression as well as CBF between the two animal models and humans. Furthermore, the consequence of such differences also seemed to vary depending on the P-gp inhibitor used. Thus, extrapolation of P-gp mediated DDIs in humans from preclinical experimental models should be conducted with caution. Lastly, unlike traditional and previously published PET-imaging studies, we used three different approaches of data analysis, and therefore three different measurements of P-gp inhibition (comparison of AUCR, ER, ER PMAP of ^{11}C-verapamil radioactivity distribution into the brain at baseline vs. those in the presence of quinidine). While each index is unique and provides accurate assessment of P-gp inhibition at the human BBB, we recommend ER of ^{11}C-verapamil radioactivity distribution into the brain be used as the primary index for P-gp activity, because unlike the other two alternatives, it is both quantitative and accounts for changes in CBF.

Conversely, in **Chapter 5**, we investigated whether P-gp at the human BBB can be induced, a question that has long been asked, but was not addressed until our study. We chose rifampin as our model P-gp inducer because it is an approved drug that has been proven clinically to induce intestinal/hepatic P-gp after as little as 6 days of oral administration. We recruited healthy human volunteers to follow this standard rifampin protocol (600 mg QD, nightly) for 11-29 days, and then quantified the magnitude of change in BBB P-gp activity in comparison to baseline (the same study group for the quinidine PET study) using PET-imaging and ^{11}C-verapamil as our P-gp PET substrate. However, our findings showed that rifampin treatment did not significantly change P-gp activity at the human BBB, even though its inductive effect was observed in the CYP3A-mediated metabolism of ^{11}C-verapamil. While insufficient rifampin systemic and/or intracellular exposure in the brain microvessel endothelial cells could

explain the lack of P-gp induction at the human BBB, another potential explanation that needs further investigation, is that PXR expression may be too low or absent at the human BBB. There has been only one study that reported PXR and CAR mRNA expression are not detected in isolated human brain microvessels, while that of AhR is. Therefore, future studies are needed to determine whether the nuclear receptors known to regulate P-gp in other tissues (e.g., PXR, CAR, GR, AhR, VDR, FXR) are also present at the human BBB. If so, quantifying the expression of such nuclear receptors at the human BBB can help identify additional pathways to induce P-gp at this critical anatomical site. It would also be interesting to compare the expression profiles of these nuclear receptors in healthy human brains vs. those with different CNS diseases, which could provide new insights into P-gp's role in specific CNS diseases and how P-gp modulation could improve their treatments.

In conclusion, the work presented in this thesis has significantly enhanced our understanding and prediction of PIs-based DDIs that are mediated by metabolic enzymes and/or transporters, as well as in our understanding of P-gp mediated DDIs at the human BBB. With the studies we have conducted, we addressed and explained many unanswered questions and key issues that we believe have contributed to the complexity of DDIs associated with HIV protease inhibitors and those mediated by P-gp at the human BBB. However, many new and interesting questions are raised from these studies, and remained to be addressed.

References

Abbott NJ, Patabendige AA, Dolman DE, Yusof SR, Begley DJ. Structure and function of the blood-brain barrier. *Neurobiol Dis*. 2010; **37** : 13-25.

Aiba T, Susa M, Fukumori S, Hashimoto Y. The effects of culture conditions on CYP3A4 and MDR1 mRNA induction by 1alpha,25-dihydroxyvitamin D(3) in human intestinal cell lines, Caco-2 and LS180. *Drug Metab Pharmacokinet*. 2005; **20** : 268-274.

Aller SG, Yu J, Ward A, et al. Structure of P-glycoprotein reveals a molecular basis for poly-specific drug binding. *Science*. 2009; **323** : 1718−1722.

Amsden GW, Nafziger AN, Foulds G, Cabelus LJ. A study of the pharmacokinetics of azithromycin and nelfinavir when coadministered in healthy volunteers. *J Clin Pharmacol* 2000; **40** : 1522-1527.

Annaert P, Ye ZW, Stieger B, Augustijns P. Interaction of HIV protease inhibitors with OATP1B1, 1B3, and 2B1. *Xenobiotica* 2010; **40** : 163-176.

Arts EJ, Hazuda DJ. HIV-1 Antiretroviral Drug Therapy. *Cold Spring Harb Perspect Med*. 2012; **2** : a007161.

Aslan S, Huang H, Uh J, et al. White matter cerebral blood flow is inversely correlated with structural and functional connectivity in the human brain. *Neuroimage.* 2011; **56** : 1145-1153.

Atazanavir sulfate (Reyataz^{TM}) drug label, Bristol-Myers Squibb, October 2004.

Bankstahl JP, Kuntner C, Abrahim A, et al. Tariquidar-induced P-glycoprotein inhibition at the rat blood-brain barrier studied with (R)-11C-verapamil and PET. *J Nucl Med*. 2008; **49** : 1328-1335.

Bart J, Willemsen AT, Groen HJ, et al. Quantitative assessment of P-glycoprotein function in the rat blood-brain barrier by distribution volume of [11C]verapamil measured with PET. *Neuroimage*. 2003; **20** : 1775-1782.

Bauer B, Yang X, Hartz AM, Olson ER, Zhao R, Kalvass JC, Pollack GM, Miller DS. In vivo activation of human pregnane X receptor tightens the blood-brain barrier to methadone through P-glycoprotein up-regulation. *Mol Pharmacol*. 2006; **70** : 1212-1219.

Bauer M, Zeitlinger M, Karch R, et al. Pgp-mediated interaction between (R)-[11C]verapamil and tariquidar at the human blood-brain barrier: a comparison with rat data. *Clin Pharmacol Ther*. 2012; **91** : 227-233.

Beaulieu E, Demeule M, Ghitescu L, Béliveau R. P-glycoprotein is strongly expressed in the luminal membranes of the endothelium of blood vessels in the brain. *Biochem J*. 1997; **326** : 539-544.

Boffito M, Dickinson L, Hill A, Back D, Moyle G, Nelson M, Higgs C, Fletcher C, Gazzard B, Pozniak A. Steady-state pharmacokinetics of saquiniavir hard-gel/ritonavir/foxamprenavir in HIV-1-infected patients. *J Acquir Immune Defic Syndr* 2004; **37** : 1376-1384.

Brophy DF, Israel DS, Pastor A, Gillotin C, Chittick GE, Symonds WT, Lou Y, Sadler BM, Polk RE. Pharmacokinetic interaction between amprenavir and clarithromycin in healthy male volunteers. *Antimicrob Agents Chemother* 2000; **44** : 978-984.

Brunton LL, Blumenthal DK, Murri N, Dandan RH, Knollmann BC. *Goodman & Gilman's The Pharmacological Basis of Therapeutics.12th ed.* New York: McGraw-Hill publishers; 2011.

Burger DM, Huisman A, Van Ewijk N, Neisingh H, Van Uden P, Rongen GA, Koopmans P, Bertz RJ. The effect of atazanavir and atazanavir/ritonavir on UDP-glucuronosyltransferase using lamotrigine as a phenotypic probe. *Clin Pharmacol Ther*. 2008; **84** : 698-703.

Buss N, Snell P, Bock J, Hsu A, Jorga K. Saquinavir and ritonavir pharmacokinetics following combined ritonavir and saquinavir (soft gelatin capsules) administration. *J Clin Pharmacol* 2001; **52** : 255-264.

Busti AJ, Bain AM, Hall RG, Bedimo RG, Leff RD, Meek C, Mehvar R. Effects of atazanavir/ritonavir or fosamprenavir/ritonavir on the pharmacokinetics of rosuvastatin. *J Cardiovasc Pharmacol* 2008; **51** : 605-610.

Chen L, Sabo JP, Philip E, Mao Y, Norris SH, MacGregor TR, Wruck JM, Garfinkel S, Castles M, Brinkman A, Valdez H. Steady-state disposition of the nonpeptidic protease inhibitor tipranavir when coadministered with ritonavir. *Antimicrob Agents Chemother* 2007; **51** : 2436-2444.

Cirrito JR, Deane R, Fagan AM, Spinner ML, Parsadanian M, Finn MB, Jiang H, Prior JL, Sagare A, Bales KR, Paul SM, Zlokovic BV, Piwnica-Worms D, Holtzman DM. P-glycoprotein deficiency at the blood-brain barrier increases amyloid-beta deposition in an Alzheimer disease mouse model. *J Clin Invest*. 2005; **115** : 3285-3290.

Cordon-Cardo C, O'Brien JP, Casals D, Rittman-Grauer L, Biedler JL, Melamed MR, Bertino JR. Multidrug-resistance gene (P-glycoprotein) is expressed by endothelial cells at blood-brain barrier sites. *Proc Natl Acad Sci U S A*. 1989; **86** : 695-698.

Dauchy S, Dutheil F, Weaver RJ, Chassoux F, Daumas-Duport C, Couraud PO, Scherrmann JM, De Waziers I, Declèves X. ABC transporters, cytochromes P450 and their main

transcription factors: expression at the human blood-brain barrier. *J Neurochem*. 2008; **107** : 1518-1528.

Denissen JF, Grabowski BA, Johnson MK, Buko AM, Kempf DJ, Thomas SB, Surber BW. Metabolism and disposition of the HIV-1 protease inhibitor ritonavir (ABT-538) in rats, dogs, and humans. *Drug Metab Dispos* 1997; **25** : 489-501.

Desai PB, Nallani SC, Sane RS, Moore LB, Goodwin BJ, Buckley DJ, Buckley AR. Induction of cytochrome P450 3A4 in primary human hepatocytes and activation of the human pregnane X receptor by tamoxifen and 4-hydroxytamoxifen. *Drug Metab Dispos 2002*; **30** : 608-612.

Dickinson L, Khoo S, Back D. Pharmacokinetics and drug-drug interactions of antiretrovirals: an update. *Antiviral Res*. 2010; **85** : 176-89.

Dixit V, Hariparsad N, Li F, Desai P, Thummel KE, Unadkat JD. Cytochrome P450 enzymes and transporters induced by anti-human immunodeficiency virus protease inhibitors in human hepatocytes: implications for predicting clinical drug interactions. *Drug Metab Dispos* 2007a; **35** : 1853-1859.

Dixit V, Hariparsad N, Desai P, Unadkat JD. In vitro LC-MS cocktail assays to determine simultaneously human cytochrome P450 activities. *Biopharm Drug Dispos* 2007b; **28** : 257-262.

Dussault I, Lin M, Hollister K, Wang EH, Synold TW, Forman BM. Peptide mimetic HIV protease inhibitors are ligands for the orphan receptor SXR. *J Biol Chem*. 2001; **276** : 33309-33312.

Ernest CS, 2nd, Hall SD, and Jones DR. Mechanism-based inactivation of CYP3A by HIV protease inhibitors. *J Pharmacol Exp Ther* 2005; **312** : 583-591.

Eyal S, Chung FS, Muzi M, et al. Simultaneous PET imaging of P-glycoprotein inhibition in multiple tissues in the pregnant nonhuman primate. *J Nucl Med.* 2009; **50** : 798-806.

Eyal S, Ke B, Muzi M, et al. Regional P-glycoprotein activity and inhibition at the human blood-brain barrier as imaged by positron emission tomography. *Clin Pharmacol Ther*. 2010; **87** : 579-585.

Eyal S, Hsiao P, Unadkat JD. Drug interactions at the blood-brain barrier: fact or fantasy? *Pharmacol Ther*. 2009; **123** : 80-104.

Fahmi OA, Kish M, Boldt S, Obach RS. Cytochrome P450 3A4 mRNA is a more reliable marker than CYP3A4 activity for detecting pregnane X receptor-activated induction of drug-metabolizing enzymes. *Drug Metab Dispos* 2010; **38** : 1605-1611.

Fichtenbaum CJ, Gerber JG, Rosenkranz SL, Segal Y, Aberg JA, Blaschke T, Alston B, Fang F, Kosel B, Aweeka F; NIAID AIDS Clinical Trials Group. Pharmacokinetic interactions between protease inhibitors and statins in HIV seronegative volunteers: ACTG Study A5047. *AIDS* 2002; **16** : 569-577.

FDA DDI guidance. The FDA Website. http://www.fda.gov/downloads/Drugs/GuidanceComplianceRegulatoryInformation/Guidances/ucm072101.pdf

Govindarajan R, Endres CJ, Whittington D, LeCluyse E, Pastor-Anglada M, Tse CM, Unadkat JD. Expression and hepatobiliary transport characteristics of the concentrative and equilibrative nucleoside transporters in sandwich-cultured human hepatocytes. *Am J Physiol Gastrointest Liver Physiol* 2008; **295** : 570-580.

Grube M, Köck K, Karner S, Reuther S, Ritter CA, Jedlitschky G, Kroemer HK. Modification of OATP2B1-mediated transport by steroid hormones. *Mol Pharmacol* 2006; **70** : 1735-1741.

Gupta A, Mugundu GM, Desai PB, Thummel KE, Unadkat JD. Intestinal human colon adenocarcinoma cell line LS180 is an excellent model to study pregnane X receptor, but not constitutive androstane receptor, mediated CYP3A4 and multidrug resistance transporter 1 induction: studies with anti-human immunodeficiency virus protease inhibitors. *Drug Metab Dispos*. 2008; **36** : 1172-1180.

Gupta A, Zhang Y, Unadkat JD, Mao Q. HIV protease inhibitors are inhibitors but not substrates of the human breast cancer resistance protein (BCRP/ABCG2). *J Pharmacol Exp Ther* 2004; **310** : 334-341.

Gurley BJ, Swain A, Williams DK, Barone G, Battu SK. Gauging the clinical significance of P-glycoprotein-mediated herb-drug interactions: comparative effects of St. John's wort, Echinacea, clarithromycin, and rifampin on digoxin pharmacokinetics. *Mol Nutr Food Res*. 2008; **52** : 772-779.

Hagenbuch B, Gui C. Xenobiotic transporters of the human organic anion transporting polypeptides (OATP) family. *Xenobiotica* 2008; **38** : 778-801.

Hamman MA, Bruce MA, Haehner-Daniels BD, Hall SD. The effect of rifampin administration on the disposition of fexofenadine. *Clin Pharmacol Ther*. 200; **69** : 114-421.

Hardman JG, Limbird LE, Gilman AG. Goodman & Gilman's The Pharmacological Basis of Therapeutics, 10/e. McGraw-Hill: New York, 2001.

Hartkoorn RC, Kwan WS, Shallcross V, Chaikan A, Liptrott N, Egan D, Sora ES, James CE, Gibbons S, Bray PG, Back DJ, Khoo SH, Owen A. HIV protease inhibitors are substrates for OATP1A2, OATP1B1 and OATP1B3 and lopinavir plasma concentrations are influenced by SLCO1B1 polymorphisms. *Pharmacogenet Genomics* 2010; **20** :112-120.

Hartz AM, Miller DS, Bauer B. Restoring blood-brain barrier P-glycoprotein reduces brain amyloid-beta in a mouse model of Alzheimer's disease. *Mol Pharmacol*. 2010; **77** : 715-723.

Hewitt N J, Buhring KU, Dasenbrock J, Haunschild J, Ladstetter B, Utesch D. Studies comparing in vivo:in vitro metabolism of three pharmaceutical compounds in rat, dog, monkey, and human using cryopreserved hepatocytes, microsomes, and collagen gel immobilized hepatocyte cultures. *Drug Metab Dispos* 2001; **29** : 1042–1050.

Hendrikse NH, Schinkel AH, de Vries EG, Fluks E, Van der Graaf WT, Willemsen AT, Vaalburg W, Franssen EJ. Complete in vivo reversal of P-glycoprotein pump function in the blood-brain barrier visualized with positron emission tomography. *Br J Pharmacol*. 1998; **124** : 1413-1418.

Hill A, van der Lugt J, Sawyer W, Boffito M. How much ritonavir is needed to boost protease inhibitors? Systematic review of 17 dose-ranging pharmacokinetic trials. *AIDS* 2009; **23** : 2237-2245.

Hogeland GW, Swindells S, McNabb JC, Kashuba AD, Yee GC, Lindley CM. Lopinavir/ritonavir reduces bupropion plasma concentrations in healthy subjects. *Clin Pharmacol Ther* 2007; **81** : 69-75.

Hsiao P, Bui T, Ho RJ, Unadkat JD. In vitro-to-in vivo prediction of p-glycoprotein-based drug interactions at the human and rodent blood-brain barrier. *Drug Metab Dispos* 2008; **36** : 481-484.

Hsiao P, Sasongko L, Link JM, et al. Verapamil P-glycoprotein Transport across the Rat Blood-Brain Barrier: Cyclosporine, a Concentration Inhibition Analysis, and Comparison with Human Data. *J. Pharmacol. Exp. Ther.* 2006; **317** : 704-710.

Huisman MT, Smit JW, Crommentuyn KM, Zelcer N, Wiltshire HR, Beijnen JH, Schinkel AH. Multidrug resistance protein 2 (MRP2) transports HIV protease inhibitors, and transport can be enhanced by other drugs. *AIDS* 2002; **16** : 2295-2301.

Hsyu PH, Lillibridge J, Daniels E, Kerr BM. Pharmacokinetic interaction of nelfinavir and methadone in intravenous drug users. *Biopharm Drug Dispos* 2006; **27** : 61-68.

Ito K, Uchida Y, Ohtsuki S, et al. Quantitative membrane protein expression at the blood-brain barrier of adult and younger cynomolgus monkeys. *J Pharm Sci.* 2011; **100** : 3939-3950.

Kaddoumi A, Choi SU, Kinman L, et al. Inhibition of P-glycoprotein activity at the primate blood-brain barrier increases the distribution of nelfinavir into the brain but not into the cerebrospinal fluid. *Drug Metab Dispos*. 2007; **35** : 1459-1462.

Kannan P, Brimacombe KR, Kreisl WC, Liow JS, Zoghbi SS, Telu S, Zhang Y, Pike VW, Halldin C, Gottesman MM, Innis RB, Hall MD. Lysosomal trapping of a radiolabeled

substrate of P-glycoprotein as a mechanism for signal amplification in PET. *Proc Natl Acad Sci U S A*. 2011; **108** : 2593-2598.

Kawamura K, Yamasaki T, Yui J, Hatori A, Konno F, Kumata K, Irie T, Fukumura T, Suzuki K, Kanno I, Zhang MR. In vivo evaluation of P-glycoprotein and breast cancer resistance protein modulation in the brain using [(11)C]gefitinib. *Nucl Med Biol*. 2009; **36** : 239-46.

Kemper EM, Cleypool C, Boogerd W, Beijnen JH, van Tellingen O. The influence of the P-glycoprotein inhibitor zosuquidar trihydrochloride (LY335979) on the brain penetration of paclitaxel in mice. *Cancer Chemother Pharmacol*. 2004; **53** : 173-178.

Kemper EM, van Zandbergen AE, Cleypool C, Mos HA, Boogerd W, Beijnen JH, van Tellingen O. Increased penetration of paclitaxel into the brain by inhibition of P-Glycoprotein. *Clin Cancer Res*. 2003; **9** : 2849-2855.

Kemper EM, Verheij M, Boogerd W, Beijnen JH, van Tellingen O. Improved penetration of docetaxel into the brain by co-administration of inhibitors of P-glycoprotein. *Eur J Cancer*. 2004b; **40** : 1269-1274.

Kent UM, Bend JR, Chamberlin BA, Gage DA, Hollenberg PF. Mechanism-based inactivation of cytochrome P450 2B1 by N-benzyl-1-aminobenzotriazole. *Chem Res Toxicol* 1997; **10** : 600-608.

Kharasch ED, Hoffer C, Whittington D, Walker A, Bedynek PS. Methadone pharmacokinetics are independent of cytochrome P4503A (CYP3A) activity and gastrointestinal drug transport: insights from methadone interactions with ritonavir/indinavir. *Anesthesiology* 2009; **110** : 660-672.

Kim RB. Drugs as P-glycoprotein substrates, inhibitors, and inducers. *Drug Metab Rev* 2002; **34** : 47-54.

Kim RB, Fromm MF, Wandel C, Leake B, Wood AJ, Roden DM, Wilkinson GR. The drug transporter P-glycoprotein limits oral absorption and brain entry of HIV-1 protease inhibitors. *J Clin Invest*. 1998; **101** : 289-294.

Kimoto E, Walsky R, Zhang H, Bi YA, Whalen KM, Yang YS, Linder C, Xiao Y, Iseki K, Fenner KS, El-Kattan AF, Lai Y. Differential modulation of cytochrome p450 activity and the effect of 1-aminobenzotriazole on hepatic transport in sandwich-cultured human hepatocytes. *Drug Metab Dispos* 2012; **40** : 407-411.

Kindla J, Müller F, Mieth M, Fromm MF, König J. Influence of non-steroidal anti-inflammatory drugs on organic anion transporting polypeptide (OATP) 1B1- and OATP1B3-mediated drug transport. *Drug Metab Dispos* 2011; **39** : 1047-1053.

Kirby BJ, Collier AC, Kharasch ED, Whittington D, Thummel KE, Unadkat JD. Complex drug interactions of HIV protease inhibitors 1: inactivation, induction, and inhibition of

cytochrome P450 3A by ritonavir or nelfinavir. *Drug Metab Dispos* 2011a; **39** : 1070-1078.

Kirby BJ, Collier AC, Kharasch ED, Vaishali D, Desai P, Whittington D, Thummel KE, Unadkat JD. Complex drug interactions of HIV protease inhibitors 2: In vivo induction and in vitro to in vivo correlation of induction of cytochrome P450 1A2, 2B6 and 2C9 by ritonavir or nelfinavir. *Drug Metab Dispos* 2011b; **39** : 2329-2337.

Kis O, Robillard K, Chan GN, Bendayan R. The complexities of antiretroviral drug-drug interactions: role of ABC and SLC transporters. *Trends Pharmacol Sci*. 2010; **31**: 22-35.

Kis O, Zastre JA, Ramaswamy M, Bendayan R. pH dependence of organic anion-transporting polypeptide 2B1 in Caco-2 cells: potential role in antiretroviral drug oral bioavailability and drug-drug interactions. *J Pharmacol Exp Ther* 2010; **334** : 1009-1022.

Kiser JJ, Gerber JG, Predhomme JA, Wolfe P, Flynn DM, Hoody DW. Drug/drug interaction between lopinavir/ritonavir and rosuvastatin in heathy volunteers. *J Acquir Immune Defic Syndr* 2008; **47** : 570–578.

Klein CE, Chiu YL, Cai Y, Beck K, King KR, Causemaker SJ, Doan T, Esslinger HU, Podsadecki TJ, Hanna GJ. Effects of acid-reducing agents on the pharmacokinetics of lopinavir/ritonavir and ritonavir-boosted atazanavir. *J Clin Pharmacol* 2008; **48** : 553-562.

Kreisl WC, Liow JS, Kimura N, et al. P-Glycoprotein Function at the Blood–Brain Barrier in Humans Can Be Quantified with the Substrate Radiotracer 11C-N-Desmethyl-Loperamide. *J Nucl Med.* 2010; **51** : 559-566.

Kumar GN, Jayanti VK, Johnson MK, Uchic J, Thomas S, Lee RD, Grabowski BA, Sham HL, Kempf DJ, Denissen JF, Marsh KC, Sun E, Roberts SA. Metabolism and disposition of the HIV-1 protease inhibitor lopinavir (ABT-378) given in combination with ritonavir in rats, dogs, and humans. *Pharm Res* 2004; **21** : 1622-1630.

Kurowski M, Sternfeld T, Sawyer A, Hill A, Möcklinghoff C. Pharmacokinetic and tolerability profile of twice-daily saquinavir hard gelatin capsules and saquinavir soft gelatin capsules boosted with ritonavir in healthy volunteers. *HIV Med* 2003; **4** : 94-100.

la Porte CJ, de Graaff-Teulen MJ, Colbers EP, Voncken DS, Ibanez SM, Koopmans PP, Hekster YA, Burger DM. Effect of efavirenz treatment on the pharmacokinetics of nelfinavir boosted by ritonavir in healthy volunteers. *Br J Clin Pharmacol* 2004; **58** : 632-640.

Lee G, Dallas S, Hong M, Bendayan R. Drug transporters in the central nervous system: brain barriers and brain parenchyma considera-tions. *Pharmacol. Rev*. 2001; **53** : 569–596

Lim ML, Min SS, Eron JJ, Bertz RJ, Robinson M, Gaedigk A, Kashuba AD. Coadministration of lopinavir/ritonavir and phenytoin results in two-way drug interaction through cytochrome P-450 induction. *J Acquir Immune Defic Syndr* 2004; **36** : 1034-1040.

Linnet K, Ejsing TB. A review on the impact of P-glycoprotein on the penetration of drugs into the brain. Focus on psychotropic drugs. *Eur Neuropsychopharmacol* 2008; **18** : 157-69.

Liow JS, Kreisl W, Zoghbi SS, et al. P-glycoprotein function at the blood-brain barrier imaged using 11C-N-desmethyl-loperamide in monkeys. *J Nucl Med*. 2009; **50** :108-115.

Liu L, Mugundu G, Kirby BJ, Divya S, Pankaj D, Unadkat JD. Quantification of human hepatocyte cytochrome P450 enzymes and transporters induced by HIV protease inhibitors using newly validated LC-MS/MS cocktail assays and RT-PCR. *Biopharm & Drug Disp* 2012a; **33** : 207-217.

Liu L, Collier AC, Link JM, Domino KB, Mankoff DA, Eary JF, Richards T, Hsiao P, Deo AK, Unadkat JD. Quinidine inhibition of P-glycoprotein at the human blood-brain barrier as measured by positron emission tomography imaging. Submitted to *Journ of Nucl Med*

Löscher W, Potschka H. Role of drug efflux transporters in the brain for drug disposition and treatment of brain diseases. *Prog Neurobiol*. 2005a; **76** : 22-76.

Löscher W, Potschka H. Blood-brain barrier active efflux transporters: ATP-binding cassette gene family. *NeuroRx*. 2005b; **2** : 86-98.

Lubberink M, Luurtsema G, van Berckel BN, et al. Evaluation of tracer kinetic models for quantification of P-glycoprotein function using (R)-[11C]verapamil and PET. *J Cereb Blood Flow Metab*. 2007; **27** : 424-433.

Luurtsema G, Molthoff CF, Schuit RC, Windhorst AD, Lammertsma AA, Franssen EJ. Evaluation of (R)-[11C]verapamil as PET tracer of P-glycoprotein function in the blood-brain barrier: kinetics and metabolism in the rat. *Nucl Med Biol*. 2005; **32** : 87-93.

Martin C, Berridge G, Higgins CF, Mistry P, Charlton P, Callaghan R. Communication between multiple drug binding sites on P-glycoprotein. *Mol Pharmacol* 2000; **58** : 624−632.

Martin P, Riley R, Back DJ, Owen A. Comparison of the induction profile for drug disposition proteins by typical nuclear receptor activators in human hepatic and intestinal cells. *Br J Pharmacol*. 2008; **153** : 805-819.

Mathias AA, Hinkle J, Shen G, Enejosa J, Piliero PJ, Sekar V, Mack R, Tomaka F, Kearney BP. Effect of ritonavir-boosted tipranavir or darunavir on the steady-state pharmacokinetics of elvitegravir. *J Acquir Immune Defic Syndr* 2008; **49** : 156-162.

Matsushima S, Maeda K, Kondo C, Hirano M, Sasaki M, Suzuki H, Sugiyama Y. Identification of the hepatic efflux transporters of organic anions using double-transfected Madin-Darby canine kidney II cells expressing human organic anion-transporting polypeptide 1B1 (OATP1B1)/multidrug resistance-associated protein 2, OATP1B1/multidrug resistance 1, and OATP1B1/breast cancer resistance protein. *J Pharmacol Exp Ther*. 2005; **314** : 1059-1067.

McRae MP, Lowe CM, Tian X, Bourdet DL, Ho RH, Leake BF, Kim RB, Brouwer KL, Kashuba AD. Ritonavir, saquinavir, and efavirenz, but not nevirapine, inhibit bile acid transport in human and rat hepatocytes. *J Pharmacol Exp Ther*. 2006; **318** : 1068-1075.

Miller DS. Regulation of P-glycoprotein and other ABC drug transporters at the blood-brain barrier. *Trends Pharmacol Sci*. 2010; **31** : 246-254.

Mugundu GM, Hariparsad N, Desai PB. Impact of ritonavir, atazanavir and their combination on the CYP3A4 induction by efavirenz in primary human hepatocytes. *Drug Metabolism Letter* 2010; **4** : 45-50.

Mukwaya G, MacGregor T, Hoelscher D, Heming T, Legg D, Kavanaugh K, Johnson P, Sabo JP, McCallister S. Interaction of ritonavir-boosted tipranavir with loperamide does not result in loperamide-associated neurologic side effects in healthy volunteers. *Antimicrob Agents Chemother* 2005; **49** : 4903-4910.

Muzi M, Mankoff DA, Link JM, et al. Imaging of Cyclosporine Inhibition of P-Glycoprotein Activity Using 11C-Verapamil in the Brain: Studies of Healthy Humans. *J Nucl Med.* 2009; **50** : 1267–1275.

Narang VS, Fraga C, Kumar N, Shen J, Throm S, Stewart CF, Waters CM. Dexamethasone increases expression and activity of multidrug resistance transporters at the rat blood-brain barrier. *Am J Physiol Cell Physiol*. 2008; **295** : C440-450.

Niemi M, Backman JT, Fromm MF, Neuvonen PJ, Kivistö KT. Pharmacokinetic interactions with rifampicin : clinical relevance. *Clin Pharmacokinet*. 2003; **42** : 819-850.

Nussey S, Whitehead S. *Endocrinology: An Integrated Approach*. Oxford: BIOS Scientific Publishers; 2001.

Ohtsuki S, Ito S, Terasaki T. Is P-glycoprotein involved in amyloid-β elimination across the blood-brain barrier in Alzheimer's disease? *Clin Pharmacol Ther*. 2010; **88** : 443-445.

Oostendorp RL, van de Steeg E, van der Kruijssen CM, Beijnen JH, Kenworthy KE, Schinkel AH, Schellens JH. Organic anion-transporting polypeptide 1B1 mediates transport of Gimatecan and BNP1350 and can be inhibited by several classic ATP-binding cassette (ABC) B1 and/or ABCG2 inhibitors. *Drug Metab Dispos* 2009; **37** : 917-923.

Ott M, Fricker G, Bauer B. Pregnane X receptor (PXR) regulates P-glycoprotein at the blood-brain barrier: functional similarities between pig and human PXR. *J Pharmacol Exp Ther*. 2009; **329** : 141-149.

Ozdemir V, Kalow W, Tang BK, Paterson AD, Walker SE, Endrenyi L, and Kashuba AD. Evaluation of the genetic component of variability in CYP3A4 activity: a repeated drug administration method. *Pharmacogenetics* 2000; **10** : 373–388.

Paine MF, Khalighi M, Fisher JM, Shen DD, Kunze KL, Marsh CL, Perkins JD and Thummel KE. Characterization of interintestinal and intraintestinal variations in human CYP3A-dependent metabolism. *J Pharmacol Exp Ther* 1997; **283** :1552-1562.

Pardridge WM. Blood–brain barrier biology and methodology. *J. Neurovirol*. 1999; **5** ; 556–569.

Parker AJ and J. Brian Houston. Rate-Limiting Steps in Hepatic Drug Clearance: Comparison of Hepatocellular Uptake and Metabolism with Microsomal Metabolism of Saquinavir, Nelfinavir, and Ritonavir. *Drug Metab Dispos* 2008; **36** : 1375–1384.

Pauli-Magnus C, von Richter O, Burk O, et al. Characterization of the major metabolites of verapamil as substrates and inhibitors of P-glycoprotein. *JPET*. 2000; **293** : 376–382.

Ray GM. Antiretroviral and statin drug-drug interactions. *Cardiol Rev*. 2009; **17** : 44-47.

Reece PA, Peikert M. Simple and selective high-performance liquid chromatographic method for estimating plasma quinidine levels. *J Chromatogr*. 1980; **181** : 207-217.

Reich T, Rusinek H. Cerebral cortical and white matter reactivity to carbon dioxide. *Stroke.* 1989; **20** : 453-457.

Reschly EJ, Krasowski MD. Evolution and function of the NR1I nuclear hormone receptor subfamily (VDR, PXR, and CAR) with respect to metabolism of xenobiotics and endogenous compounds. *Curr Drug Metab*. 2006; **7** : 349-365.

Saah AJ, Winchell GA, Nessly ML, Seniuk MA, Rhodes RR, Deutsch PJ. Pharmacokinetic profile and tolerability of indinavir-ritonavir combinations in healthy volunteers. *Antimicrob Agents Chemother* 2001; **45** : 2710-2715.

Sadeque AJ, Wandel C, He H, Shah S, Wood AJ. Increased drug delivery to the brain by P-glycoprotein inhibition. *Clin Pharmacol Ther*. 2000; **68** : 231-237.

Sadler BM, Chittick GE, Polk RE, Slain D, Kerkering TM, Studenberg SD, Lou Y, Moore KH, Woolley JL, Stein DS. Metabolic disposition and pharmacokinetics of [14C]-amprenavir, a human immunodeficiency virus type 1 (HIV-1) protease inhibitor, administered as a single oral dose to healthy male subjects. *J Clin Pharmacol* 2001; **41** : 386-396.

Saquinavir (Fortovase) soft gelatin capsules drug label, Hoffmann-Lab Roche, December 2003.

Sasongko L, Link JM, Muzi M, et al. Imaging P-glycoprotein transport activity at the human blood-brain barrier with positron emission tomography. *Clin Pharmacol Ther*. 2005; **77** : 503-514.

Seneca N, Zoghbi SS, Liow JS, et al. Human brain imaging and radiation dosimetry of 11C-N-desmethyl-loperamide, a PET radiotracer to measure the function of P-glycoprotein. *J Nucl Med*. 2009; **50** : 807-813.

Skarke C, Jarrar M, Erb K, Schmidt H, Geisslinger G, Lötsch J. Respiratory and miotic effects of morphine in healthy volunteers when P-glycoprotein is blocked by quinidine. *Clin Pharmacol Ther*. 2003;**74** : 303-311.

Shawahna R, Uchida Y, Declèves X, et al. Transcriptomic and quantitative proteomic analysis of transporters and drug metabolizing enzymes in freshly isolated human brain microvessels. *Mol Pharm.* 2011; **8** : 1332-1341.

Su Y, Zhang X, Sinko PJ. Human organic anion-transporting polypeptide OATP-A (SLC21A3) acts in concert with P-glycoprotein and multidrug resistance protein 2 in the vectorial transport of Saquinavir in Hep G2 cells. *Mol Pharm* 2004; **1** : 49-56.

Sun H, Dai H, Shaik N, Elmquist WF. Drug efflux transporters in the CNS. *Adv Drug Deliv Rev* 2003; **55** : 83-105.

Thiebaut F, Tsuruo T, Hamada H, Gottesman MM, Pastan I, Willingham MC. Immunohistochemical localization in normal tissues of different epitopes in the multidrug transport protein P170: evidence for localization in brain capillaries and crossreactivity of one antibody with a muscle protein. *J Histochem Cytochem*.1989; **37** : 159-164.

Thompson MA, Aberg JA, Hoy JF, Telenti A, Benson C, Cahn P, Eron JJ, Günthard HF, Hammer SM, Reiss P, Richman DD, Rizzardini G, Thomas DL, Jacobsen DM, Volberding PA. Antiretroviral treatment of adult HIV infection: 2012 recommendations of the International Antiviral Society-USA panel. *JAMA*. 2012; **308** : 387-402.

Tracy TS, Korzekwa KR, Gonzalez FJ, Wainer IW. Cytochrome P450 isoforms involved in metabolism of the enantiomers of verapamil and norverapamil. *Br J Clin. Pharmacol*. 1999; **47** : 545-552.

Tröger U, Lins H, Scherrmann JM, Wallesch CW, Bode-Böger SM. Tetraparesis associated with colchicine is probably due to inhibition by verapamil of the P-glycoprotein efflux pump in the blood-brain barrier. *BMJ*. 2005; **331** : 613.

Uchida Y, Ohtsuki S, Katsukura Y, et al. Quantitative targeted absolute proteomics of human blood-brain barrier transporters and receptors. *J Neurochem*. 2011; **117** : 333-345.

Unadkat JD, Chung F, Sasongko L, et al. Rapid solid-phase extraction method to quantify [(11)C]-verapamil, and its [(11)C]-metabolites, in human and macaque plasma. *Nucl Med Biol*. 2008; **35** : 911-917.

Unadkat JD and Y. Wang, *Protease Inhibitors*, in *Metabolic Drug Interactions*, R.H. Levy, et al., Editors. 2000, Lippincott Williams & Wilkins: Philadelphia. p. 647-652.

van der Lee MJ, Blenke AA, Rongen GA, Verwey-van Wissen CP, Koopmans PP, Pharo C, Burger DM. Interaction study of the combined use of paroxetine and fosamprenavir-ritonavir in healthy subjects. *Antimicrob Agents Chemother*. 2007; **51** : 4098-4104.

van der Lee MJ, Dawood L, ter Hofstede HJ, de Graaff-Teulen MJ, van Ewijk-Beneken Kolmer EW, Caliskan-Yassen N, Koopmans PP, Burger DM. Lopinavir/ritonavir reduces lamotrigine plasma concentrations in healthy subjects. *Clin Pharmacol Ther*. 2006; **80** : 159-168.

van der Sandt IC, Vos CM, Nabulsi L, Blom-Roosemalen MC, Voorwinden HH, de Boer AG, Breimer DD. Assessment of active transport of HIV protease inhibitors in various cell lines and the in vitro blood--brain barrier. *AIDS* 2001; **15** : 483-491.

Vandenbossche J, Huisman M, XuY, Sanderson-Bongiovanni D, Soons P. Loperamide and P-glycoprotein inhibition: assessment of the clinical relevance. *J Pharm Pharmacol*. 2010; **62** : 401−412.

Vogelgesang S, Cascorbi I, Schroeder E, Pahnke J, Kroemer HK, Siegmund W, Kunert-Keil C, Walker LC, Warzok RW. Deposition of Alzheimer's beta-amyloid is inversely correlated with P-glycoprotein expression in the brains of elderly non-demented humans. *Pharmacogenetics*. 2002; **12** : 535-541.

Wood R, Eron J, Arasteh K, Teofilo E, Trepo C, Livrozet JM, Yeo J, Millard J, Wire MB, Naderer OJ. A 42-week open-label study to assess the pharmacokinetics, antiretroviral activity, and safety of amprenavir or amprenavir plus ritonavir in combination with abacavir and lamivudine for treatment of HIV-infected patients. *Clin Infect Dis* 2004; **39** : 591-594.

www.accessdata.fda.gov/drugsatfda_docs/label/2010/021567s023lbl.pdf

www.drugbank.ca

Wyen C, Fuhr U, Frank D, Aarnoutse RE, Klaassen T, Lazar A, Seeringer A, Doroshyenko O, Kirchheiner JC, Abdulrazik F, Schmeisser N, Lehmann C, Hein W, Schömig E, Burger DM, Fätkenheuer G, Jetter A. Effect of an antiretroviral regimen containing ritonavir boosted lopinavir on intestinal and hepatic CYP3A, CYP2D6 and P-glycoprotein in HIV-infected patients. *Clin Pharmacol Ther* 2008; **84** : 75-82.

Yanni SB, Augustijns PF, Benjamin DK Jr, Brouwer KL, Thakker DR, Annaert PP. In vitro investigation of the hepatobiliary disposition mechanisms of the antifungal agent micafungin in humans and rats. *Drug Metab Dispos* 2010; **38** : 1848-56.

Ye ZW, Sandrine Camus, Patrick Augustijns, and Pieter Annaert. Interaction of Eight HIV Protease Inhibitors with the Canalicular Efflux Transporter ABCC2 (MRP2) in Sandwich-cultured Rat and Human Hepatocytes. *Biopharm Drug Dispos* 2010; **31** : 178–188.

Yuen N, Anderson SE, Glaser N, Tancredi DJ, O'Donnell ME. Cerebral blood flow and cerebral edema in rats with diabetic ketoacidosis. *Diabetes*. 2008; **57** : 2588-2594.

Zolnerciks JK, Booth-Genthe CL, Gupta A, Harris J, Unadkat JD. Substrate- and species-dependent inhibition of P-glycoprotein-mediated transport: implications for predicting in vivo drug interactions. *J Pharm Sci*. 2011; **100** : 3055-3061.

Vitae

Li (Lilly) Liu was born in China, and move to the US with her parents at the age of 12. Since then she has lived in Mahattan, New Jersey, Kansas, San Francisco, Canada, and Seattle. Lilly graduated from Lowell High School in 2002; and the received her bachelors in Biochemistry and Molecular Cell Biology in 2006. After undergoing multiple undergraduate research scholarships and fellowships related to the disciplines of pharmaceutical sciences, pharmacology, and biochemistry, she decided to pursue her doctoral degree in the Department of Pharmaceutics, University of Washington in 2006. Lilly began her doctoral training under the mentorship of Professor Jashvant D. Unadkat in 2007. While in Professor Unadkat's lab, Lilly has dedicated her thesis research in investigating drug-drug interactions (DDIs) produced by the HIV protease inhibitors; and P-gp mediated DDIs at the human blood-brain barrier (BBB) using PET-imaging in healthy volunteers. Lilly is the recipients of multiple awards, fellowship, and graduate student research grants (e.g., 2011 ISSX poster presentation award, Rank #1; TL1 Pre-doctoral multidisciplinary clinical research fellowship; 2009 and 2011 CFAR support grants, ISSX travel grants, Covance travel grants)

Appendix

Induction of mRNA and Activity

	CYP3A4		CYP3A5		CYP3A		
	mRNA Fold Δ		mRNA Fold Δ		Activity Fold Δ		
Treatment (10 µM)	Mean	SEM	Mean	SEM	Mean	SEM	% of RIF
RIF	5.49	2.62	3.23	1.57	5.66	1.65	100.00%
APV	19.51	12.49	1.39	0.94	1.61	0.95	85.16%
RTV	4.29	0.92	4.02	6.25	1.49	0.34	36.65%
NFV	1.27	0.40	3.71	2.98	4.25	0.54	48.82%
NFV 1µM	8.53	NA	2.70	NA	2.53	NA	42.70%
SQV	2.71	1.67	1.89	1.51	1.91	0.39	30.98%
ATV	3.47	1.42	1.51	0.71	2.58	0.77	49.78%
LPV	1.44	0.65	2.82	3.51	1.91	0.65	42.53%
TPV	2.98	2.55	1.09	0.33	2.58	0.44	49.73%
TPV 1µM	8.00	NA	2.03	NA	2.03	NA	39.20%
IDV	1.33	0.57	2.14	0.81	2.12	0.84	40.83%
N/A = not available, N = 2							

Induction of mRNA and Activity

	CYP2B6				
	mRNA Fold Δ		Activity Fold Δ		
Treatment (10 µM)	Mean	SEM	Mean	SEM	% of RIF
RIF	2.60	1.51	5.09	1.31	100.00%
APV	3.19	0.61	2.11	0.80	94.82%
RTV	2.29	0.51	2.65	0.85	51.51%
NFV	1.10	1.20	3.51	0.89	63.34%
NFV 1µM	1.42	NA	2.43	NA	46.52%
SQV	0.89	0.80	2.14	0.87	55.11%
ATV	1.13	0.58	2.89	0.86	75.51%
LPV	1.07	1.22	3.45	0.53	81.18%
TPV	1.85	1.71	2.15	0.53	56.30%
TPV 1µM	2.35	NA	1.70	NA	44.22%
IDV	0.60	0.46	1.85	0.66	48.23%
NA = not available, N = 2					

Induction of mRNA and Activity

	CYP2C8				
	mRNA Fold Δ		Activity Fold Δ		
Treatment (10 µM)	Mean	SEM	Mean	SEM	% of RIF
RIF	2.27	0.84	3.82	0.73	100.00%
APV	6.18	3.25	1.12	0.52	61.22%
RTV	2.45	1.58	1.16	0.19	29.40%
NFV	1.56	0.93	1.94	0.46	32.47%
NFV 1µM	7.77	NA	1.07	NA	17.02%
SQV	2.84	2.14	1.06	0.52	33.75%
ATV	2.41	1.43	1.22	0.33	36.83%
LPV	0.89	0.47	1.95	0.49	63.20%
TPV	0.84	0.56	1.59	0.38	48.17%
TPV 1µM	3.68	NA	2.28	NA	122.80%
IDV	2.35	1.32	1.45	0.33	43.80%
NA = not available, N = 2					

Induction of mRNA and Activity

	CYP2C9				
	mRNA Fold Δ		Activity Fold Δ		
Treatment (10 µM)	Mean	SEM	Mean	SEM	% of RIF
RIF	2.49	0.74	1.74	0.34	100.00%
APV	4.51	2.22	1.42	0.39	89.02%
RTV	2.93	1.78	1.17	0.27	97.08%
NFV	2.70	1.39	1.65	0.07	76.68%
NFV 1µM	3.50	NA	1.11	NA	70.35%
SQV	2.14	1.26	1.22	0.41	98.00%
ATV	1.69	0.62	1.41	0.13	97.08%
LPV	1.54	0.99	1.08	0.15	82.47%
TPV	0.77	0.30	1.10	0.13	75.58%
TPV 1µM	2.52	NA	1.04	NA	71.81%
IDV	1.47	0.74	0.77	0.26	53.03%
NA = not available, N = 2					

Induction of mRNA

	MDR1		MRP2		MRP4		OATP1B1		OATP1B3	
	mRNA Fold Δ		mRNA Fold Δ		mRNA Fold Δ		mRNA Fold Δ		mRNA Fold Δ	
Treatment (10 μM)	Mean	SEM	Mean	SEM	Mean	SEM	Mean	SEM	Mean	SEM
RIF	2.38	0.98	1.37	0.44	0.98	0.41	2.56	0.88	1.00	0.00
APV	2.66	1.08	1.60	0.50	1.03	0.40	7.34	2.47	1.76	0.85
RTV	2.89	2.16	2.16	1.17	1.49	1.02	5.31	2.64	0.88	0.17
NFV (10 μM)	2.71	1.59	1.76	0.91	2.08	1.45	2.43	0.73	4.81	2.23
NFV (1 μM)	3.36	NA	1.97	NA	1.39	NA	4.17	NA	2.00	NA
SQV	1.42	1.07	1.10	0.56	1.35	0.92	2.82	1.04	1.33	0.34
ATV	0.86	0.41	0.80	0.27	0.53	0.22	1.64	0.70	1.65	0.47
LPV	1.17	0.60	1.34	0.67	1.62	1.05	4.65	1.91	1.25	0.32
TPV (10 μM)	2.06	1.54	0.60	0.18	1.90	1.20	2.79	1.09	8.82	0.53
TPV (1 μM)	1.49	NA	0.89	NA	1.08	NA	2.95	NA	1.25	NA
IDV	0.87	0.28	0.78	0.20	0.60	0.28	2.77	0.91	1.91	0.52

NA = not available, N = 2

Cocktail Assay 1 Validation

	% Activity				
	CYP1A	CYP3A	CYP2D6	CYP2C9	CYP2A6
HLM 143	78.78	75.02	82.27	81.39	91.88
HLM 166	87.82	70.35	72.63	71.33	101.86
HLM 155	97.18	77.51	88.28	80.61	108.26
MEAN	87.93	74.29	81.06	77.78	100.67
STDEV	9.20	3.63	7.90	5.59	8.25

Cocktail Assay 2 Validation

	% Activity			
	CYP2C19	CYP2C8	CYP2B6	CYP2E1
HLM 143	75.03	95.22	94.63	81.19
HLM 166	75.60	95.31	97.55	85.80
HLM 155	74.62	77.02	84.39	60.43
MEAN	75.08	88.66	92.19	75.80
STDEV	0.49	10.09	6.91	13.52

(+)ABT; H3-ES hepatocyte uptake

	Cell:Media ratio/Protein Conc (mL/mg)				
BSP (µM)	1st	2nd	3rd	Mean	Stdev
0 µM	2.21	1.11	2.34	1.88	0.67
20 µM	0.85	0.34	1.10	0.76	0.39
100 µM	0.59	0.30	0.58	0.49	0.17

(-)ABT; H3-ES hepatocyte uptake

	Cell:Media ratio/Protein Conc (mL/mg)		
BSP (µM)	1st	2nd	Mean
0 µM	1.41	2.67	2.04
20 µM	0.52	1.15	0.84
100 µM	0.38	0.76	0.57

H3-PI tempreature dependent uptake transport studies

Cell:Media ratio/Protein Conc (mL/mg)

	(+)ABT; H3-NFV hepatocyte uptake					(+)ABT; H3-RTV hepatocyte uptake				
			4°C					4°C		
Time	1st	2nd	3rd	Mean	Stdev	1st	2nd	3rd	Mean	Stdev
0min	0.09	0.13	0.08	0.10	0.02	0.06	0.10	0.09	0.08	0.02
10min	0.63	0.54	0.57	0.58	0.05	0.15	0.13	0.15	0.14	0.01
20min	0.58	0.55	0.75	0.63	0.11	0.19	0.15	0.16	0.17	0.02
			37°C					37°C		
Time	1st	2nd	3rd	Mean	Stdev	1st	2nd	3rd	Mean	Stdev
0min	0.09	0.14	0.11	0.11	0.02	0.08	0.08	0.09	0.08	0.01
10min	0.72	0.61	0.79	0.71	0.09	0.20	0.16	0.25	0.20	0.04
20min	0.71	0.70	0.70	0.70	0.00	0.23	0.16	0.16	0.18	0.04

	(+)ABT; H3-LPV hepatocyte uptake					(+)ABT; H3-APV hepatocyte uptake				
			4°C					4°C		
Time	1st	2nd	3rd	Mean	Stdev	1st	2nd	3rd	Mean	Stdev
0min	0.13	0.37	0.47	0.32	0.17	0.16	0.12	0.05	0.11	0.06
10min	0.36	0.27	0.31	0.31	0.04	0.49	0.16	0.58	0.41	0.23
20min	0.39	0.57	0.51	0.49	0.09	0.56	0.16	0.56	0.43	0.23
			37°C					37°C		
Time	1st	2nd	3rd	Mean	Stdev	1st	2nd	3rd	Mean	Stdev
0min	0.23	0.57	0.81	0.54	0.30	0.17	0.17	0.08	0.14	0.05
10min	0.36	0.77	0.97	0.70	0.31	0.78	0.75	1.23	0.92	0.27
20min	0.59	1.13	1.80	1.17	0.61	1.11	0.92	2.01	1.35	0.59

H3-PI competitive inhibition uptake transport studies

Cell:Media ratio/Protein Conc (mL/mg)

	(+)ABT; H3-NFV hepatocyte uptake						(+)ABT; H3-RTV hepatocyte uptake				
NFV (μM)	1st	2nd	3rd	Mean	Stdev	RTV (μM)	1st	2nd	3rd	Mean	Stdev
0μM	0.71	0.61	0.70	0.67	0.06	0μM	0.22	0.21	0.19	0.20	0.02
20μM	0.67	0.54	0.85	0.69	0.16	20μM	0.22	0.23	0.20	0.22	0.01
100μM	0.64	0.55	0.82	0.67	0.14	100μM	0.21	0.17	0.18	0.19	0.02
RTV (μM)	1st	2nd	3rd	Mean	Stdev	NFV (μM)	1st	2nd	3rd	Mean	Stdev
0μM	0.71	0.61	0.70	0.67	0.06	0μM	0.22	0.21	0.19	0.20	0.02
20μM	0.54	0.71	0.76	0.67	0.12	20μM	0.20	0.24	0.20	0.21	0.02
100μM	0.63	0.81	0.77	0.74	0.09	100μM	0.22	0.22	0.17	0.20	0.02
BSP (μM)	1st	2nd	3rd	Mean	Stdev	BSP (μM)	1st	2nd	3rd	Mean	Stdev
0μM	0.71	0.61	0.70	0.67	0.06	0μM	0.22	0.21	0.19	0.20	0.02
20μM	0.55	0.58	0.76	0.63	0.12	20μM	0.21	0.22	0.21	0.21	0.01
100μM	0.67	0.78	0.85	0.77	0.09	100μM	0.19	0.26	0.22	0.22	0.03

	(+)ABT; H3-LPV hepatocyte uptake						(+)ABT; H3-APV hepatocyte uptake				
LPV (μM)	1st	2nd	3rd	Mean	Stdev	APV (μM)	1st	2nd	3rd	Mean	Stdev
0 μM	0.59	0.71	0.86	0.72	0.13	0 μM	0.81	1.08	1.71	1.20	0.46
20 μM	0.64	0.86	1.04	0.85	0.20	20 μM	0.15	0.22	0.22	0.20	0.04
100 μM	0.64	0.82	0.90	0.79	0.14	100 μM	0.10	0.10	0.19	0.13	0.05
BSP (μM)	1st	2nd	3rd	Mean	Stdev	BSP (μM)	1st	2nd	3rd	Mean	Stdev
0 μM	0.49	0.79	0.81	0.69	0.18	0 μM	1.01	1.29	1.34	1.21	0.18
20 μM	0.58	0.98	0.84	0.80	0.20	20 μM	0.87	1.37	1.52	1.25	0.34
100 μM	0.64	0.93	0.83	0.80	0.15	100 μM	0.83	1.33	1.43	1.20	0.32

(+)ABT; H3-APV hepatocyte uptake and BEI

	(+) Ca Cell:Media ratio/Protein Conc (mL/mg)				
APV (µM)	1st	2nd	3rd	Mean	Stdev
0µM	0.63	0.60	0.66	0.63	0.03
20µM	0.12	0.09	0.08	0.10	0.02
100µM	0.07	0.11	0.05	0.08	0.03
	(-) Ca Cell:Media ratio/Protein Conc (mL/mg)				
APV (µM)	1st	2nd	3rd	Mean	Stdev
0µM	0.42	0.40	0.42	0.42	0.01
20µM	0.09	0.05	0.06	0.07	0.02
100µM	0.05	0.07	0.04	0.05	0.02
			BEI		
APV (µM)	1st	2nd	3rd	Mean	Stdev
0µM	32.92%	33.59%	36.45%	34.32%	1.87%
20µM	25.76%	42.39%	34.83%	34.33%	8.33%
100µM	26.39%	38.38%	19.78%	28.18%	9.43%

(+)ABT; H3-APV hepatocyte uptake and BEI

	(+) Ca Cell:Media ratio/Protein Conc (mL/mg)					
elacridar (µM)	1st	2nd	3rd	4th	Mean	Stdev
0µM	2.02	0.83	0.63	0.60	1.02	0.67
20µM	1.83	0.71	0.58	0.63	0.94	0.59
100µM	0.49	0.47	0.50	0.46	0.48	0.02
	(-) Ca Cell:Media ratio/Protein Conc (mL/mg)					
elacridar (µM)	1st	2nd	3rd	4th	Mean	Stdev
0µM	0.90	0.49	0.42	0.40	0.55	0.23
20µM	0.58	0.17	0.37	0.43	0.39	0.17
100µM	0.40	0.39	0.53	0.39	0.43	0.07
			BEI			
elacridar (µM)	1st	2nd	3rd	4th	Mean	Stdev
0µM	55.58%	41.14%	32.78%	33.58%	40.77%	10.57%
20µM	68.31%	75.52%	36.71%	32.85%	53.35%	21.70%
100µM	16.86%	18.04%	2.01%	15.26%	13.04%	7.45%

(+)ABT; H3-EG hepatocyte uptake and BEI

	(+) Ca Cell:Media ratio/Protein Conc (mL/mg)				
elacridar (μM)	1st	2nd	3rd	Mean	Stdev
0 μM	0.16	0.12	0.16	0.14	0.02
100 μM	0.07	0.06	0.08	0.07	0.01
	(-) Ca Cell:Media ratio/Protein Conc (mL/mg)				
elacridar (μM)	1st	2nd	3rd	Mean	Stdev
0 μM	0.10	0.07	0.09	0.09	0.02
100 μM	0.06	0.05	0.07	0.06	0.01
			BEI		
elacridar (μM)	1st	2nd	3rd	Mean	Stdev
0 μM	34.02%	39.66%	39.67%	37.78%	3.26%
100 μM	2.16%	9.27%	9.15%	6.86%	4.08%

H3-ES or PIs B-->A transport in MDCKII-OATP1B1 cells

BSP (μM)	1st	2nd	3rd
0μM	0.26	0.27	0.28
100μM	0.05	0.11	0.08

RTV (μM)	1st	2nd	3rd	4th	5th	6th	7th
0μM	0.30	0.39	0.34	0.52	0.33	0.39	0.60
20μM	0.43	0.49	NA	0.86	NA	NA	NA
100μM	0.25	0.23	0.26	0.46	NA	NA	NA
BSP (μM)	1st	2nd	3rd				
20μM	0.30	0.39	0.54				
100μM	0.34	0.33	0.48				

NFV (μM)	1st	2nd	3rd	4th	5th	6th	7th
0μM	0.33	0.40	0.35	0.60	0.26	0.37	0.65
20μM	0.17	0.32	NA	0.58	NA	NA	NA
100μM	0.20	0.23	0.16	0.64	NA	NA	NA
BSP (μM)	1st	2nd	3rd				
20μM	0.29	0.54	0.77				
100μM	0.34	0.41	0.75				

LPV (μM)	1st	2nd	3rd	4th	5th	6th	7th
0μM	0.21	0.23	0.25	0.45	0.23	0.27	0.44
20μM	0.30	0.43	NA	0.63	NA	NA	NA
100μM	0.12	0.17	0.13	0.39	NA	NA	NA
BSP (μM)	1st	2nd	3rd				
20μM	0.23	0.28	0.40				
100μM	0.25	0.28	0.49				

APV (μM)	1st	2nd	3rd	4th	5th	6th	7th
0μM	0.61	0.68	0.66	1.35	0.62	0.70	1.45
20μM	0.56	0.72	NA	1.00	NA	NA	NA
100μM	0.38	0.42	0.34	0.64	NA	NA	NA
BSP (μM)	1st	2nd	3rd				
20μM	0.62	0.74	1.16				
100μM	0.67	0.74	1.06				

CBF: water K1 (mL/min/100 g tissue)

	Brain (Gray + White)			Gray Matter			White Matter		
Subject	Baseline	Quinidine	Rifampin	Baseline	Quinidine	Rifampin	Baseline	Quinidine	Rifampin
SUB1	42.86	44.53	37.88	49.06	51.63	43.93	28.41	27.37	23.28
SUB2	39.48	NA	69.27	45.69	NA	79.89	26.51	NA	45.69
SUB3	37.40	29.28	55.60	43.51	33.08	63.63	22.60	19.43	35.40
SUB4	35.63	20.27	41.52	41.45	24.29	50.53	24.58	12.39	34.18
SUB5	50.93	30.32	32.82	60.86	35.48	36.82	32.96	19.53	25.47
SUB6	39.45	54.16	22.34	48.08	67.48	26.66	24.50	33.47	13.66
SUB7	29.83	56.71	NA	33.91	65.10	NA	20.81	39.09	NA
SUB8	74.03	45.98	110.99	85.47	52.59	127.06	49.51	32.91	73.62
SUB9	30.84	37.87	27.94	35.76	44.07	32.70	20.63	25.78	18.37
SUB10	22.59	12.65	32.44	26.34	15.56	37.35	16.50	8.49	24.51
Mean (quinidine)	40.39	36.86	NA	47.16	43.25	NA	26.72	24.27	NA
Stdev (quinidine)	15.00	14.99	NA	17.48	17.72	NA	9.77	10.17	NA
Mean (rifampin)	41.47	NA	47.87	48.47	NA	55.40	27.35	NA	32.69
Stdev (rifampin)	14.49	NA	27.74	16.79	NA	31.56	9.52	NA	18.13

NA = not available, PET study not performed; not calculated

verapamil K1p (mL/min/g tissue)

Subject	Model	Brain (Gray + White)			Gray Matter			White Matter		
		Baseline	Quinidine	Rifampin	Baseline	Quinidine	Rifampin	Baseline	Quinidine	Rifampin
SUB1	1TC, 10min	0.049	0.067	NA	0.058	0.077	NA	0.029	0.041	NA
	1TC, 5min	0.055	NA	0.046	0.067	NA	0.056	0.029	NA	0.021
SUB2	1TC, 10min	NA	NA	NA	NA	NA	NA	NA	NA	NA
	1TC, 5min	0.032	NA	0.039	0.040	NA	0.050	0.019	NA	0.017
SUB3	1TC, 10min	0.047	0.067	NA	0.054	0.077	NA	0.028	0.041	NA
	1TC, 5min	0.060	NA	0.040	0.069	NA	0.050	0.036	NA	0.020
SUB4	1TC, 10min	0.049	0.059	NA	0.058	0.069	NA	0.030	0.038	NA
	1TC, 5min	0.050	NA	0.054	0.062	NA	0.059	0.028	NA	0.042
SUB5	1TC, 10min	0.037	0.051	NA	0.045	0.063	NA	0.020	0.032	NA
	1TC, 5min	0.034	NA	0.036	0.048	NA	0.048	0.020	NA	0.019
SUB6	1TC, 10min	0.048	0.061	NA	0.060	0.075	NA	0.028	0.036	NA
	1TC, 5min	0.049	NA	0.052	0.062	NA	0.066	0.025	NA	0.026
SUB7	1TC, 10min	0.039	0.059	NA	0.046	0.067	NA	0.022	0.040	NA
	1TC, 5min	NA	NA	NA	NA	NA	NA	NA	NA	NA
SUB8	1TC, 10min	0.044	0.085	NA	0.052	0.097	NA	0.027	0.059	NA
	1TC, 5min	0.046	NA	0.058	0.055	NA	0.067	0.025	NA	0.035
SUB9	1TC, 10min	0.034	0.051	NA	0.041	0.062	NA	0.019	0.031	NA
	1TC, 5min	0.034	NA	0.047	0.043	NA	0.059	0.016	NA	0.022
SUB10	1TC, 10min	0.036	0.058	NA	0.044	0.068	NA	0.025	0.042	NA
	1TC, 5min	0.036	NA	0.035	0.044	NA	0.044	0.022	NA	0.023
	Mean 1TC, 10min	0.043	0.062	NA	0.051	0.073	NA	0.025	0.040	NA
	Stdev 1TC, 10min	0.006	0.010	NA	0.007	0.011	NA	0.004	0.008	NA
	Mean 1TC, 5min	0.044	NA	0.045	0.054	NA	0.056	0.024	NA	0.025
	Stdev 1TC, 5min	0.010	NA	0.008	0.011	NA	0.008	0.006	NA	0.008

NA = not available, PET study not performed; not calculated

verapamil Blood to Plasma ratio

Subject	Baseline	Quinidine	Rifampin
SUB1	0.77	0.74	0.79
SUB2	0.80	NA	0.74
SUB3	0.75	0.84	0.93
SUB4	0.81	0.86	0.81
SUB5	0.74	0.78	0.75
SUB6	0.79	0.83	0.80
SUB7	0.74	0.81	NA
SUB8	0.78	0.84	0.79
SUB9	0.76	0.79	0.76
SUB10	0.76	0.81	0.77
Mean	0.77	0.81	0.79
Stdev	0.02	0.04	0.06

NA = not available, PET study not performed; not calculated

verapamil K1b (mL/min/g tissue)

Subject	Model	Brain (Gray + White)			Gray Matter			White Matter		
		Baseline	Quinidine	Rifampin	Baseline	Quinidine	Rifampin	Baseline	Quinidine	Rifampin
SUB1	1TC, 10min	0.064	0.090	NA	0.038	0.055	NA	0.075	0.104	NA
	1TC, 5min	0.072	NA	0.058	0.038	NA	0.026	0.086	NA	0.070
SUB2	1TC, 10min	NA	NA	NA	NA	NA	NA	NA	NA	NA
	1TC, 5min	0.040	NA	0.053	0.024	NA	0.023	0.050	NA	0.067
SUB3	1TC, 10min	0.063	0.080	NA	0.037	0.048	NA	0.073	0.093	NA
	1TC, 5min	0.080	NA	0.043	0.049	NA	0.021	0.092	NA	0.054
SUB4	1TC, 10min	0.061	0.068	NA	0.037	0.044	NA	0.072	0.081	NA
	1TC, 5min	0.062	NA	0.066	0.034	NA	0.052	0.076	NA	0.073
SUB5	1TC, 10min	0.050	0.066	NA	0.027	0.040	NA	0.061	0.080	NA
	1TC, 5min	0.046	NA	0.048	0.026	NA	0.025	0.065	NA	0.064
SUB6	1TC, 10min	0.061	0.073	NA	0.036	0.043	NA	0.076	0.091	NA
	1TC, 5min	0.062	NA	0.065	0.032	NA	0.033	0.079	NA	0.083
SUB7	1TC, 10min	0.052	0.072	NA	0.029	0.050	NA	0.062	0.083	NA
	1TC, 5min	NA	NA	NA	NA	NA	NA	NA	NA	NA
SUB8	1TC, 10min	0.057	0.100	NA	0.035	0.070	NA	0.067	0.115	NA
	1TC, 5min	0.059	NA	0.073	0.033	NA	0.045	0.071	NA	0.084
SUB9	1TC, 10min	0.045	0.065	NA	0.025	0.039	NA	0.054	0.078	NA
	1TC, 5min	0.046	NA	0.062	0.022	NA	0.029	0.057	NA	0.078
SUB10	1TC, 10min	0.048	0.072	NA	0.032	0.052	NA	0.058	0.084	NA
	1TC, 5min	0.047	NA	0.045	0.029	NA	0.030	0.058	NA	0.057
	Mean 1TC, 10min	0.056	0.076	NA	0.033	0.049	NA	0.066	0.090	NA
	Stdev 1TC, 10min	0.007	0.012	NA	0.005	0.010	NA	0.008	0.012	NA
	Mean 1TC, 5min	0.057	NA	0.057	0.032	NA	0.032	0.070	NA	0.070
	Stdev 1TC, 5min	0.013	NA	0.010	0.008	NA	0.010	0.014	NA	0.011

NA = not available, PET study not performed; not calculated

verapamil ER

Subject	Model	Brain (Gray + White)			Gray Matter			White Matter		
		Baseline	Quinidine	Rifampin	Baseline	Quinidine	Rifampin	Baseline	Quinidine	Rifampin
SUB1	1TC, 10min	0.150	0.202	NA	0.133	0.199	NA	0.154	0.202	NA
	1TC, 5min	0.167	NA	0.152	0.133	NA	0.113	0.176	NA	0.160
SUB2	1TC, 10min	NA	NA	NA	NA	NA	NA	NA	NA	NA
	1TC, 5min	0.102	NA	0.076	0.089	NA	0.050	0.110	NA	0.084
SUB3	1TC, 10min	0.168	0.273	NA	0.166	0.249	NA	0.168	0.280	NA
	1TC, 5min	0.214	NA	0.077	0.215	NA	0.060	0.211	NA	0.085
SUB4	1TC, 10min	0.170	0.337	NA	0.151	0.354	NA	0.175	0.332	NA
	1TC, 5min	0.174	NA	0.159	0.139	NA	0.153	0.184	NA	0.145
SUB5	1TC, 10min	0.098	0.216	NA	0.083	0.207	NA	0.100	0.225	NA
	1TC, 5min	0.090	NA	0.146	0.080	NA	0.098	0.107	NA	0.175
SUB6	1TC, 10min	0.156	0.135	NA	0.146	0.129	NA	0.158	0.134	NA
	1TC, 5min	0.157	NA	0.293	0.130	NA	0.239	0.164	NA	0.313
SUB7	1TC, 10min	0.174	0.128	NA	0.140	0.127	NA	0.183	0.127	NA
	1TC, 5min	NA	NA	NA	NA	NA	NA	NA	NA	NA
SUB8	1TC, 10min	0.077	0.218	NA	0.071	0.214	NA	0.078	0.218	NA
	1TC, 5min	0.080	NA	0.066	0.066	NA	0.061	0.083	NA	0.066
SUB9	1TC, 10min	0.145	0.172	NA	0.119	0.152	NA	0.152	0.178	NA
	1TC, 5min	0.148	NA	0.221	0.105	NA	0.159	0.159	NA	0.238
SUB10	1TC, 10min	0.213	0.566	NA	0.196	0.616	NA	0.219	0.540	NA
	1TC, 5min	0.208	NA	0.140	0.173	NA	0.122	0.220	NA	0.152
	Mean 1TC, 10min	0.150	0.250	NA	0.134	0.250	NA	0.154	0.248	NA
	Stdev 1TC, 10min	0.041	0.136	NA	0.039	0.154	NA	0.042	0.127	NA
	Mean 1TC, 5min	0.149	NA	0.148	0.125	NA	0.117	0.157	NA	0.158
	Stdev 1TC, 5min	0.049	NA	0.074	0.047	NA	0.060	0.048	NA	0.079

NA = not available, PET study not performed; not calculated

verapamil k2 (1/min)

Subject	Model	Brain (Gray + White)			Gray Matter			White Matter		
		Baseline	Quinidine	Rifampin	Baseline	Quinidine	Rifampin	Baseline	Quinidine	Rifampin
SUB1	1TC, 10min	0.107	0.096	NA	0.062	0.057	NA	0.120	0.106	NA
	1TC, 5min	0.197	NA	0.131	NA	NA	NA	0.228	NA	0.170
SUB2	1TC, 10min	NA	NA	NA	NA	NA	NA	NA	NA	NA
	1TC, 5min	0.065	NA	0.120	NA	NA	NA	0.113	NA	0.166
SUB3	1TC, 10min	0.098	0.090	NA	0.055	0.051	NA	0.110	0.100	NA
	1TC, 5min	0.121	NA	0.106	NA	NA	NA	0.151	NA	0.164
SUB4	1TC, 10min	0.086	0.071	NA	0.045	0.043	NA	0.097	0.081	NA
	1TC, 5min	0.101	NA	0.108	NA	NA	0.069	0.135	NA	0.124
SUB5	1TC, 10min	0.095	0.102	NA	0.028	0.054	NA	0.111	0.120	NA
	1TC, 5min	0.033	NA	0.069	NA	NA	NA	0.153	NA	0.138
SUB6	1TC, 10min	0.084	0.091	NA	0.045	0.049	NA	0.097	0.104	NA
	1TC, 5min	0.087	NA	0.127	NA	NA	NA	0.127	NA	0.166
SUB7	1TC, 10min	0.094	0.090	NA	0.034	0.065	NA	0.110	0.097	NA
	1TC, 5min	NA	NA	NA	NA	NA	NA	NA	NA	NA
SUB8	1TC, 10min	0.092	0.126	NA	0.048	0.096	NA	0.104	0.136	NA
	1TC, 5min	0.121	NA	0.143	NA	NA	0.044	0.152	NA	0.166
SUB9	1TC, 10min	0.076	0.095	NA	0.019	0.046	NA	0.094	0.113	NA
	1TC, 5min	0.092	NA	0.124	NA	NA	NA	0.131	NA	0.171
SUB10	1TC, 10min	0.064	0.074	NA	0.031	0.046	NA	0.077	0.086	NA
	1TC, 5min	0.047	NA	0.050	NA	NA	NA	0.082	NA	0.097
	Mean 1TC, 10min	0.088	0.093	NA	0.041	0.056	NA	0.102	0.105	NA
	Stdev 1TC, 10min	0.013	0.016	NA	0.014	0.016	NA	0.013	0.017	NA
	Mean 1TC, 5min	0.096	NA	0.109	NA	NA	0.057	0.141	NA	0.151
	Stdev 1TC, 5min	0.048	NA	0.030	NA	NA	0.017	0.040	NA	0.026

NA = not available, PET study not performed; not calculated

Blood, Plasma dose normalized AUC (min/L)

	Baseline			Quinidine			Rifampin		
Subject	5 min	10 min	20 min	5 min	10 min	20 min	5 min	10 min	20 min
SUB1 Arter B	0.179	0.217	0.263	0.162	0.203	0.253	0.192	0.262	0.346
SUB1 Arter P	0.241	0.288	0.347	0.203	0.253	0.318	0.264	0.342	0.441
SUB2 Arter B	0.156	0.196	0.261	NA			0.127	0.171	0.209
SUB2 Arter P	0.215	0.268	0.331				0.182	0.238	0.299
SUB3 Arter B	0.174	0.218	0.267	0.218	0.272	0.333	0.267	0.343	0.423
SUB3 Arter P	0.236	0.297	0.359	0.243	0.312	0.387	0.279	0.360	0.456
SUB4 Arter B	0.209	0.255	0.316	0.173	0.215	0.237	0.198	0.268	0.352
SUB4 Arter P	0.258	0.316	0.382	0.202	0.255	0.280	0.243	0.329	0.429
SUB5 Arter B	0.185	0.246	0.309	0.196	0.246	0.302	0.190	0.253	0.327
SUB5 Arter P	0.245	0.327	0.411	0.224	0.287	0.359	0.260	0.342	0.437
SUB6 Arter B	0.159	0.197	0.239	0.161	0.205	0.252	0.172	0.225	0.289
SUB6 Arter P	0.206	0.254	0.307	0.198	0.249	0.306	0.223	0.288	0.365
SUB7 Arter B	0.178	0.230	0.292	0.168	0.225	0.292	NA		
SUB7 Arter P	0.246	0.315	0.397	0.212	0.282	0.360			
SUB8 Arter B	0.230	0.284	0.307	0.182	0.238	0.263	0.201	0.265	0.347
SUB8 Arter P	0.298	0.368	0.397	0.218	0.284	0.312	0.260	0.337	0.439
SUB9 Arter B	0.224	0.280	0.305	0.183	0.244	0.273	0.186	0.257	0.353
SUB9 Arter P	0.311	0.385	0.417	0.239	0.314	0.347	0.241	0.337	0.456
SUB10 Arter B	0.160	0.195	0.210	0.130	0.166	0.182	0.146	0.182	0.227
SUB10 Arter P	0.217	0.263	0.283	0.160	0.204	0.224	0.195	0.241	0.298
Mean Arter B (quinidine)	0.189	0.236	0.279	0.175	0.224	0.265			
Stdev Arter B (quinidine)	0.026	0.033	0.036	0.025	0.031	0.043	NA		
Mean Arter P (quinidine)	0.251	0.313	0.367	0.211	0.271	0.322			
Stdev Arter B (quinidine)	0.034	0.044	0.047	0.025	0.034	0.049			
Mean Arter B (rifampin)	0.186	0.232	0.275				0.186	0.247	0.319
Stdev Arter B (rifampin)	0.028	0.035	0.036	NA			0.039	0.051	0.067
Mean Arter P (rifampin)	0.247	0.307	0.359				0.239	0.313	0.402
Stdev Arter P (rifampin)	0.036	0.046	0.047				0.033	0.046	0.065

NA = not available, PET study not performed; not calculated

Brain tissue dose normalized AUC (min/L)

	Baseline								
	Brain (Gray & White)			Gray Matter			White Matter		
Subject	5 min	10 min	20 min	5 min	10 min	20 min	5 min	10 min	20 min
SUB1	0.027	0.065	0.127	0.030	0.073	0.140	0.019	0.046	0.094
SUB2	0.016	0.041	0.083	0.018	0.045	0.092	0.012	0.031	0.064
SUB3	0.026	0.063	0.123	0.029	0.070	0.135	0.018	0.046	0.091
SUB4	0.021	0.051	0.078	0.024	0.058	0.088	0.015	0.037	0.058
SUB5	0.010	0.033	0.070	0.011	0.038	0.080	0.006	0.023	0.051
SUB6	0.020	0.049	0.096	0.023	0.057	0.110	0.013	0.034	0.069
SUB7	0.025	0.059	0.115	0.028	0.066	0.127	0.017	0.043	0.087
SUB8	0.034	0.083	0.162	0.038	0.093	0.179	0.025	0.062	0.125
SUB9	0.030	0.071	0.139	0.034	0.080	0.156	0.021	0.051	0.104
SUB10	0.024	0.057	0.111	0.028	0.065	0.124	0.019	0.045	0.090
Mean (quinidine)	0.024	0.059	0.113	0.027	0.067	0.127	0.017	0.043	0.086
Stdev (quinidine)	0.007	0.014	0.029	0.008	0.016	0.031	0.005	0.011	0.023
Mean (rifampin)	0.023	0.057	0.110	0.026	0.064	0.123	0.016	0.042	0.083
Stdev (rifampin)	0.007	0.016	0.031	0.008	0.017	0.033	0.005	0.012	0.024

Brain tissue dose normalized AUC (min/L)

	Quinidine								
	Brain (Gray & White)			Gray Matter			White Matter		
Subject	5 min	10 min	20 min	5 min	10 min	20 min	5 min	10 min	20 min
SUB1	0.030	0.075	0.153	0.034	0.084	0.169	0.021	0.054	0.113
SUB2		NA			NA			NA	
SUB3	0.034	0.084	0.169	0.038	0.093	0.185	0.024	0.061	0.126
SUB4	0.039	0.092	0.143	0.044	0.104	0.161	0.028	0.067	0.107
SUB5	0.027	0.065	0.130	0.032	0.074	0.146	0.020	0.049	0.100
SUB6	0.037	0.097	0.197	0.045	0.114	0.229	0.026	0.069	0.143
SUB7	0.037	0.093	0.189	0.041	0.103	0.208	0.028	0.071	0.148
SUB8	0.052	0.126	0.249	0.058	0.139	0.271	0.040	0.098	0.201
SUB9	0.036	0.086	0.175	0.041	0.097	0.195	0.026	0.064	0.135
SUB10	0.031	0.076	0.153	0.035	0.085	0.169	0.025	0.063	0.129
Mean (quinidine)	0.036	0.088	0.173	0.041	0.099	0.193	0.026	0.066	0.134
Stdev (quinidine)	0.007	0.017	0.036	0.008	0.019	0.039	0.006	0.014	0.030

NA = not available, PET study not performed; not calculated

Brain tissue dose normalized AUC (min/L)

	Rifampin								
	Brain (Gray & White)			Gray Matter			White Matter		
Subject	5 min	10 min	20 min	5 min	10 min	20 min	5 min	10 min	20 min
SUB1	0.026	0.066	0.135	0.029	0.073	0.149	0.017	0.046	0.099
SUB2	0.016	0.038	0.077	0.018	0.043	0.086	0.010	0.026	0.056
SUB3	0.028	0.067	0.135	0.031	0.075	0.148	0.019	0.047	0.100
SUB4	0.024	0.061	0.125	0.026	0.065	0.133	0.021	0.053	0.109
SUB5	0.022	0.059	0.122	0.026	0.067	0.139	0.015	0.041	0.091
SUB6	0.022	0.056	0.114	0.026	0.066	0.131	0.015	0.039	0.082
SUB7		NA			NA			NA	
SUB8	0.032	0.080	0.163	0.036	0.088	0.177	0.024	0.061	0.130
SUB9	0.022	0.058	0.123	0.025	0.065	0.137	0.015	0.041	0.092
SUB10	0.022	0.053	0.107	0.025	0.060	0.119	0.017	0.042	0.086
Mean (rifampin)	0.024	0.060	0.122	0.027	0.067	0.136	0.017	0.044	0.094
Stdev (rifampin)	0.005	0.011	0.023	0.005	0.012	0.024	0.004	0.010	0.020

NA = not available, PET study not performed; not calculated

AUC Ratio (brain tissue to blood)

	Baseline								
	Brain (Gray & White)			Gray Matter			White Matter		
Subject	5 min	10 min	20 min	5 min	10 min	20 min	5 min	10 min	20 min
SUB1	0.14888	0.299898	0.481341	0.167905	0.335647	0.533135	0.103206	0.214076	0.357003
SUB2	0.101681	0.207849	0.316968	0.114199	0.23202	0.351424	0.0752	0.156717	0.244078
SUB3	0.15177	0.290433	0.45999	0.169618	0.322372	0.506074	0.105924	0.208515	0.341918
SUB4	0.101365	0.199967	0.246583	0.116175	0.227135	0.278457	0.072352	0.146746	0.184142
SUB5	0.051549	0.132655	0.226496	0.060416	0.153011	0.258438	0.03455	0.093636	0.16528
SUB6	0.124014	0.247827	0.400326	0.145347	0.288293	0.460336	0.084692	0.173251	0.28972
SUB7	0.14039	0.256111	0.395733	0.158483	0.285737	0.436545	0.097871	0.186491	0.299822
SUB8	0.14882	0.293655	0.529339	0.166701	0.326515	0.58247	0.108228	0.219071	0.408769
SUB9	0.133668	0.252761	0.456675	0.152712	0.285942	0.510497	0.092821	0.181596	0.341224
SUB10	0.151412	0.294394	0.52966	0.172563	0.332129	0.591939	0.11668	0.232424	0.427397
Mean (quinidine)	0.128	0.252	0.414	0.146	0.284	0.462	0.091	0.184	0.313
Stdev (quinidine)	0.033	0.055	0.111	0.036	0.060	0.121	0.025	0.043	0.090
Mean (rifampin)	0.124	0.247	0.405	0.141	0.278	0.453	0.088	0.181	0.307
Stdev (rifampin)	0.034	0.057	0.116	0.037	0.062	0.126	0.025	0.044	0.093

AUC Ratio (brain tissue to blood)

	Quinidine								
	Brain (Gray & White)			Gray Matter			White Matter		
Subject	5 min	10 min	20 min	5 min	10 min	20 min	5 min	10 min	20 min
SUB1	0.184505	0.372408	0.604152	0.206955	0.414973	0.667096	0.128225	0.265708	0.446365
SUB2		NA			NA			NA	
SUB3	0.155887	0.309399	0.508246	0.173532	0.341935	0.556812	0.10894	0.222887	0.379126
SUB4	0.222618	0.428107	0.605539	0.253259	0.483581	0.680359	0.159199	0.313299	0.450692
SUB5	0.140039	0.265984	0.429495	0.160804	0.30241	0.483061	0.101872	0.199026	0.33101
SUB6	0.232214	0.473862	0.779958	0.276571	0.558077	0.909316	0.159474	0.335761	0.567827
SUB7	0.188128	0.373715	0.617965	0.209453	0.413361	0.679041	0.14124	0.286529	0.483665
SUB8	0.285667	0.529472	0.948724	0.316478	0.582509	1.032513	0.218536	0.413808	0.765925
SUB9	0.196263	0.353163	0.642654	0.223452	0.397727	0.715473	0.140644	0.262014	0.493683
SUB10	0.242045	0.46149	0.843345	0.272797	0.513854	0.927296	0.19366	0.379101	0.711258
Mean (quinidine)	0.205	0.396	0.664	0.233	0.445	0.739	0.150	0.298	0.514
Stdev (quinidine)	0.045	0.084	0.164	0.051	0.096	0.181	0.038	0.070	0.144

NA = not available, PET study not performed; not calculated

AUC Ratio (brain tissue to blood)

	Rifampin								
	Brain (Gray & White)			Gray Matter			White Matter		
Subject	5 min	10 min	20 min	5 min	10 min	20 min	5 min	10 min	20 min
SUB1	0.133657	0.250386	0.389295	0.151614	0.280396	0.430061	0.088778	0.175385	0.287416
SUB2	0.123573	0.220546	0.367742	0.142607	0.251158	0.413323	0.081998	0.153682	0.268182
SUB3	0.104375	0.196214	0.318898	0.117276	0.218388	0.350849	0.070656	0.138262	0.235396
SUB4	0.122058	0.228132	0.355495	0.131169	0.24444	0.378777	0.104582	0.196854	0.310842
SUB5	0.116136	0.231777	0.373869	0.136077	0.267035	0.423927	0.077709	0.163831	0.277402
SUB6	0.129916	0.250781	0.394531	0.152767	0.291837	0.453947	0.087762	0.175044	0.284914
SUB7		NA			NA			NA	
SUB8	0.161199	0.302887	0.470252	0.178202	0.331745	0.509765	0.119684	0.232408	0.373735
SUB9	0.118986	0.224155	0.347252	0.13656	0.25407	0.388385	0.081436	0.160236	0.259353
SUB10	0.15337	0.293648	0.469898	0.173913	0.330425	0.524782	0.119416	0.232863	0.379185
Mean (rifampin)	0.129	0.244	0.387	0.147	0.274	0.430	0.092	0.181	0.297
Stdev (rifampin)	0.018	0.035	0.052	0.020	0.038	0.058	0.018	0.033	0.049

NA = not available, PET study not performed; not calculated

SPE Baseline

	5 min					10 min					20 min				
Subject	Polar	D-617	D-703,702	Verapamil	SUM	Polar	D-617	D-703,702	Verapamil	SUM	Polar	D-617	D-703,702	Verapamil	SUM
SUB1	8.39%	4.70%	2.03%	93.39%	108.51%	24.65%	3.50%	2.11%	73.43%	103.69%	24.82%	21.76%	1.68%	55.48%	103.75%
SUB2	9.05%	4.80%	2.75%	78.66%	95.26%	9.69%	4.95%	1.35%	77.09%	93.08%	21.30%	9.49%	1.91%	51.67%	84.36%
SUB3	2.19%	0.63%	0.46%	90.95%	94.23%	4.28%	1.58%	0.54%	89.23%	95.62%	12.91%	6.72%	0.81%	79.35%	99.79%
SUB4	6.31%	2.95%	1.73%	92.19%	103.19%	16.39%	7.90%	1.83%	76.94%	103.06%	27.78%	15.05%	1.08%	56.90%	100.81%
SUB5	10.94%	5.03%	2.87%	79.50%	98.35%	11.04%	5.80%	2.71%	85.65%	105.20%	33.94%	12.53%	2.51%	53.23%	102.22%
SUB6	7.20%	6.04%	4.44%	84.78%	102.46%	6.66%	3.52%	2.54%	85.21%	97.94%	18.36%	12.65%	2.77%	71.85%	105.63%
SUB7	16.95%	9.50%	5.42%	69.95%	101.83%	27.30%	11.60%	5.26%	56.89%	101.04%	28.84%	15.69%	3.14%	51.07%	98.73%
SUB8	3.87%	2.02%	2.11%	90.72%	98.72%	15.33%	7.88%	3.58%	73.00%	99.79%	27.06%	11.17%	1.51%	60.65%	100.39%
SUB9	13.23%	4.43%	3.07%	80.77%	101.50%	21.15%	7.44%	3.21%	65.39%	97.19%	41.21%	11.55%	1.91%	46.02%	100.69%
SUB10	16.37%	4.32%	2.48%	74.98%	98.15%	21.14%	9.35%	4.56%	65.67%	100.73%	25.56%	12.49%	2.12%	55.88%	96.05%
Mean (quinidine)	9.49%	4.40%	2.73%	84.14%	100.77%	16.44%	6.51%	2.93%	74.60%	100.47%	26.72%	13.29%	1.95%	58.94%	100.89%
Stdev (quinidine)	5.25%	2.53%	1.48%	8.36%	4.03%	7.93%	3.19%	1.43%	10.82%	3.18%	8.17%	4.08%	0.77%	10.45%	2.78%
Mean (rifampin)	8.61%	3.88%	2.44%	85.10%	100.04%	14.48%	5.77%	2.49%	76.85%	99.59%	25.88%	12.60%	1.81%	59.00%	99.30%
Stdev (rifampin)	4.45%	1.69%	1.08%	6.88%	4.39%	7.04%	2.57%	1.21%	8.54%	4.00%	8.31%	4.14%	0.63%	10.39%	6.20%

SPE Quinidine

	5 min					10 min					20 min				
Subject	Polar	D-617	D-703,702	Verapamil	SUM	Polar	D-617	D-703,702	Verapamil	SUM	Polar	D-617	D-703,702	Verapamil	SUM
SUB1	12.84%	5.29%	2.08%	84.27%	104.49%	14.13%	9.38%	2.39%	74.04%	99.94%	22.00%	22.27%	1.00%	51.25%	96.52%
SUB2			NA					NA					NA		
SUB3	12.33%	4.36%	1.62%	87.32%	105.63%	15.12%	5.88%	2.08%	80.33%	103.42%	19.25%	10.78%	0.42%	63.06%	93.52%
SUB4	8.67%	2.87%	0.91%	86.61%	99.06%	18.61%	7.46%	0.67%	77.43%	104.18%	34.50%	13.53%	0.30%	58.09%	106.41%
SUB5	11.09%	4.48%	2.22%	85.68%	103.47%	14.87%	7.34%	2.21%	79.57%	103.99%	31.74%	12.45%	1.65%	52.79%	98.63%
SUB6	5.23%	4.62%	3.27%	86.70%	99.82%	9.75%	6.00%	3.08%	77.18%	96.00%	21.33%	13.23%	2.62%	59.83%	97.01%
SUB7	15.15%	8.72%	4.67%	73.18%	101.72%	16.74%	9.46%	3.89%	64.64%	94.73%	33.97%	17.38%	2.32%	47.46%	101.13%
SUB8	8.11%	3.43%	2.28%	88.92%	102.74%	16.39%	6.40%	1.92%	75.18%	99.90%	37.64%	11.27%	1.23%	51.07%	101.21%
SUB9	15.64%	6.16%	3.54%	74.97%	100.31%	25.82%	11.26%	2.89%	59.79%	99.76%	38.95%	15.26%	1.47%	39.70%	95.37%
SUB10	12.11%	4.60%	5.47%	77.86%	100.04%	16.51%	8.01%	3.46%	68.72%	96.70%	10.92%	19.47%	3.53%	61.44%	95.36%
Mean (quinidine)	11.24%	4.95%	2.90%	82.83%	101.92%	16.44%	7.91%	2.51%	72.99%	99.85%	27.81%	15.07%	1.62%	53.85%	98.35%
Stdev (quinidine)	3.39%	1.70%	1.47%	5.88%	2.30%	4.29%	1.82%	0.95%	7.09%	3.53%	9.70%	3.90%	1.05%	7.52%	3.99%

NA = not available, PET study not performed; not calculated

SPE Rifampin

	5 min					10 min					20 min				
Subject	Polar	D-617	D-703,702	Verapamil	SUM	Polar	D-617	D-703,702	Verapamil	SUM	Polar	D-617	D-703,702	Verapamil	SUM
SUB1	7.81%	2.63%	1.17%	84.38%	96.00%	25.51%	7.99%	1.47%	68.44%	103.41%	38.08%	15.08%	0.51%	42.64%	96.31%
SUB2	9.66%	3.37%	0.83%	78.51%	102.37%	31.38%	8.85%	1.05%	69.73%	111.00%	29.34%	15.93%	1.15%	57.17%	103.59%
SUB3	9.99%	5.91%	3.13%	76.17%	95.19%	15.24%	7.62%	3.65%	64.42%	90.93%	38.18%	10.66%	2.82%	42.63%	94.29%
SUB4	11.85%	5.59%	2.41%	74.47%	94.32%	39.01%	9.47%	0.38%	52.34%	101.19%	50.06%	12.97%	1.67%	35.26%	99.96%
SUB5	12.36%	3.98%	2.06%	82.94%	101.33%	28.31%	5.99%	1.65%	70.56%	106.52%	48.40%	8.77%	1.37%	46.79%	105.32%
SUB6	14.81%	5.68%	4.53%	78.51%	103.53%	28.58%	6.87%	3.72%	56.59%	95.76%	41.95%	8.94%	2.67%	44.34%	97.90%
SUB7			NA					NA					NA		
SUB8	9.63%	5.78%	3.13%	72.99%	91.53%	30.96%	5.16%	1.12%	56.89%	94.13%	49.98%	8.62%	1.31%	37.85%	97.77%
SUB9	9.31%	4.93%	3.72%	74.86%	92.83%	40.90%	4.74%	1.79%	51.24%	98.66%	52.28%	7.77%	2.02%	36.14%	98.21%
SUB10	12.96%	5.30%	3.38%	76.72%	98.36%	36.73%	7.48%	3.20%	53.75%	101.16%	49.67%	8.89%	2.57%	37.12%	98.25%
Mean (rifampin)	10.93%	4.80%	2.71%	77.73%	97.27%	30.73%	7.13%	2.00%	60.44%	100.31%	44.22%	10.85%	1.79%	42.21%	99.07%
Stdev (rifampin)	2.20%	1.19%	1.20%	3.83%	4.33%	7.80%	1.60%	1.22%	7.83%	6.26%	7.75%	3.05%	0.79%	6.89%	3.45%

NA = not available, PET study not performed; not calculated

quinidine plasma conc during infusion

	µg/Ml (total)						µM (total)						µM (unbound)					
Subject	0 min	15 min	30 min	45 min	60 min	80 min	0 min	15 min	30 min	45 min	60 min	80 min	0 min	15 min	30 min	45 min	60 min	80 min
SUB1	0	1.743	2.525	2.478	3.718	2.950	0	5.371	7.784	7.640	11.460	9.093	0	0.806	1.168	1.146	1.719	1.364
SUB2	0	1.271	1.676	2.234	3.075	2.611	0	3.848	4.807	6.891	9.475	8.037	0	0.577	0.721	1.034	1.421	1.206
SUB3	0	0.835	1.676	2.054	2.942	2.662	0	2.557	4.807	6.416	8.992	8.299	0	0.383	0.721	0.962	1.349	1.245
SUB4	0	1.081	1.867	2.332	3.382	3.068	0	3.471	5.385	7.137	10.135	9.339	0	0.521	0.808	1.071	1.520	2.148
SUB5	0	2.054	2.759	3.236	2.867	2.366	0	6.331	8.505	9.974	8.838	7.292	0	0.950	1.276	1.496	1.326	1.094
SUB6	0	0.654	1.505	1.780	2.473	1.728	0	2.014	4.639	5.486	7.624	5.326	0	0.302	0.696	0.823	1.144	0.799
SUB7	0	0.363	1.076	2.203	2.913	2.675	0	1.118	3.316	6.790	8.979	8.244	0	0.168	0.497	1.019	1.347	1.237
SUB8	0	0.190	0.535	1.090	2.489	1.478	0	0.586	1.648	3.360	7.671	4.556	0	0.088	0.247	0.504	1.151	0.683
SUB9	0	0.363	1.076	2.203	2.913	2.675	0	1.118	3.316	6.790	8.979	8.244	0	0.168	0.497	1.019	1.347	1.237
SUB10	0	0.702	0.912	1.769	2.597	2.413	0	2.162	2.810	5.451	8.006	7.439	0	0.324	0.422	0.818	1.201	1.116